TAMPEREEN TEKNILLINEN YLIOPISTO
TAMPERE UNIVERSITY OF TECHNOLOGY

SHOKOUFEH TEYMOURI

CHEMICAL SURFACE MODIFICATION OF POLYIMIDE FILM FOR ENHANCED COLLAGEN IMMOBILIZATION AND CELLULAR INTERACTIONS

Master of Science Thesis

Examiners: Professor Minna Kellomäki, MSc Maiju Hiltunen
Examiners and topic approved in the Faculty of Science and Environmental Engineering Council meeting on 7th November, 2012

ABSTRACT

TAMPERE UNIVERSITY OF TECHNOLOGY
Master´s Degree Programme in Biomedical Engineering
TEYMOURI, SHOKOUFEH: Chemical surface modification of polyimide film for enhanced collagen immobilization and cellular interactions
Master of science thesis, 79 Pages, 5 Appendix pages
August 2013
Major: Biomaterials
Examiners: Professor Minna Kellomäki, MSc Maiju Hiltunen
Keywords: chemical surface modification, polyimide, collagen IV, retinal pigment epithelium

Different natural and synthetic polymers have been studied as an insulator and carrier for retinal prosthesis or as a scaffold for cell transplantation. The use of synthetic polymers outmatches natural polymers in some aspects including degradation, processability and strength. The synthetic polymers can be surface modified by proteins to promote their hydrophilicity, cell adhesion, and biocompatibility. Chemical surface modification is one of the stable means of protein immobilization in which proteins can be grafted covalently onto the surface. The generated covalent coupling protects the protein from shear stresses applied on the biomaterial and changes in pH of environment.

The aim of this thesis was to modify the surface of polyimide (PI) membrane by covalent coupling of adhesive molecule collagen IV to improve the retinal cell interaction with PI substrates. Therefore, acrylic acid graft polymerization was carried out on the plasma treated membrane and the number of carboxyl groups on the membranes was determined using Toluidine Blue O (TBO) method. Lastly, a peptide bond was produced between collagen and carboxyl groups by means of carbodiimides and N-hydroxysuccinimide crosslinkers. The surface morphology and hydrophilicity of membranes were obtained by atomic force microscopy (AFM) and water contact angle measurements. The fluorescent labelling was applied to compare the surface density of immobilized collagen and its stability on the membranes. The modified PI substrate was further evaluated by *in vitro* study of ARPE-19 cell interactions.

The results showed that the 25 % acrylic acid (AAc) monomer concentration provides more carboxyl groups on the membrane surface compared to 35 % AAc monomer concentration. The presence of grafted poly(acrylic acid) chains at the acrylic acid grafted membrane surface was also determined by Attenuated total reflectance-Fourier transform infrared (ATR-FTIR) spectroscopy. Collagen-modified PI was found to be more hydrophilic in comparison to control membranes. Considering the AFM results, the surface modification protocol did not significantly affect the final surface roughness of membranes. High ranges of variation in the intensities were observed between the parallel samples in both collagen density determination and stability tests. The protein ZO-1 was observed more on surface modified membrane and ARPE-19 cells acquired more hexagonal cell morphology on them.

As a conclusion, the concentration of grafted carboxyl groups on the membrane was strongly dependent on the concentration of AAc monomer solution. The surface modified membrane tested in this study show good potential as ARPE-19 cell substrate. However, means to prevent the aberrant cell division are suggested. The autofluorescence property of the membrane was the main issue in determination of collagen surface density. In addition, a more surface sensitive method like XPS is suggested to detect the presence of different functional groups on surface after each step in the protocol.

PREFACE

This work was carried out in the Biomaterial laboratory of Biomedical Engineering Department (presently known as Department of Electronics and Communications Engineering) at Tampere University of Technology, partly in the Ophthalmology Group of REGEA Institute of Regenerative Medicine at the University of Tampere, and partly in Department of Automation Science and Engineering (ASE) at Tampere University of Technology. It was funded by the Academy of Finland grant "Active Biomaterials for Retinal Prosthesis".

First of all, I would like to express my sincere gratitude to my supervisors Professor, Dr Tech Minna Kellomäki and M.Sc. Maiju Hiltunen for an interesting and challenging topic, valuable counselling and feedback throughout the process. They gave me a lot of trust and flexibility on the project. Furthermore, I am grateful to M.Sc. Maiju Hiltunen for her patience and constructive comments. Without her, I could not have dealt with such a challenging project. Her office door was always open for my questions and she never hesitated for helping me.

Also I am grateful to Head of Ophthalmology Group, Docent, PhD Heli Skottman, for collaboration, and providing cells and materials for cell culturing studies. In addition, I would like to thank PhD Kati Juuti-Uusitalo, M.Sc. Anni Sorkio, B.Sc. Elina Pajulla for their time, valuable input, and teaching me how in vitro cell culturing works. Special thank goes for Micro- and Nanosystems research group in ASE department, M.Sc Joni Leivo for teaching the fluorescence microscope and supporting materials for collagen immunostaining, M.Sc. Tomi Ryynänen for teaching me the basics of plasma treatment, M.Sc. Samu Hemmilä for teaching the contact angle measurements, and M.Sc Joose Kreutzer for his always willing support during the process in practical part.

I owe my gratitude to M.Sc. Niina Ahola for teaching the UV/VIS Spectrophotometer, M.Sc. Maiju Hiltunen for teaching the AFM imaging, PhD Kati Juuti-Uusitalo for confocal microscope images, M.Sc. Elli Käpylä for teaching the contact angle measurements, and B.Sc. Elina Pajulla for teaching the fluorescence microscope.

A warm thank goes also for my friends for all the support and encouragement during the process.

Finally, I want to thank my parents who are thousand kilometres far away from me but always being helpful and supportive during my life. They have always encouraged me in my studies and goals.

Tampere, August 2013
Shokoufeh Teymouri

CONTENTS

ABBREVIATIONS

AAc	Acrylic acid
AFM	Atomic force microscopy
AMD	Age-related macular degeneration
APTES	3-aminopropyltriethoxysilane
Ar	Argon
ARPE-19	Spontaneously transformed human adult RPE cell line
ATR-FTIR	Attenuated total reflectance-Fourier transform infrared
BCB	Benzocyclobutene
BMSF	Bombyx mori silk fibroin
BSA	Albumin from bovine serum
CRALBP	Cellular retinaldehyde-binding protein
CS	Chondroitin sulfate
CVD	Chemical vapour deposition
DAPI	4´, 6´ diamidino-2-phenylidole
DNA	Deoxyribonucleic acid
DPBS	Dulbecco's Phosphate Buffered Saline
ECM	Extracellular matrix
EDC or EDAC	Carbodiimides
EDC	N-(3-dimethylaminopropyl)-N-ethylcarbodiimide hydrochloride
F-actin	Filamentous actin
FNAB	1-Fluoro-2-nitro-4-azidobenzene
HA	Hyaluronic acid
HEMA	2-hydroxyethyl methacrylate
hESC	Human embryonic stem cell
hESC-RPE	hESC-derived RPE
hiPSCs	Human induced pluripotent stem cells
HS	Heparin sulphate
Ir	Iridium
LCP	Liquid crystal polymers
MEAs	Microelectrode arrays
MPDA	Microphotodiode array
NDS	Normal donkey serum
NHS	N-hydroxysuccinimide
NHS-esters	Succinimidyl-esters
NHS-PFPA	N-hydroxysuccinimide-derivatized PFPA
NVOC	4,5-dimethoxy-2-nitrobenzyl chloroformate
O_2	Oxygen
PC	Parylene C
PCL	Poly(ε-caprolactone)

PDL	Poly(D-lysine)
PDMS	Poly(dimethylsiloxane)
PEO	Poly(ethylene oxide)
PET	Poly(ethylene terephthalate)
PFA	Paraformaldehyde
PFCL	Perfluorocarbon liquid
PFPA	Perfluorophenylazide
PGA	Poly(glycolic acid)
PGS	Poly(glycerol sebacate)
PI	Polyimide
PLA	Poly(lactic acid)
PLGA	Poly(lactic-co-glycolic acid)
PLL	Poly(L-lysine)
PLLA	Poly(L-lactic acid)
PMAA	Poly(methacrylic acid)
PMMA	Poly(methyl methacrylate)
PNIPAAm	Poly(N-isopropylacrylamide)
ppNIPAM	Plasma-polymerized(N-isopropylacrylamide)
R_a	Roughness average
RGDS	Arg-Gly-Asp-Ser
RP	Retinitis pigmentosa
RPCs	Retinal progenitor cells
RPE	Retinal pigment epithelium
SiO_2	Silicium oxide
SS-PEG	Succinimidyl succinate-polyethylene glycol
ST-PEG	Styryl-polyethylene glycol
TBO	Toluidine Blue O
Ti	Titanium
TJ	Tight junction
ZO-1	Zonula occludens-1

1. INTRODUCTION

Retinitis pigmentosa (RP) and age-related macular degeneration (AMD) are diseases that lead to the impairment of photoreceptor cells. [1] RP and AMD are common and account for several million of the blind population in the world. [1] When vision is lost, there are two different approaches in research progress to help these people: retinal implant devices and RPE cell transplantation. Different natural and synthetic polymers have been studied as an insulator and carrier for retinal prosthesis or as a scaffold for cell transplantation. The use of synthetic polymers outmatches natural polymers in some aspects including degradation, processability and strength. The mechanical performance of biomaterial is governed by bulk properties, whereas, the surface properties dictate the tissue-biomaterial interactions. [1, 2]

Synthetic polymers can be surface modified by proteins to promote their hydrophilicity, cell adhesion, and biocompatibility. Physical surface modification is a simple and common approach in which the proteins can simply absorb on the surface through attractive forces such as ionic, hydrophobic, or van der Waals. However, shear forces and changes in pH of the solution can easily remove the physically absorbed protein layer. Chemical modification is a more stable means of protein immobilization compared to physical modification. In this strategy, proteins can be grafted onto the surface covalently with good stability. The covalent bond is formed between the molecules of the substrate and the functional groups of proteins. [2-4]

Polyimides are one of synthetic polymers with high-performance in medical implants. They are flexible, bio-inert and electrically insulating, thus suitable for biosensor encapsulation or as a substrate for subretinal and epiretinal prosthesis. [5-8]. In addition, the physically coated PI membranes with adhesive molecules such as collagen type IV and laminins (both from mouse and human placenta) promoted the maturation of hESC-derived RPE (hESC-RPE). However, the cell attachment and growth was poor on uncoated PI membrane. Laminin and collagen IV are both major constituents of RPE basal lamina, which serves as an anchoring surface for the RPE. [9]

The aim of this Master's thesis was to covalently immobilize collagen type IV on the surface of track etched polyimide membrane (ipCELLCULTURE™) with a chemical surface modification protocol. The chemical surface modification was chosen to achieve a more stable biomolecule-coated layer on polyimide membrane surface. The protocol was obtained from the existing literature with some modifications [2, 3, 10-21]. In this protocol, a covalent bounding is formed between the grafted carboxyl groups on the surface of PI membrane and the amine groups of collagen IV. To determine the density of grafted carboxyl groups on PI membrane and the presence of various functional

groups after each step of protocol, Toluidine Blue O (TBO) method and Attenuated total reflectance-Fourier transform infrared (ATR-FTIR) spectroscopy were used, respectively. The surface morphology and hydrophilicity of membranes were obtained by atomic force microscopy (AFM) and water contact angle measurements. The fluorescent labelling was applied to study the surface density of immobilized collagen and its stability on the membranes. Another goal was to investigate the effect of covalent crosslinking for cell culturing purposes and especially on ARPE-19 cell differentiation. ARPE-19 cell differentiation was studied by immunocytochemical staining and confocal microscope through observation in cell morphological changes. In all experiments, uncoated and physically coated PI membranes were used as control.

THEORETICAL PART

2. RETINAL DISEASES AND TREATMENTS

2.1. Retina and retinal diseases

The retina in the eye absorbs photons of light and converts them into neural electrical signals (Figure 2.1). Approximately 1 million axons of the ganglion cells form the optic nerve which carries the neural signals to the visual cortex at the back of brain. The visual cortex processes the signals into meaningful image perception. The 200 µm thin retina is composed of approximately 126 million photoreceptors in two types of rods and cones which convert light signals to electrical ones. The rods are responsible for peripheral and night vision, and the cones function best in colour vision and bright daylight. The middle layer of retina contains bipolar cells which collect neural signals from the photoreceptors and then transmit them to the outermost layer of the retina, and ultimately to the brain. On the way, all neural cell layers involving horizontal cells, bipolar cells, amacrine cells, and ganglion cells participate in signal processing and convergence. [22]

The retinal pigment epithelium (RPE) is a cellular monolayer located between the choriocapillaris and photoreceptor layers of the retina. It provides essential metabolic support for the normal function of the neurosensory retina. Also, it plays an important role in local cellular and extracellular homeostasis and maintenance of the extra photoreceptor matrix. The separation of the neurosensory retina from the underlying RPE is one of the most common causes of photoreceptor cell loss. [23-25]

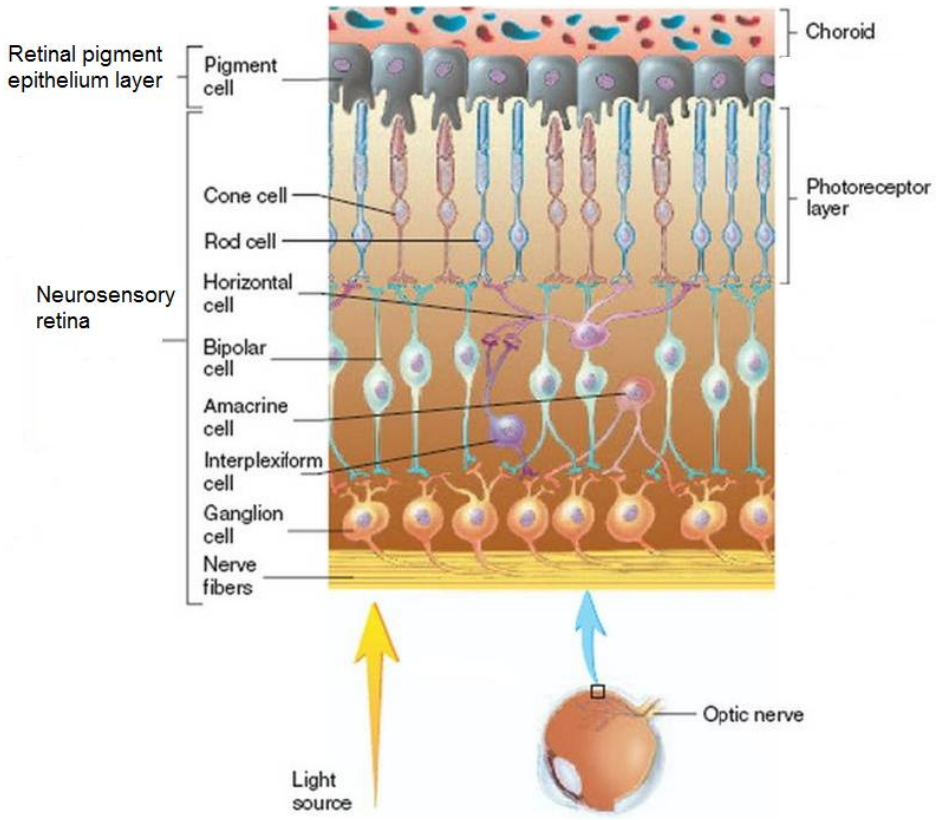

Figure 2.1. *The detailed structure of retina. The retina has two main layers, the neurosensory retina and RPE layer. [26]*

Retinitis pigmentosa (RP) and age-related macular degeneration (AMD) are diseases that lead to the impairment of photoreceptor cells. [1] RP and AMD are common and account for several million of the blind population in the world. [1] In the United States, 300000 new patients with AMD are diagnosed annually among adults older than 65, 10% of whom become blind each year. [27] Also, the incidence of RP is 1 per 4000 live births worldwide. [28] Effective medical treatments for RP and AMD have not been established yet. A number of approaches, including gene therapy and pharmacological measures, are currently being pursued in the hope of preventing blindness. [6] However, when vision is lost, there are two different approaches in research progress to help these people: retinal implant devices and RPE cell transplantation. While the photoreceptor cells degenerate with RP and AMD, many other retinal cells (bipolar, horizontal, amacrine, and ganglion) are still present even after many years of blindness. Accordingly, it will be possible to restore some level of visual function using retinal implant devices to electrically stimulate the remaining retinal network. [1, 29] The damaged retina could also be repaired by healthy retinal tissue by RPE cell transplantation. In this method, if a population of healthy cells that are able to integrate into the retina and reconnect to the synaptic pathways of the remaining host are placed in the subretinal space, then these cells may prevent the consequent loss of photoreceptor cells in the early stages of disease and restore vision. [30, 31]

2.2. Retinal implant devices

Retinal implant devices are applied for patients blinded primarily by photoreceptor loss such as RP and some forms of AMD. [32] They can be classified according to the location of the device: on the retinal surface (epiretinal), or in the subretinal space. Currently several research groups are developing retinal prostheses worldwide. Epiretinal implants are being investigated by research groups such as Eckmiller and his colleagues [33], Klauke and her colleagues [34], Humayun et al. [35], Rizzo and co-workers [36]. Alan Y.Chow and colleagues [37] and Eberhart Zrenner in Tübingen [6] are also developing subretinal implants.

The epiretinal implants consist of an electrode array implanted on top of the inner limiting membrane, connected by a cable or wirelessly to a microprocessor, power source and a camera. The camera captures the image and sends it to the microprocessor, which processes the data and sends the impulses to the electrode array to stimulate the retinal ganglion cells (Figure 2.2). [7, 35] The epiretinal implant design keeps a significant portion of the device in the eyeglass frame rather than implanted. Therefore, it leads to less tissue damage and reduces the inflammatory reactions and the risk of failure. In addition, it optimizes the ease of replacement or upgrading the components. [32, 35] However, the epiretinal implant is relatively far from its target cells, requiring more energy to stimulate visual sensation than if the electrodes are placed near to their target cells. [38]

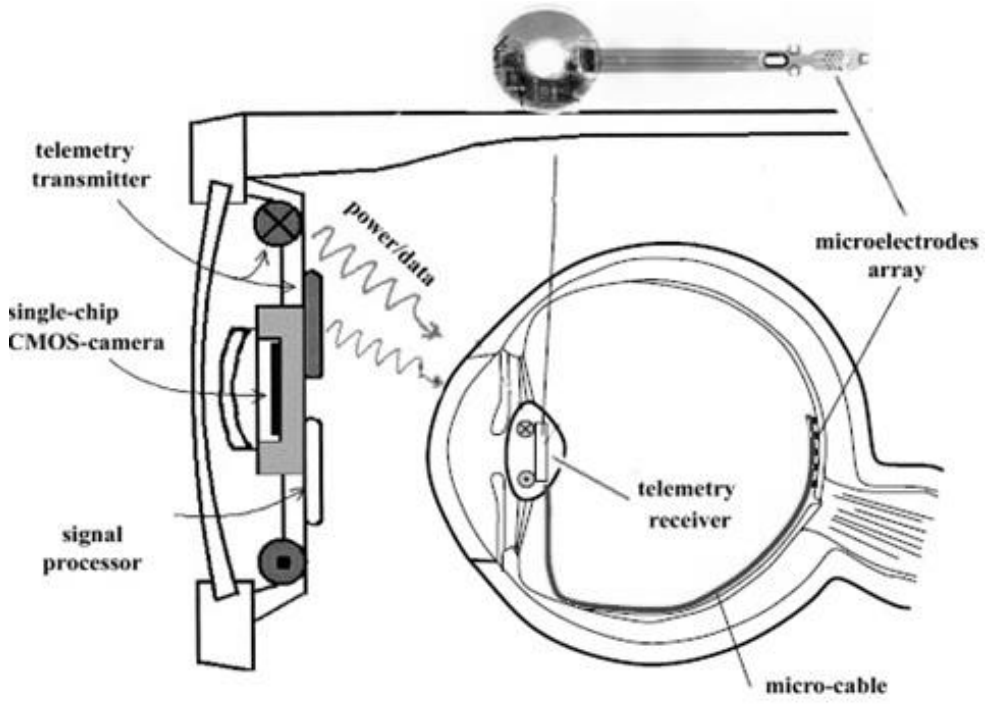

Figure 2.2. *Components of the epiretinal electronic prosthesis. The camera captures the image and sends it to the microprocessor, and then the electrode array receives the impulses to stimulate the retinal ganglion cells. According to [22, 34].*

The subretinal prosthesis is targeted to replace the degenerated outer retinal layers. It involves the implantation of a subretinal microphotodiode array (MPDA) with microelectrodes arranged in arrays between the pigment epithelium layer and the outer layer of the retina. Then the photodetectors capture the light and subsequentially convert the light energy into electrical impulses to stimulate the intact remaining retinal cells in the same region of the received light energy (Figure 2.3 a). [7, 35, 39] The subretinal prosthesis directly replaces damaged photoreceptor cells and is positioned in close proximity to the remaining bipolar cells, which may also permit smaller stimulus thresholds. However, there are limited space for the microprocessor and power source in the subretinal space and therefore an increased likelihood of thermal injury to the neural tissue. In addition, due to the limited amount of light that can reach the device, MPDA do not deliver sufficient energy to stimulate the retina. [40] Therefore, an external power source is a necessity, and with it comes the surgical implantation problems (Figure 2.3 b). [32, 35] Zrenner et al. demonstrated that the blind patients with subretinal microelectode arrays with 1500 photodiodes can read letters, locate bright objects on a dark table, and describe and name objects like a fork and knife on a table. However, the results show that the visual acuity is still poor relative to normal vision. Perhaps, these devices can be used for mobility and orientation of patients. [6]

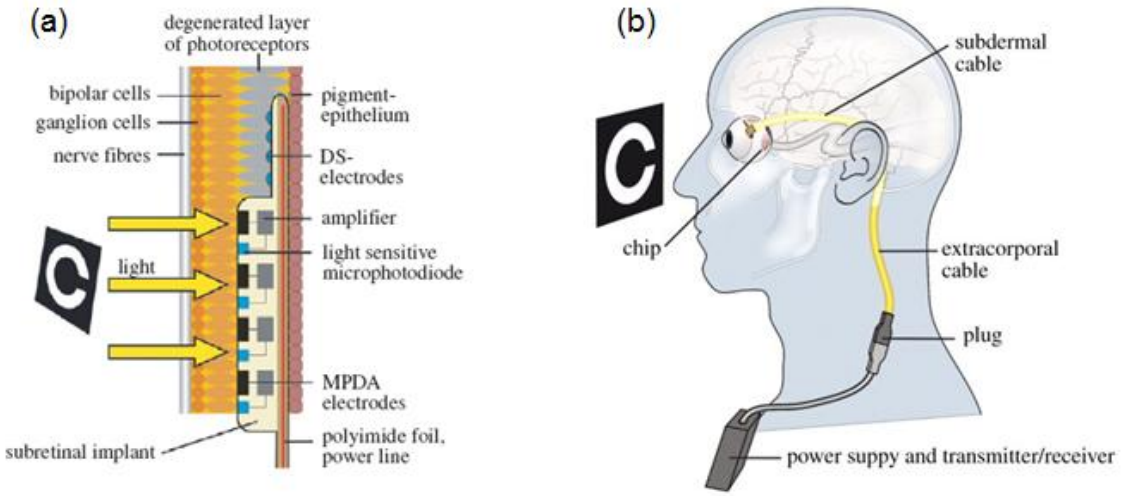

Figure 2.3. *Components of subretinal implant device and their position in the body. (a) the position of subretinal MPDA between the pigment epithelium layer and the outer layer of the retina, (b) an external power source in subretinal implant devices. [6]*

2.2.1. Polymers in retinal prosthesis

Besides microelectronic aspects and the demand of developing minimally invasive implantation techniques, there are some priorities that must be taken into consideration by retinal implants in order to function well and restore the vision. The biocompatibility of

the implant materials is an important issue so that the device would function reliably over many decades. [41] The implant materials must be durable and relatively inert so that their impact on remaining retinal tissue is minimal. [40] The general requirements of retinal implant materials are listed in Table 2.1. Also, Appendix 1 represents some of the renown polymers which have been used in retinal prosthesis considering their properties.

Table 2.1. *The general requirements of retinal prosthesis materials. [8, 42, 43]*

The ideal properties of retinal implant material →Explanation
• Thin → to slide easily between layers of eye • Stiff → to be inserted in the eye cavity without buckling • Flexible → to preserve its original shape after folding or rolling • Biocompatible • Mechanically stable • Light-weighted • Barrier against both biofluids and also possible compounds leaching out of the implant • Have low moisture absorption • Have stable interfacial (cell and tissue) adhesion in aqueous environment

The implanted elements of retinal prosthesis are in contact with corrosive biological fluid. Therefore, the device must be protected to avoid corrosion and release of toxic substances from implant. [44] In general – the protection of the tissue against implant and the protection of the implant against the surrounding tissue– demonstrate the importance of an encapsulation material which is biostable over the intended lifespan of the implant. [45]

To date, several polymer materials including poly(dimethylsiloxane) (PDMS), silicone, polyimide (PI), or parylene C (PC) have been used as an insulator and carrier for platinum, gold, or iridium (Ir) based microelectrode arrays (MEAs), conductive lines, and interconnecting pads. [22, 42, 46, 47] These polymers are thin, flexible, and biocompatible — suitable characteristics for minimally invasive retinal electrode arrays. [42]

Güven et al. studied the long-term and mechanical biocompatibility of PDMS arrays manufactured by soft-lithography technique. The PDMS array was implanted epiretinally in dog's eyes for 6 months, with a single retinal tack in each case to fix the array in place. In general, there was no ocular infection and the device was attached to retina, while the layered retinal structure under the array was preserved. [46]

Majji et al. studied the biocompatibility of the hand fabricated electrode array which was made of platinum disc shaped electrodes in a silicone matrix. The electrically inactive electrode array was implanted onto the retinal surface of dog's eyes. The electrode array remained firmly fixed to the retina by the metal retinal tacks for up to 1 year of follow-up and no retinal detachment or infection occurred throughout the follow-up period. [48] The flexibility and softness of silicone elastomer can minimize the unintended damage during implantation and its durability is sufficient to protect an implanted prosthetic device for more than 20 years. However, softness and nonplanar surface of silicone elastomer is not suitable for microfabricating thin film electrode arrays and it is difficult to shape the silicone matrix into thin sheet. [48-50]

PI is easy to handle and can be shaped into any configuration. [50] Seo et al. studied human RPE cell culturing on flexible PI as a substrate material for gold based MEA with aim to assess the biocompatibility and cell behavior of PI. As a result, the PI based MEA showed good affinity to human RPE and caused no harmful effects. In addition, *in vivo* biocompatibility tests in the rabbit eyes showed very good stability and safety by 12 weeks. [50]

In another study done by Kim et al., human RPE cells were cultured on a PI electrode array to evaluate adhesion and survival of the cells. RPE cells showed good affinity to MEA and there appeared no abnormal morphological changes or no piled-up growth. In addition, there was no histological difference between control and operated rabbit eyes except some damaged photoreceptors in subretinally implanted group, which might be due to the photoreceptor damage during operation. The PI electrode array itself showed good stability at the first year follow-up. In a few electrodes, moth-eaten fragmentation of the border of the PI around the electrode opening site was observed. Electrode detachment from its PI bed was not observed even in such a case. [8]

Sachs et al. studied the intracortical responses evoked by subretinal electrical stimulation by platinized titanium nitrite electrodes on a PI film. Perfluorocarbon liquid (PFCL) was used to provide close contact between the electrode array and the outer retina. The retina was attached over the stimulation array in acute trials for up to 12 h in the eyes of cats. Neither displacement of the film nor any other adverse events, especially inflammatory reactions, were detected during experiments. [7]

Later, Zrenner et al. implanted subretinally a MPDA on a 20 µm thick PI foil carrying an additional test field with 16 electrodes for direct electrical stimulation in blind patients for short-term stimulation. The patients were able to localize and recognise the objects and read letters, however, the biocompatibility assessment of the device was not mentioned in this study. [6]

The film thickness should be kept below some tenths of a micrometer to slide easily into the fragile retina. However, the stiff edges of a thin film structure of PI may cause unwanted scratches during insertion and movement of the arrays into the target position. Therefore, Kim et al. developed a silicone-PI hybrid MEA to combine the suitability of the silicone elastomer for implantation and the microfabrication technology of the PI-based MEA. *In vivo* epiretinal and subretinal implantations were successfully performed

during the 4-week follow-up period without damage to the MEA or the operation site in the rabbit eye. [49]

Although the retinal stimulation electrode arrays fabricated on PI, PC, and silicone have been reported to be safe and effective in previous *in vivo* and *in vitro* studies, there are concerns related to the water absorption and interfacial adhesion properties of these polymers in aqueous environment for long-term applications. Lee et al. have studied liquid crystal polymers (LCP) which are flexible, mechanically stable and have lower moisture absorption compared with PI, PC, and silicone. The LCP based MEAs were implanted in rabbit eyes to evaluate the long-term biocompatibility and stability of the material. No retinal neural loss or inflammation around the arrays space, and no sign of degradation were observed after 4 months implantation. [42]

Any implanted electronic device is exposed to movements and should be attached in a stable manner to its intended anatomical location. In retinal implant, a stable array position is critical in maintaining steady image resolution and stimulation current levels. A dislocated implant can cause a visual disturbance and retinal injury, and therefore should be removed. [48] There are different attachment methods according to different approaches and locations along the visual pathways. The subretinal prosthesis could be kept in place by the adherence forces between the sensory retina and the RPE, where the movement of small implant is restricted. [32] However, the epiretinal prosthesis requires retinal tacks pushed through the implant, retina, and sclera to fix a stimulating MEA on to ganglion cells of the retina. [31, 51]

The conventional retinal tacks made of titanium (Ti) are traumatic, large and cause distortion or tearing of small and flexible PI based MEAs. Around the insertion area of metal alloy tacks, hyper-pigmentation and hypo-pigmentation of the RPE was noted, although damage did not appear to spread. [38, 46, 48] Silicon retinal tacks could be good candidates as the substitute for the conventional Ti tack in the retinal prosthesis system as they made minimal or no damage to PI electrode array. To overcome the fragmentation of the gripping site of the tack, Seo et al. deposited 3 μm thick PC film on the entire surface of silicon-micromachined retinal tack and implanted the tack in the rabbit's eyes for 4 weeks. The results revealed no inflammatory infiltrates in retina, and no corrosion of the silicon retinal tack due to the body fluid. The PC coating was also well-preserved with tight cellular adhesion for 4 weeks and it improved the durability and chronic biocompatibility. [51] Bioadhesives and magnets are the other methods examined for fixation of epiretinal implants. [32, 38] Previous reports showed that adhesive hydrogels such as succinimidyl succinate-polyethylene glycol (SS-PEG) and styryl-polyethylene glycol (ST-PEG) were effective but short-lasting and SS-PEG was toxic to the retina [52]. The plasma-polymerized (N-isopropylacrylamide) (ppNIPAM) is non-toxic to neural tissue and can detach from the retinal surface *in vitro* by lowering the temperature of the physiological medium [53]. The ppNIPAM coated implants provided retinal adhesion without evidence of ocular toxicity and inflammation in rabbit eyes during 6 weeks experiments [54]. However, the use of adhesives for epiretinal attachment remains a research topic [38].

2.3. RPE cells transplantation

In many types of retinal degeneration, the photoreceptors lose their function, while the inner layers of retina and associated cell types still maintain their architecture for a time period. Therefore, the idea of transplantation comes from this preservation to deliver to the subretinal space a population of healthy cells that are able to integrate into the retina and replace receptor function. These cells may reconnect to the remaining host visual synaptic pathways and restore the vision. [30]

Mature photoreceptors, progenitor cells, retinal sheets and RPE cells have been tested in animal models from 1 to 7 months. The results show varying degrees of improved vision. However, the subretinal cell transplantation has not yet resulted in an effective clinical treatment. [30]

It is possible to deliver cells into the subretinal space either by the cell suspension injection or scaffold. The cell suspension injection in the form of transplanted retinal cells or tissue, leads to the random orientation of photoreceptors and insufficient cells survivals. The scaffolds can provide structural support for cells, deliver cells or drugs and direct cell behavior. They contain relevant cell populations that after transplantation, the cells differentiate and organize into appropriately functioning cell layers. Also, they provide more RPE cells and retinal progenitor cell survival during transplantation compared to cell suspension injection strategy. Therefore, they are considered as desirable subretinal transplantation strategy and may be a promising treatment to restore vision in patients with retinal degeneration. [30, 55]

One of the difficulties in growing RPE cells in culture is that the RPE cells undergo morphological and physiological changes in the absence of an appropriate adhesion substrate. They re-enter the cell cycle and proliferate, lose melanin pigment, and alter their normal epithelial appearance to either a macrophage- or a fibroblast-like morphology. The fibronectin enriched surfaces, three dimensional collagen gels, plastic tissue culture surfaces, and presence of photoreceptor debris in culture lead to alteration in morphology of RPE cells. [23, 25] The properties of an ideal culture system for RPE cells are presented in Table 2.2.

Table 2.2. *The properties of an ideal scaffold substrate used for RPE cells. [23, 55, 56]*

Ideal properties of scaffold substrate for RPE cells
• Regulate nutrients and waste products to and from the neural tissue • Biocompatible and biodegradable • Easily processable and availability • Maintain normal cell physiology and morphology • Support the cell attachment • Allow gentle manipulation of cells in and out of the matrix

2.3.1. Substrates for RPE transplantation

Different natural and synthetic substrates have been studied to design a scaffold for cell transplantation. One of the straightforward methods in this aim is to use the membranes and tissues of the donor tissue without any cellular component. The human amniotic membrane, human lens capsule, and Bruch's membrane are the few examples. These scaffolds often mimic natural mechanical properties and are biocompatible. However, the donor shortage and disease transmission are the concerns that must be considered about these substrates. [30]

The natural polymers that exist in extracellular matrix (ECM) also play an important role in scaffold applications. However, the consistency and mechanical properties of scaffold must be controlled. The other issues concerning this approach are the purity of polymers with animal origin, disease transmission, and patient allergies to some components. [30] Collagen, laminin, fibrin, alginate, and hyaluronic acid (HA) are some examples of natural biocompatible polymers that are discussed in more detail in this chapter.

2.3.1.1 Natural polymers

Collagen

Collagen is a primary component of ECM and has a fibrous structure that provides tensile strength to tissues such as tendons, cartilage and skin. It is the most abundant structural protein inside the body with 30 different types that vary in amount in each tissue. [56-58] Collagen has been investigated as haemostatic agent, drug carrier vehicle, and osteogenic and bone filling material to promote the cell adhesion [59]. Collagen I, III, IV and V are the major components of Bruch's membrane that have been used as scaffold for cell attachment, proliferation and differentiation with different mechanical properties and degradation rates [30, 59]. In a study of Lu et al., thin collagen I films (2 μm) allowed the nutrient flow across the membrane to ARPE-19 cells (a spontaneously arising human RPE cell line with similar morphological and functional characteristics to adult human RPE) during 15 h of incubation. In addition, the membrane supported the cell growth and formation of tight epithelial monolayer. [56, 60] Collagen I serves as one of the major binding proteins for RPE cells and has been examined as a coating on the scaffolds to support the anchorage-dependent RPE cell attachment [61]. In addition, in a study by Vaajasaari et al. human embryonic stem cells (hESCs) and human induced pluripotent stem cells (hiPSCs) differentiated toward functional RPE cells on collagen IV–coated substrates in serum free culture medium. [62]

Alginate

Alginate is a natural linear copolymer that contains 1,4-linked β-D mannuronic acid and α-L guluronic acid (Figure 2.4). These residues can bind with cross-linking divalent (Ca^{2+}, Ba^{2+}, Sr^{2+}) or trivalent cations (Al^{3+}, Fe^{3+}) to form hydrogels at room temperature

(RT). Alginate matrices maintain normal cell phenotype and physiological functions during the propagation of chondrocytes and hepatocytes. [23] In addition, alginate provides a structural support for implanted cells and has been widely used for cell entrapment as hydrogels or microcapsules. [57, 63] The microcapsules are coated by a cationic polyelectrolyte to slow down the swelling and degradation of the microcapsules, while the risk of immunological reactions and fibrotic growth may increase. The guluronic acid and mannuronic acid contents of alginate play an important role in controlling the microcapsule structure. [63]

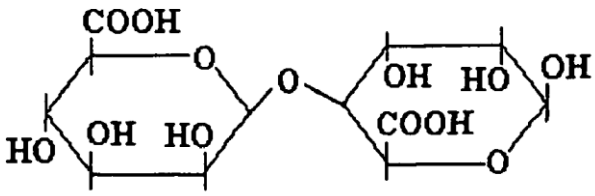

β-D-mannuronic acid (M) α-L-gluluronic acid (G)

Figure 2.4. *The structure of alginate. [64]*

In order to investigate the suitability of alginate as an ideal culture system for RPE cells, porcine RPE cells were cultured on the alginate matrix for 14 days so that the cell number increased significantly and their normal morphologic appearance and pigmentation were reversed. [23] In a study by Wikström, ARPE-19 cells encapsulated in microcapsules of alginate that was cross-linked with different divalent cations (Ca^{2+}, Ba^{2+}, Sr^{2+} and combination of Ca^{2+} and Ba^{2+}). The microcapsules were coated first with poly-L-lysine (PLL) and then with alginate. Then, they were incubated at 37 °C and 7 % CO_2 for *in vitro* cell viability studies. Alginate microcapsules that were crosslinked with Ca^{2+} and Ba^{2+} ions showed the best ARPE-19 cells viability and protein secretion for at least 110 days. [63, 65]

Hyaluronic acid

Hyaluronic acid (HA) is a natural linear polysaccharide composed of a repeating disaccharide β-D-(1→3) glucuronic acid and β-D-(1→4)-N-acetyl-glucosamine units (Figure 2.5). HA is an essential constituent of native ECM and tissues. [66] It is a major component of the vitreous body of eye. 21.9 % and 8 % of the RPE and the inter photoreceptor matrix are made of HA.

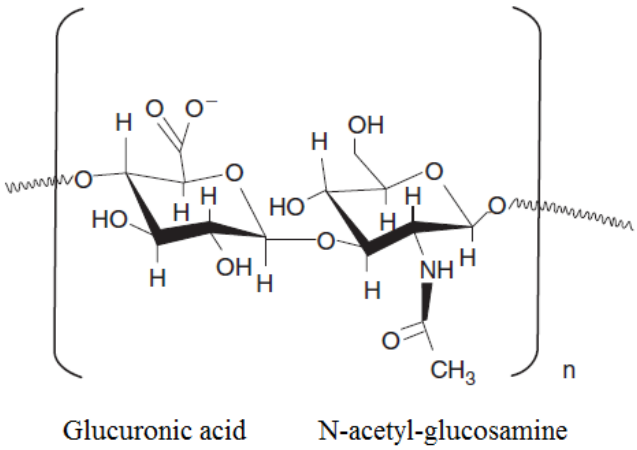

Figure 2.5. *The structure of HA. [57]*

It plays an important role in co-regulation of cell behaviour during fetal growth and development, wound healing processes, inflammation and tumorigenesis [57, 66, 67]. In the past decade, HA and its derivatives have been investigated as new biomaterials for use in cell therapy, tissue engineering scaffolds, drug delivery, and treatment of knee osteoarthritis. [66, 68] HA improves cellular adhesion, proliferation and migration; it can be incorporated into the final copolymers to enhance the ability of the scaffolds to act as cellular substrates. [25] The injectable Poly(N-isopropylacrylamide) PNIPAAm/ HA-based copolymers demonstrated excellent compatibility with human RPE cells *in vitro*. The presence of HA in the scaffolds provided an adhesion substrate for anchorage-dependant RPE cells. [25]

The architecture, mechanics, and degradation of HA hydrogels are controllable which makes them ideal for cell delivery to a subretinal space while decreasing invasiveness of the procedure. [69]

Laminin

Laminins are a major ECM protein component of the basal lamina (one of the layers of the basement membrane). They are composed of an α-chain, a β-chain, and a γ-chain, found in five, four, and three genetic variants, respectively. The chain compositions determine the name of laminin molecules. [70] The presence of laminin in basal lamina has effects on cell differentiation, migration, and adhesion, as well as phenotype and survival [71]. Laminin influences differentiation of progenitor cells toward mature retinal phenotypes. [72] In a study by Christopher et al., poly(glycerol sebacate) (PGS) membranes were coated with electrospun nanofiber composed of laminin and poly(ε-caprolactone) (PCL). The membranes were cultured for 7–14 days with E40 porcine retinas. Laminin promoted neurite in-growth into the membrane and facilitated neuronal connection between graft and host. Laminin-PCL blend nanofibers promoted sufficient cell adhesion of isolated photoreceptor layers to PGS membranes *in vitro*. [73]

Laminins play an important role in maintenance and survival of tissues, acting as an integral part of the structural scaffolding in almost every tissue. Laminins can bind to other laminin molecules to form sheets in the basal lamina. [74] This crosslink structure provides binding regions for cell membranes and ECM molecules adhesion [75].

2.3.1.2 Synthetic polymers

Another approach in scaffold fabrication is the use of synthetic polymers outmatching natural polymers in some aspects. The polymer composition and its corresponding properties such as degradation, processability and strength can be tailored in scaffolds composed of synthetic polymers. The polymer can be either degradable or non-degradable depending on the intended application.

Poly(lactic acid) (PLA), poly(glycolic acid) (PGA)

Poly(lactic acid) (PLA), poly(glycolic acid) (PGA), and poly(lactic-co-glycolic acid) (PLGA) are the most common synthetic biodegradable polymers used in scaffolds (Figure 2.6) [30, 76]. These polymers are biocompatible, easily processable to desired configurations of controlled thickness, and can be metabolized by the body after degradation [55]. Crystallinity, molecular weight, and the ratio of lactic to glycolic acid subunits are the controllable parameters that allow specifying the degradation profile of PLGA [76].

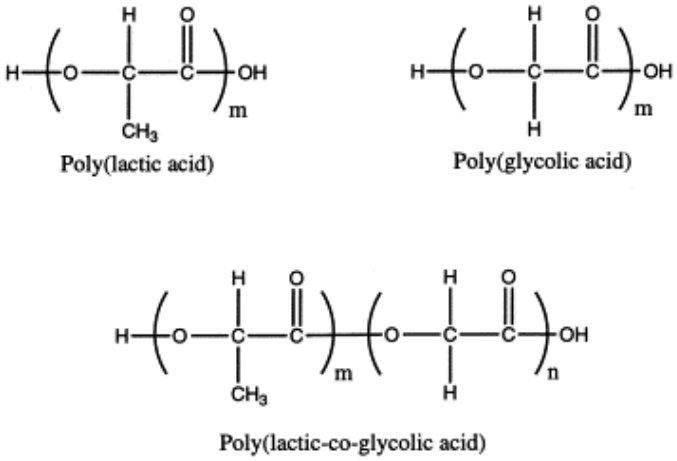

Figure 2.6. *The structure of PLA, PGA, and PLGA. [77]*

PLGA has shown ocular biocompatibility and has been used as substrates for human fetal RPE cell monolayers and spheroids culturing [76]. The polymer blend of PLGA with poly(L-lactic acid) PLLA forms a more flexible scaffold with stability in extensive elongation [30]. The PLLA/PLGA polymer has been studied as a scaffold to deliver retinal progenitor cells (RPCs) to the mouse subretinal space. As a result, there were a significant increase both in the number of surviving cells and delivered cells into the mouse retina. RPCs migrated into the retina and differentiated into cells that morpho-

logically resemble retinal neurons. The bulk degradation of scaffold started 2 weeks after implantation as an increase in the pore size. [72, 78] In addition, the thickness of PLLA scaffolds (150-250 μm) are greater than the photoreceptor layer of the rodent retina (30 μm), thus leads to damage to the retina [76].

Poly(glycerol sebacate)

Polyglycerol sebacate (PGS) is a biodegradable elastomer that exhibits high flexibility (Figure 2.7). PGS has low elastic modulus of 1.66 MPa and the mechanical properties of this polymer are more similar to those of retinal tissue with elastic modulus of 0.1 MPa. The scaffolds can be scrolled and inserted into syringe for subretinal transplantation. Therefore, the cells are protected from shear stresses during transplantation and the incidence of trauma is reduced. [76]

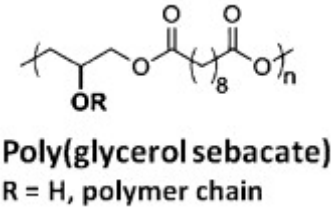

Figure 2.7. *The structure of PGS. [79]*

PGS degrades by surface erosion and minimum swelling, thus the pH of subretinal environment is less negatively affected and the loss of mechanical strength relative to mass occurs slowly. [76] The degradation time of PGS in vivo is about 4-8 weeks. In a recent study by Redenti et al., micro-fabricated PGS scaffolds promoted the initial mouse RPCs differentiation *in vitro* and subsequent *in vivo* delivery to the mouse subretinal space. PGS scaffolds demonstrate RPC compatibility and high numbers of RPCs migrated into host retinal tissue. [72]

Poly(ε-caprolactone)

Poly(ε-caprolactone) (PCL) is a biodegradable polyester that can be used as a thin substrate for retinal tissue engineering (Figure 2.8). PCL has been utilized as a nanostructured scaffold to deliver RPCs to the subretinal space. The scaffold promoted RPCs retention and provided appropriate permeability. It also increased expression of mature bipolar and photoreceptor markers in mouse retina. [80] PCL is highly permeable, allowing the nutrient molecules pass the substrate. It degrades about 2-3 years due to its hydrophobic and semi-crystalline structure. The PCL degradation occurs from its surface at a much slower rate compared to PGLA. [30, 76]

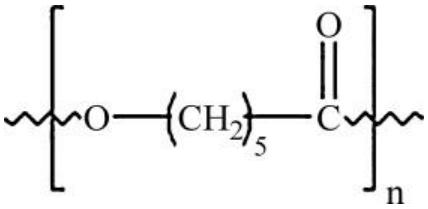

Figure 2.8. *The structure of PCL. [81]*

Poly(methyl methacrylate)

Poly(methyl methacrylate) (PMMA) is a non-degradable polymer that require second post-surgery to remove the substrate out of the subretinal space (Figure 2.9). This may increase the risk of retinal detachment and inflammation in ocular tissue.

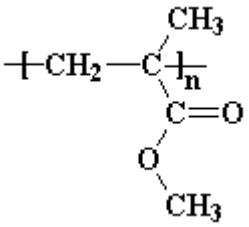

Figure 2.9. *The structure of PMMA. [82]*

In a study done by Tao et al., RPCs were delivered on micromachined ultra-thin PMMA scaffolds (6 μm thickness) and transplanted into the subretinal space of the mouse. Porous PMMA scaffolds demonstrated greater extent RPC retention and adhesion during transplantation compared to non-porous scaffolds. In addition, RPCs migrated into the host retinal layers and expressed at least three markers of mature retinal cells. Ultra-thin film PMMA scaffolds served as a biocompatible substrate for cell delivery *in vivo* without foreign body response during 4 weeks transplantation. [83]

Polyimide

Polyimides are the other synthetic polymer with high-performance in medical implants. They are bio-inert and electrically insulating, thus suitable for biosensor encapsulation or as a substrate for subretinal and epiretinal prosthesis [5-7]. In addition, PI is flexible and can recover its original shape after the implant is folded or rolled [8]. It can also undergo micromachining processes for implant fabrication [22]. PI has demonstrated ocular biocompatibility and is approved by regulatory agencies for intraocular use. In a study by Julien et al., gelatin-coated PI membranes were implanted in the subretinal space of rat eye for four weeks. It was observed that the living cells penetrated to the porous membranes that may help the mechanical anchoring of the implant to tissue [84]. In addition, PI supports adhesion and growth of fibroblasts [5]. The coated PI membranes with adhesive molecules have also promoted the maturation of hESC-derived RPE (hESC-RPE) [9].

3. SURFACE MODIFICATION OF POLYMERS USING PROTEINS

Many natural materials such as fibronectin, laminin and collagens show excellent biocompatibility and cell adhesion. However, they do not have good mechanical strength and stability, while synthetic polymers have remarkable mechanical properties and processability. Although the mechanical performance of biomaterial is governed by bulk properties, the surface properties dictate the tissue-biomaterial interactions. Therefore, synthetic polymers could be surface modified by proteins to promote their hydrophilicity, cell adhesion and biocompatibility. [2, 3]

Surface modification is a widely adopted method to improve the biocompatibility of material surface without changing the bulk properties. In addition, it provides a strong support for the desired cell attachment and subsequently enhances the tissue adhesion. [3, 10, 13] Guenther et al. studied the adhesion and survival of rat retinal cells on different materials used for fabrication of multi-photodiode array. The cell adherence on substrates of silicium oxide (SiO_2) and Ir without coating were low, whereas plating efficiency increased to 90 % after the substrates were coated with either poly(D-lysine) (PDL), poly(L-lysine) (PLL) or laminin. After 3 weeks cell culturing almost no retinal cells survived on uncoated materials, whereas 60-80 % of the cells still survived on precoated Ir and the best results were obtained with PLL. [85] In addition, coating of polymers with proteins or antibiotics prevents bacterial colonization on implants and could provide a therapeutic effect for implant. [44]

There are three different techniques of protein immobilization onto the substrate: physical, chemical, and photochemical immobilizations (Figure 3.1), which are presented in more detail in the following subchapters. [86] The strategy that is chosen to attach proteins onto the substrate can largely determine the properties of the protein-coated surface. The protein immobilization method must ensure accessibility of the protein's active site and provide a homogeneous surface orientation of proteins without affecting their function and conformation. [12]

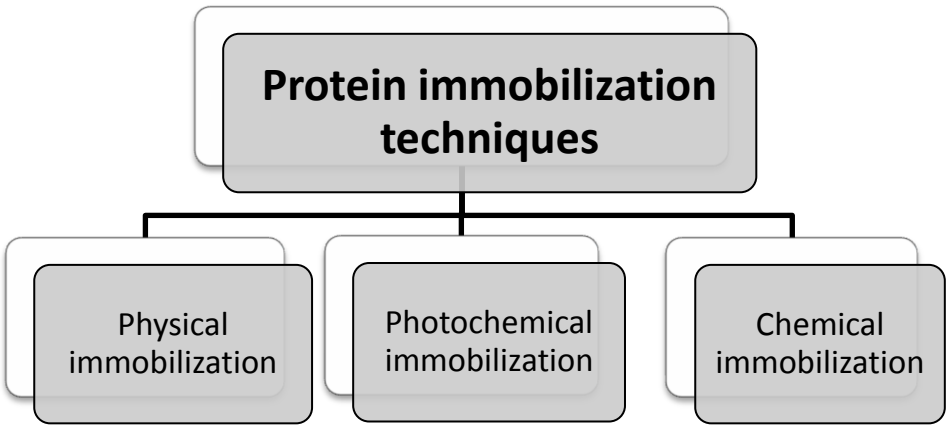

Figure 3.1. *Classification of different methods of protein immobilization on the substrate.*

3.1. Physical immobilization

This method is a simple and common approach to modify the polymer surface via physical absorption. Proteins can simply absorb on the surface without changing the structure of either, through attractive forces such as ionic, hydrophobic, or van der Waals. [3, 86, 87] However, high shear forces and changes in pH of the solution can easily remove the physically absorbed protein layer. [3]

Chang et al. coated PC films with fibronectin by a physical coating process. The cell adhesion and spreading of fibroblasts and hepatocytes after 6 h were comparable to untreated PC films, and standard tissue culture substrates such as polystyrene. High hydrophobicity and low polarity on the smooth surface of untreated PC film causes low attachment and proliferation of fibroblasts. [88]

Shadforth et al. prepared the bombyx mori silk fibroin (BMSF) intended to use as a carrier substrate for human RPE cell transplantation. The BMSF membranes were coated physically with either vitronectin, serum-supplemented culture medium, laminin or collagen IV. After 4 h incubation, the attached ARPE-19 cells on all treated membranes, except fibronectin membranes, were more than that of untreated-membranes. The amount of attached cells on vitronectin-treated membranes were significantly higher, compared to other ECM proteins, similar to that reported for tissue culture plastic. [60]

Subrizi et al. studied the effect of different proteins on hESC-RPE differentiation and maturation toward RPE phenotype. The hESC-RPE cells were cultured on PI membranes which were physically coated by proteins like collagen type I and IV from human placenta, laminins both from mouse and human placenta, HA, heparin sulphate (HS) and HyStem^{TM}. The cell attachment and growth on uncoated PI membrane was poor. In addition, the cells did not grow on HA and HS coated membranes. While, on collagen, laminin and HyStem^{TM} coated membranes, the cells acquired RPE monolayer morphology and pigmentation. Laminin and collagen IV are both major constituents of RPE basal lamina, which serves as the anchoring surface for the RPE. In addition,

laminin is considered as a suitable coating material due to its availability at GMP grade and supporting the strict standards required for clinical applications. However, HyStem^{TM} hydrogel was not recommended for future use in cell replacement therapy since the hESC-RPE monolayers easily detached from the membrane upon handling. [9]

3.2. Photochemical modification

Photochemical protein immobilization is a novel method that results in spatially oriented and spatially localized covalent coupling of proteins onto the surface. Photochemical protein patterning methods use photoreagents, which can be activated upon UV light, to bind target molecules by one of the four scenarios outlined in Figure 3.2. In the first scenario, the surface is coated with photoreagents and incubated with a protein solution. Upon masked irradiation of the solution-covered substrate, localized regions are activated and proteins are bound to the substrate via those active sites (Figure 3.2. a). In another method, a substrate is incubated with photoreagents. Upon irradiation, the photoreagents within localized regions are activated and bound to the surface in these regions, leaving a pendant group. Then the substrate is incubated with a protein solution and proteins bind to the pendant groups (Figure 3.2. b). Thirdly, photoreagents is attached to the surface and then be exposed to appropriate irradiation. Then, the caging groups are removed within localized regions and the proteins bind with the active molecules on the substrate in these areas (Figure 3.2. c). Lastly, a substrate is incubated in a solution that contains proteins and photoreagents with several photochemical species. After irradiation, the photoreagents within localized regions are activated and bound to the substrate and proteins within the patterned areas (Figure 3.2. d). [10, 86, 89]

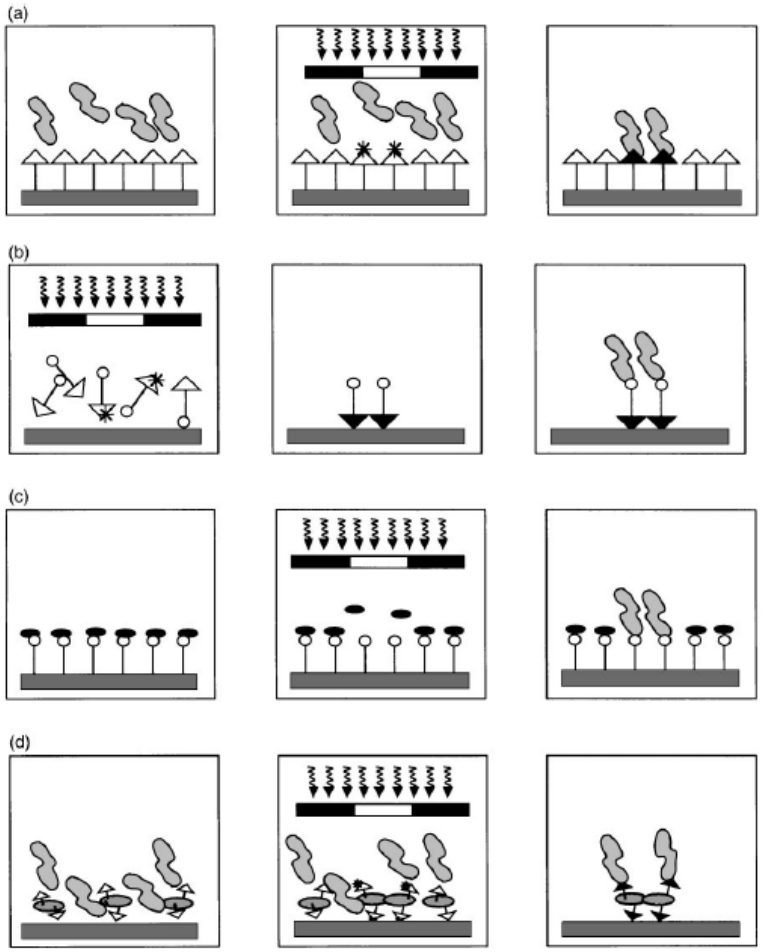

Figure 3.2. *Scenarios for photochemical protein immobilization. (a) A substrate is covered with photoreagents and incubated with a protein solution. Upon UV irradiation, the activated regions bind protein in solution. (b) A substrate is incubated with photoreagents and irradiated; after incubation with protein, protein binds in the localized regions. (c) A substrate is covered with photoreagents and irradiated. The caging group is removed and protein binds within the localized active regions. (d) A substrate is incubated with photoreagents and a protein solution. Upon UV irradiation, the activated photoreagents bind to the substrate and the protein. [86]*

3.2.1. Photoreactive groups

The most commonly used photoreagents are arylazides, nitrobenzyl, and diazirines groups. [12, 86] Upon photolysis at the appropriate UV wavelength, arylazides form reactive nitrenes which rapidly react with double bonds or insert into C-H and N-H sites (Figure 3.3). [12, 86, 89]

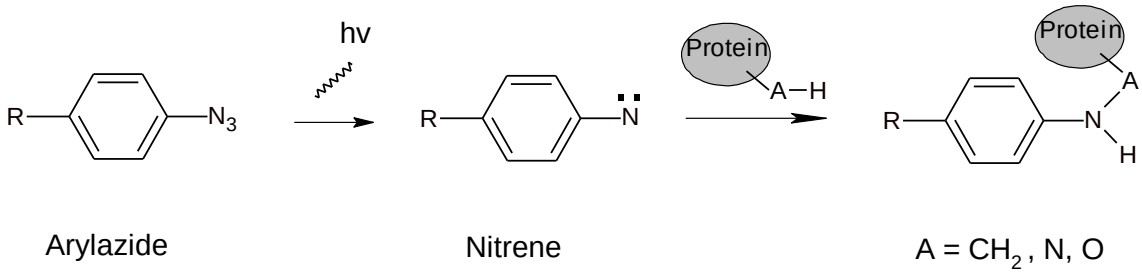

Figure 3.3. *Arylazide chemistry. [90]*

The arylazide chemistry was used by Kannoujia et al. for detection of L-ascorbic acid by ascorbate oxidase immobilized onto polycarbonate strip. Polycarbonate strip was coated with 1-Fluoro-2-nitro-4-azidobenzene (FNAB) which is classified in the group of arylazide photolinkers. Upon exposure to UV irradiation, FNAB transformed to highly reactive nitrene which binds to the polycarbonate surface and forms an activated surface labile fluoro group. After dipping the activated strips into solution containing ascorbate oxidase, the enzymes were immobilized on the strips. [91]

In addition, perfluorophenylazide (PFPA) photochemistry is based on the arylazide chemistry. It has four fluorines on the aryl ring, which improve the efficiency of nitrene insertion into electron rich sites. In a study that was done by Pei et al., PFPA was used both to covalently attach poly(ethylene oxide) (PEO) to amino-functionalized glass slides, and to covalently immobilize carbohydrates to PEO. First a monolayer of PFPA was formed on the surface by treating the amino groups on the array glass slide with N-hydroxysuccinimide-derivatized PFPA (NHS-PFPA). Then the sample was immersed in a solution of PEO and exposed to UV irradiation to attach a thin layer of PEO to the surface, with the same mechanism shown in Figure 3.2 b. Subsequently, PFPA-derivatized carbohydrates were immobilized in an array format on the PEO surface by photoinitiated insertion chemistry. [92]

Nitrobenzyl groups are caging photoreagents that attach to a molecule and prevent its normal activity. The caging group can be broken down upon irradiation of appropriate UV wavelength to a ketone, carbon dioxide and a liberated active molecule (Figure 3.4) [12, 86] Cheng and Cao grafted covalently the photocleavable 4,5-dimethoxy-2-nitrobenzyl chloroformate (NVOC) on primary amines of chitosan substrate. Upon UV illumination through the photomask, the photoactive 2-nitrobenzyl was photocleaved and the protected amine groups were deliberated for further immobilization. The localized active amine groups were first coated with cell repulsive PEG. Then, the rest of the amine groups were liberated by UV irradiation without photomask and subsequently coated with cell adhesive sequence Arg-Gly-Asp-Ser (RGDS). The applied mechanism is same as the third scenario in photochemical protein immobilization (Figure 3.2 c). After 2 days of cell seeding, it was observed that line-patterned of fibroblasts were formed on the RGDS patterns of RGDS/PEG-grafted chitosan films. [93]

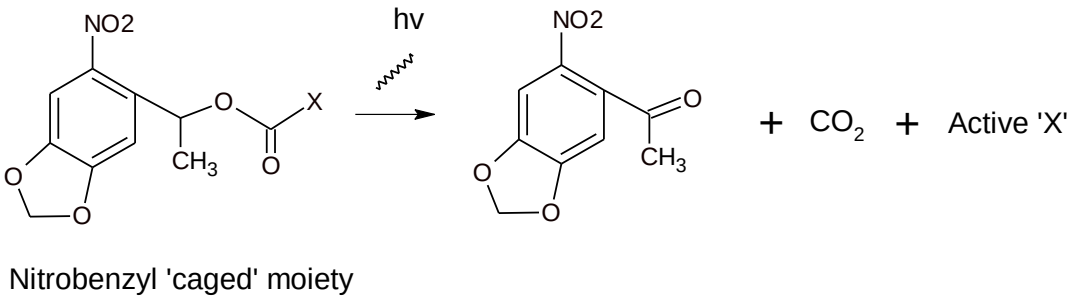

Figure 3.4. *Nitrobenzyl caging chemistry. Upon UV irradiation, ketone, carbon dioxide and the active moiety are formed. [86]*

The other photoreagents are diazirines which form reactive carbenes upon exposure to light. Carbenes react with proteins very rapidly and generate strong covalent links between the protein and the surface (Figure 3.5). [86, 94]

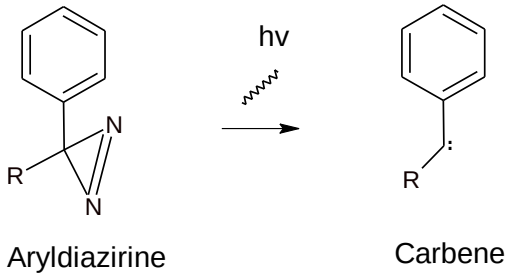

Figure 3.5. *Aryldiazirine chemistry. [86]*

3.3. Chemical modification

Chemical modification is a more stable means of protein immobilization on the substrate compared to physical modification. In this strategy, proteins can be grafted onto the surface covalently with good stability. [4] Zhang et al. immobilized gelatin on PC film through covalent reactions. It was concluded that covalently immobilized gelatin provides higher protein-substrate affinity as well as greater attachment and proliferation of human dermal fibroblasts during 7 days cell culture observation compared with physically coated proteins. [10]

In chemical immobilization, the covalent bond is formed between the molecules of the substrate and the functional groups of proteins. Most commercial polymers must undergo surface pretreatment prior to protein attachment due to their inert nature. [95] In addition, a number of cross-linkers are commercially available to activate the functional groups on the surface for attracting the proteins and covalent coupling reactions between the substrate and proteins. [89]

Proteins are made of long chains of 20 different amino acids. Amino acids consist of amine (-NH_2) group, carboxyl (-COOH) group, a hydrogen (-H) atom and an organic side group (R) attached to the carbon atom. Therefore in proteins, the functional groups such as primary amines (–NH_2), carboxyls (–COOH), sulfhydryls (–SH) account for the majority of crosslinking and chemical modification techniques. Some typical examples of cross-linkers and the available functional groups on proteins are listed in Table 3.1 and the more detailed information about crosslinkers is presented in Appendix 2.

In this study, the methods of carboxyl-group functionalization of the polymeric surface and some amine reactive crosslinkers used in chemical immobilization of proteins are explained. Also at the end of this chapter, some examples related to chemical immobilization of proteins on polymers, using methods similar to the research methods used in this study, are provided.

Table 3.1. *The available functional groups and related amino acids in proteins, and the required crosslinkers used for covalent immobilization. According to [12, 90, 96].*

Functional group on protein	**Amino acids**	**Cross-linkers**
Amine (-NH_2)	Lysine, N-terminus of polypeptide chain	– Carbodiimides – Succinimidyl ester – Aldehydes – Sulfonyl chlorides – Epoxides
Carboxyl (-COOH)	Glutamic acid, Aspartic acid, C-terminus of protein	– Carbodiimides – Succinimidyl ester
Sulfhydryl (-SH)	Cysteine	– Maleimides – Disulfide reagents – Vinyl sulfone

The covalent immobilization is a common approach in biological sensors for immobilization of probes (Deoxyribonucleic acid (DNA) or proteins) on the solid surface, since in this case the sensor can withstand assay protocols more easily without probe loss. [11] In addition, covalent immobilization has been employed in the design of biomedical devices to induce controlled and rapid healing with antimicrobial properties. [97, 98] Zhang et al. immobilized covalently antibiotics and collagen molecules on Ti surface to accelerate the bone healing and to control infection. [13] Also in another application, Wissink et al. immobilized heparin on a non-cytotoxic crosslinked collagen substrate for endothelial cell seeding, inhibition of blood coagulation and consequently improving the blood biocompatibility of synthetic vascular grafts. [99]

3.3.1. Surface pretreatment

In order to covalently immobilize protein molecules on the chemically inert surface of polymeric biomaterials, it is necessary that the polymer first undergo surface pretreatment. Therefore, the reactive groups such as hydroxyl (-OH), carboxyl (-COOH) or amino groups are introduced as coupling sites on the polymer surface prior to protein attachment. [95, 100, 101] There are different approaches to graft the mentioned reactive groups on polymer surface, which are presented in Appendix 3. In this study, the methods of grafting carboxyl groups on the polymeric substrate are briefly introduced.

3.3.1.1 Carboxylated surfaces

By far the most common method to covalently attach proteins to the surface uses the amine groups in the side chain of lysine and the N-terminus of polypeptide chain. [89] For this aim, first the inert surface of polymer must be modified by functional groups to be able to react with proteins. The carboxyl group is one of the common functional groups, which are able to bind with the amine groups of protein. [3] There are various strategies to create carboxyl groups on the substrate (see Appendix 3).

One approach to create carboxylated surface is photo-oxidization and subsequent UV-induced polymerization. This method does not need special instruments and can be performed easily compared to other methods described below. In a study done by Ma et al., first the peroxide groups were introduced onto the PLLA surface by immersing the films in hydrogen peroxide solution under UV irradiation. The peroxide groups were then used to initiate the graft polymerization of poly(methacrylic acid) (PMAA) on PLLA substrate under UV irradiation. Therefore, carboxyl groups were introduced at the chemically inert PLLA surface through UV-induced grafting of PMAA. The hydrophilicity of PMMA-grafted films obviously decreased due to the presence of carboxyl groups compared with the unmodified PLLA films. [100]

The other approach to introduce carboxyl groups on polymer surfaces is plasma treatment with CO_2 or CO. Depending on the substrate, after CO_2 plasma treatment different C and O groups such as hydroxyls, aldehydes, ketones, and esters as well as carboxyl groups could be formed on the surface. [102] In CO_2 plasma treatment of PI film, the imide groups are cleaved to form COOH and amide groups. However, only 4.8 to 7.6 % of the C_{1s} peak accounts for COOH-groups in XPS analysis of gas plasmas including CO, O_2, and CO_2; and the rest of the peak is caused by the carbon atom of polyimide chains [103]. The plasma polymerization using monomers such as acrylic acid (AAc) and propanoic acid also can create carboxyl densities as high as 15 to 20.5 % of the C_{1s} peak. [102]

In order to increase the specificity and density of carboxyl groups, instead of a single step plasma polymerization, two-step process including plasma treatment and post-plasma grafting by chemical reactions have been investigated. [102] The plasma treatment using inert gas such as argon (Ar), causes changes to a limited depth (several molecular layers) without changing the bulk properties and creates peroxide groups on the

surface of polymers. [3, 101] The radicals or peroxide groups can also be produced by ozone oxidation, gamma irradiation, electron beam or laser treatment. [3, 101] Then the proxide groups are used for radical grafting with COOH- terminated compounds such as AAc [104], succinic anhydride [13, 102], PMAA [101] and β-propiolactone [102]. AAc is commonly used in grafting of carboxyl groups on the surface. The carbon-carbon double bond in the structure of AAc binds easily with the polymers, while the chemical and physical properties of polymers are intact. [3] The amount of carboxyl groups grafted on the surface is affected by several parameters such as plasma power, plasma exposure time, concentration of AAc, reaction temperature, and reaction time. [15, 16, 102]

In a study done by Ying et al., poly(ethylene terephthalate) (PET) films were pre-treated with Ar plasma. Then the carboxyl groups were grafted onto the films by UV-induced graft copolymerization of AAc. According to the results, the concentration of the surface-grafted carboxyl groups increased significantly at AAc monomer concentrations above 2 wt%. [2] The same method was also applied on ultra thin PCL films for AAc graft polymerization. The amount of AAc grafted on film increased as the concentration of AAc monomer solutions increased in the range of 3-9 %. [3]

The carboxyl groups could be grafted also by subsequent thermal-induced polymerization; However, this method takes more time compared to UV-induced graft copolymerization. [16, 105-107] Gupta et al. used Ar plasma treatment and subsequent thermal-induced graft polymerization to introduce carboxyl groups to PET films. The longer plasma exposure time showed higher AAc grafting. The degree of grafting at different plasma exposure time increased with the increase in reaction time and reached saturation at 6 h in each case. The study was carried out from 30 °C to 70 °C and degree of grafting showed higher values at reaction temperature of 50 °C. It was also observed that grafting density sharply increased at a monomer concentration of 20 % until it reached a maximum at 40 % AAc monomer concentration (Figure 3.6). This increase was caused due to the accessibility of the monomer to the primary radicals. Beyond 40 % monomer concentration, the extensive homopolymerization and the resultant increase in viscosity of grafting medium hindered the diffusion of the remaining monomers to the propagating sites. Therefore, the degree of grafting decreased with further increase in monomer concentration and gel formed beyond 50 % monomer concentration. [15, 16]

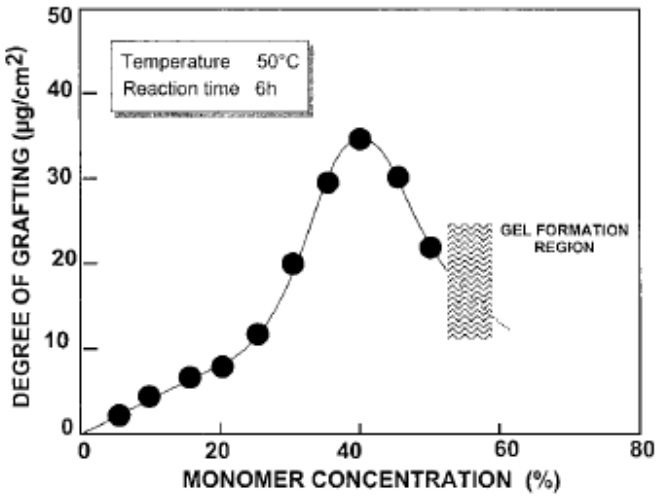

Figure 3.6. *Variation of the degree of AAc grafting with AAc monomer concentration. The AAc grafting was done at 50 ℃ for 6 h. [15]*

3.3.2. Amine-reactive cross-linkers

After the creation of carboxylated surface, the carboxyl groups on the surface will be activated by crosslinkers. Then the active sites are generated, where the protein molecules can be immobilized through their amine groups. This section will focus on the most common amine-reactive crosslinkers, i.e., carbodiimides (EDC or EDAC) and N-hydroxysuccinimide (NHS).

3.3.2.1 Carbodiimides

EDC or EDAC affect conjugation of carboxyl (-COOH) groups on the polymer surface to primary amines of proteins ($-NH_2$). They are zero-length crosslinkers since they do not become part of the final crosslink between the reacting groups. EDC react and activate the OH group of carboxylic acid to form an active intermediate O-acylurea (Figure 3.7 part 1). This intermediate can directly react with amines to produce peptide bond (Figure 3.7 part 2). The generated O-acylurea is unstable in aqueous medium and the failure to react with amines results in hydrolysis and formation of a byproduct N-acylurea, which is unreactive with amines (Figure 3.7 part 3). Also, the O-acylurea can react with a neighboring carboxyl group and yield an anhydride product at the surface with the release of the urea (Figure 3.7 part 4). [11, 89, 90, 108, 109] NHS crosslinker could be included in EDC coupling protocols to create a more stable amine-reactive intermediate and to reduce the hydrolysis of the O-acylurea.

In EDC coupling protocols, the crosslinking is performed at a pH between 4.5 to 7.5; even though, reaction conditions of pH 4.5-5 are generally recommended. [14, 89, 94] Tris, glycine and acetate buffers should be avoided as they react with the crosslink-

ers. In addition, phosphate buffers reduce coupling efficiency and the carbodiimide concentration should be increased in this case. [108]

The activation of surface-bound carboxylic acids with EDC in aqueous media is complete within 0.5-2 h at pH 4-6, at 0-5 °C. whereas, the reaction of carbodiimides with amines is slow compared to reaction with acids. Also, the coupling in buffered media takes 12-24 h at pH 5-7, at 0-10 °C. [109]

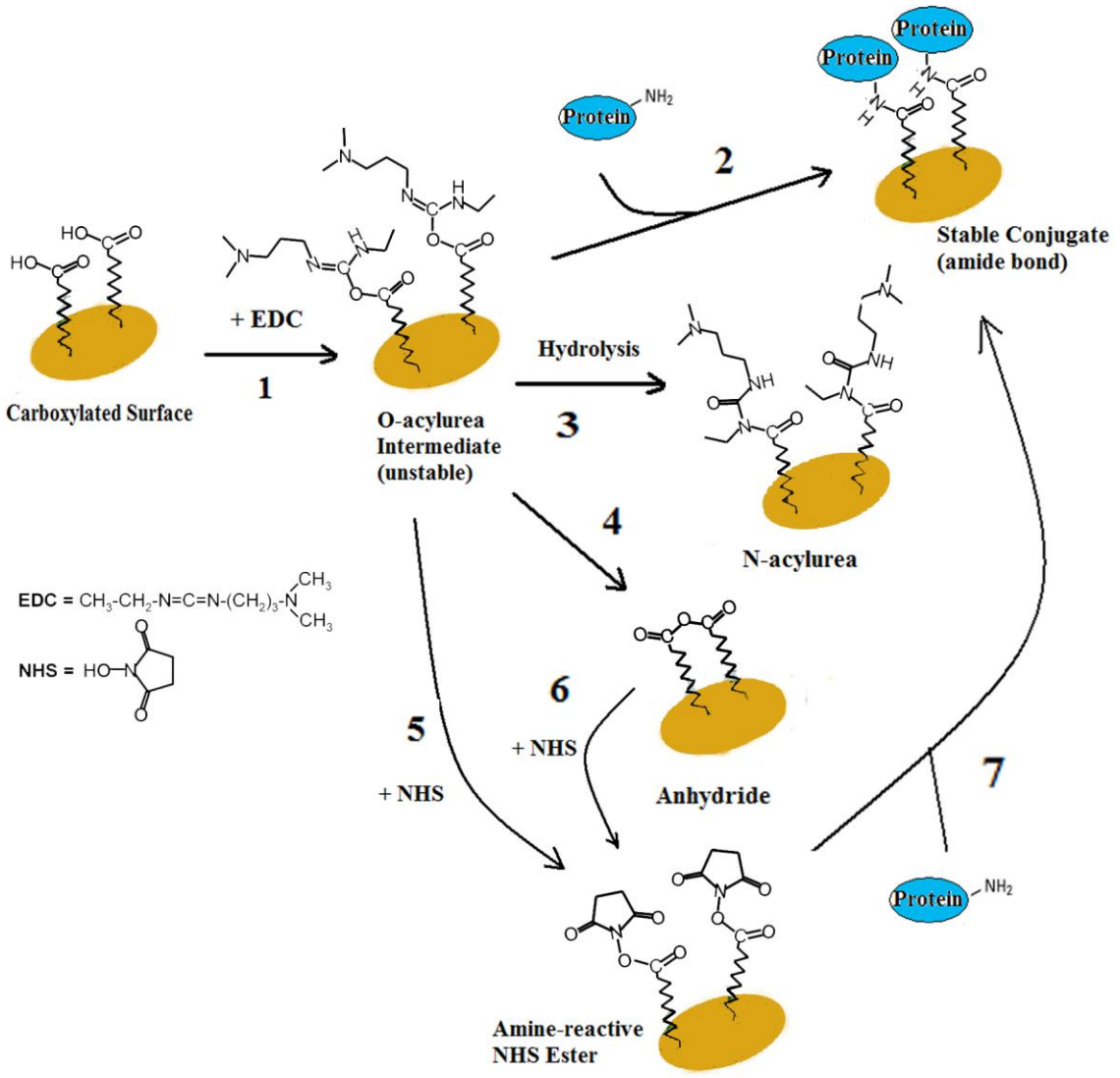

Figure 3.7. *Scheme of the NHS/EDC activation reactions. At the first step (reaction 1), the EDC interact with carboxyl groups on the substrate which results in the formation of O-acylurea. Subsequently, various paths (reactions 2-5) account for the experimentally detected products (peptide bond, urea, anhydride, succinimidyl ester). The kinetic competition between the various paths determines the final surface composition. Drawn according to [11, 94].*

3.3.2.2 N-hydroxysuccinimide esters

Succinimidyl ester (-COOSuc)-terminated surface layer is the most commonly used for coupling with protein amine groups. The reaction between the protein's amine groups and the -COOSuc surface forms strong covalent peptide bonds. [12, 96] In most cases, the -COOSuc surface is obtained by reaction of a surface bearing carboxyl end groups with NHS, in the presence of carbodiimides. [10, 13, 99, 110] This reaction is often referred to as surface "activation". In this reaction, the carboxyl groups on the surface react with EDC, resulting in O-acylurea; Then the NHS react with O-acylurea to form amine-reactive succinimidyl esters (NHS-esters) on the surface with the release of urea corresponding to the initial carbodiimide reactant (Figure 3.7 part 5). The NHS can also react with anhydride to yield amine-reactive NHS-esters (Figure 3.7 part 6). [11] Compared to O-acylurea, the NHS-esters are more resistant to hydrolysis with the half-life measured in one to several hours (at pH 7.0-7.5) and even days depending on temperature and pH. [89, 108] In the presence of amine groups, NHS esters irreversibly form the amide bonds, and the NHS is released in the medium (Figure 3.7 part 7) [90].

Coupling efficiency depends on several parameters, i.e., pH value, reactant concentration, reaction time and temperature. [11, 12] The NHS ester is more reactive and stable towards hydrolysis at neutral pH in phosphate-buffered saline at RT for 30 min to 2 hours. [12, 14] The reaction times at lower temperatures should be increased to give similar results. [14, 100]

The concentration of NHS and EDC vary from one study to another from a few 0.1 M down to the mM range. [11, 111, 112] Sam et al. activated the carboxyl groups grafted on porous silicon layers by EDC and NHS in cold water. As can be seen in Figure 3.8 and 3.7, when [NHS] > [EDC], due to the fast kinetics of reactions 5 and 6, slow succinimidyl ester formation takes place. Therefore, the unreacted acid groups remains at the surface (zone 1). Conversely, when [EDC] > [NHS], the kinetics of reactions 5 and 6 are slow. Anhydride and urea are therefore formed as the byproduct of reactions 3 and 4 and again the surface activation is incomplete (zone 3). When [EDC] and [NHS] are both high, the surface concentration of O-acylurea reaches a significant level which is consumed by reactions 3 and 5 (likely nominated by reaction 3 and yield the generation of high amount of N-acylurea at the surface) (zone 2). The optimal concentration of NHS and EDC for the activation of carboxylic acids was found at the center of graph in the range of 5mM < [EDC] ~ [NHS] < 10mM. [11, 109]

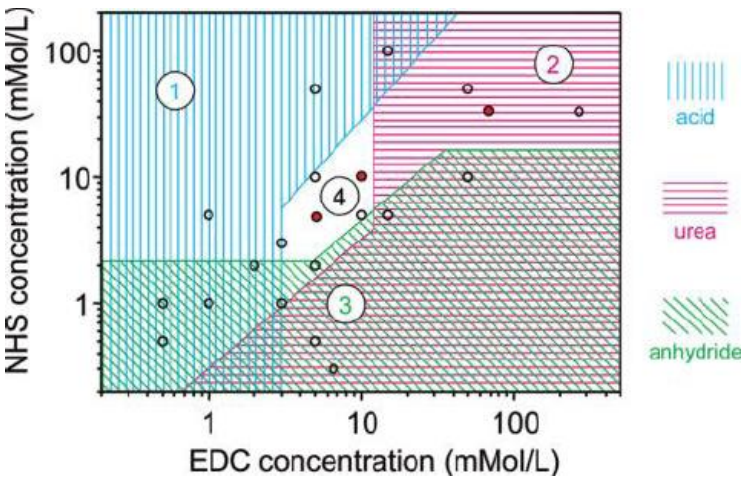

Figure 3.8. *The influence of EDC and NHS concentration on the chemical composition of the surface after activation. The boundaries of the zones are approximately drawn from the shape of the experimental infrared spectra. [11]*

3.3.3. Chemically immobilized proteins

There are various biomolecules covalently immobilized on the carboxyl grafted surface using amine-reactive crosslinkers. Zhang et al. studied the effect of Ti surface modification on collagen immobilization and fibroblast proliferation. The Ti surface was first coated with 2-hydroxyethyl methacrylate (HEMA) chains and then the pendant hydroxyl end groups of grafted HEMA chains were subsequently converted into carboxyl groups. It was observed that the surface density of collagen on Ti-grafted HEMA polymer with carboxyl groups were higher than surfaces-grafted HEMA polymer without carboxyl groups. In addition, due to the high amount of collagen immobilized on these substrates, the cell density was higher after 2 days of 3T3 fibroblast cell culturing. [13]

Gupta et al. studied collagen immobilization on the surface of AAc-grafted PET. It was observed that in the absence of crosslinkers such as EDC or NHS, some deprotonated carboxylic acid functions interacts with positively charged protonated amines on the collagen to form an ionically crosslinked surface. As collagen is not covalently bonded to the surface, after washing only 50 % of the collagen remained on the surface. Also due to the weak interaction with the surface, the collagen might interact with cell culture medium proteins and be replaced by other serum proteins. [106, 107]

Ying et al. studied the galactose ligand immobilization on AAc-grafted PET film. The surface carboxyl groups were activated by EDC and NHS. The amount of immobilized galactose ligand increased with the surface graft concentration of the AAc polymer. After 4 days of culture, the modified surfaces with a high galactose concentration allowed efficient hepatocyte attachment, resulting in formation of large aggregates or spheroids. However, the hepatocytes maintained the characteristic monolayer morphology on collagen-coated PET. [2]

Cheng et al. immobilized the collagen on AAc-grafted PCL film using EDC crosslinker. According to XPS spectra results, the graft collagen concentration on the surface, expressed as the [N]/[C] ratio, increased as the concentration of AAc monomer solutions increased. Also the number of human dermal fibroblasts on collagen coated film increased with culture time during 8 days, while only a few cells were observed on the unmodified PCL film at day 8. [3] Lee et al. also found that the amount of immobilized collagen on AAc-grafted silicone rubber membrane is dependent on the immobilization time. It was observed that the concentration of immobilized collagen increases with time and then it levels off beyond 24 h (Figure 3.9). [105]

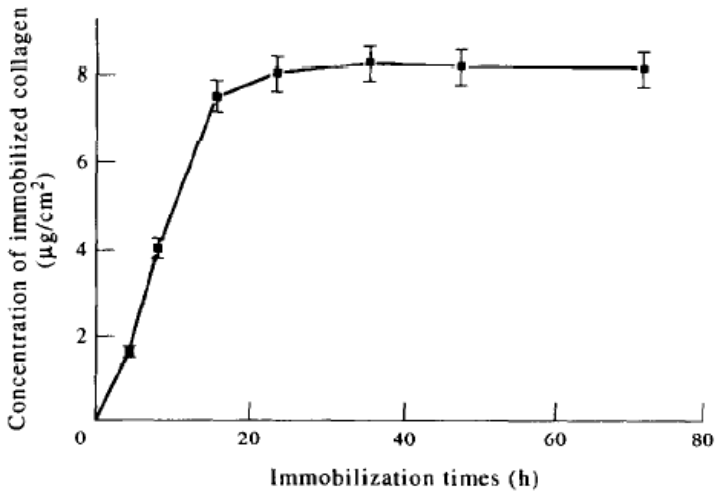

Figure 3.9. *The effect of immobilization time on the collagen concentration coated onto the silicone rubber membrane. [105]*

Xia et al. studied the gelatin immobilization on AAc-grafted PLLA. It was shown that the surface density of gelatin on AAc-grafted PLLA, measured by rhodamine-carboxyl interaction method, was significantly higher than that on PLLA. This implies the advantage of covalent immobilization over physical coating. The gelatin on either PLLA or AAc-grafted PLLA did not show significant loss after seven-day immersion in PBS. However, in the presence of enzymes and different pH values, the physically absorbed gelatin might be less stable. The adhesion and spreading of human umbilical vein endothelial cells improved significantly by gelatin-modified PLLA. [104]

Collagen crosslinking via EDC/NHS chemistry has been shown to yield biocompatible materials both in contact with endothelial cells and in subcutaneous implantation in rats. [113] Fitzpatrick et al. also studied the grafting of amine-terminated PNIPAAm chains to carboxylic acid groups on the backbone of type I bovine collagen by EDC/NHS chemistry. The produced scaffold was intended to use as vehicle for transplantation of RPE cells to subretinal space. The crosslink between the collagen and the polymer did not yield toxic material. Also viability of human RPE cells was high on days 4, 7, and 14 when seeded within 3D matrix of scaffold. [61]

EXPERIMENTAL PART

4. MATERIALS AND METHODS

4.1. Materials

The track etched polyimide membrane (ipCELLCULTURE™) was supplied by it4ip s.a.; (Seneffe, Belgium, Ref 300M25/721M103/25). The membrane was 25 mm in diameter, 24 µm in thickness, with the pore size of 1 µm. It was made from Kapton-like type H PI films. The chemical structure of kapton-H polyimide is shown in Figure 4.1. The PI membranes were sterilized by autoclave (cycle ca. 1.5 hours, 121 °C, and dry program) prior to use in cell culture studies.

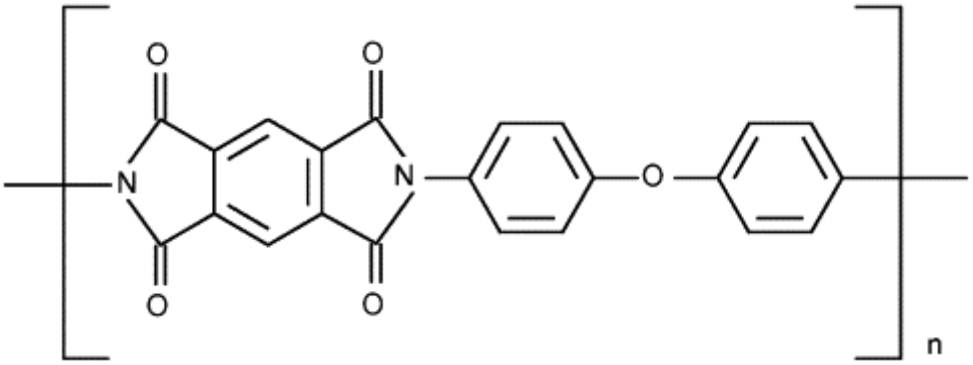

Figure 4.1. *The molecular structure of repeating unit of kapton-H polyimide. [114]*

The non-porous PI membrane was also supplied by it4ip s.a.; (Seneffe, Belgium, Ref 3000M25/000N003/00). The membrane was 24 µm in thickness. The process of production and treatment of both porous and non-porous membranes were same.

Deionised water was used as solvent in solutions. Otherwise, it is mentioned in the text. The chemicals used in the steps of protocol are listed below:

- Aqueous acrylic acid (99 %, Sigma Aldrich)
- Toluidine Blue O (dye content~80 %, Sigma Aldrich)
- Sodium hydroxide (NaOH) (99 %, Merck (Darmstadt, Germany))
- Acetic acid (CH_3COOH) (99 %, J.T.Baker)
- Sodium chloride (NaCl) (99.5 %, J.T.Baker)
- Potassium chloride (KCl, J.T.Baker)
- Potassium dihydrogen phosphate (KH_2PO_4) (99 %, J.T.Baker)

- Sodium hydrogen phosphate anhydrous (Na_2HPO_4, J.T.Baker)
- N-hydroxysuccinimide (NHS) (98 %, Sigma Aldrich)
- N-(3-dimethylaminopropyl)-N-ethylcarbodiimide hydrochloride (EDC) (crystalline, Sigma Aldrich)
- Type IV collagen from human placenta (Sigma Aldrich)
- Dulbecco's phosphate buffered saline without Ca and Mg 10×DPBS (Lonza, Belgium)
- The medium consists of couple of components:
    - Fetal bovine serum (Sigma Aldrich)
    - Glutamax and F12-medium (Life Technologies)
    - Pen/strep (Fisherscientific)

4.2. Surface modification

In this study, the carboxyl groups were grafted on the surface of PI membrane. Then, the collagen type IV was covalently immobilized on PI membrane surface by means of crosslinkers.

The surface modification protocol of PI membrane is illustrated in Figure 4.2. Four steps are involved in this protocol, presented in more details in the following subchapters: (1) argon plasma pretreatment, (2) AAc graft polymerization, (3) surface activation and (4) collagen immobilization. Plasma treatment, carboxyl functionalization of substrates, surface activation and collagen immobilization were carried out under clean room conditions for cell culture studies. No sterilization was applied on membranes prepared for surface characterization.

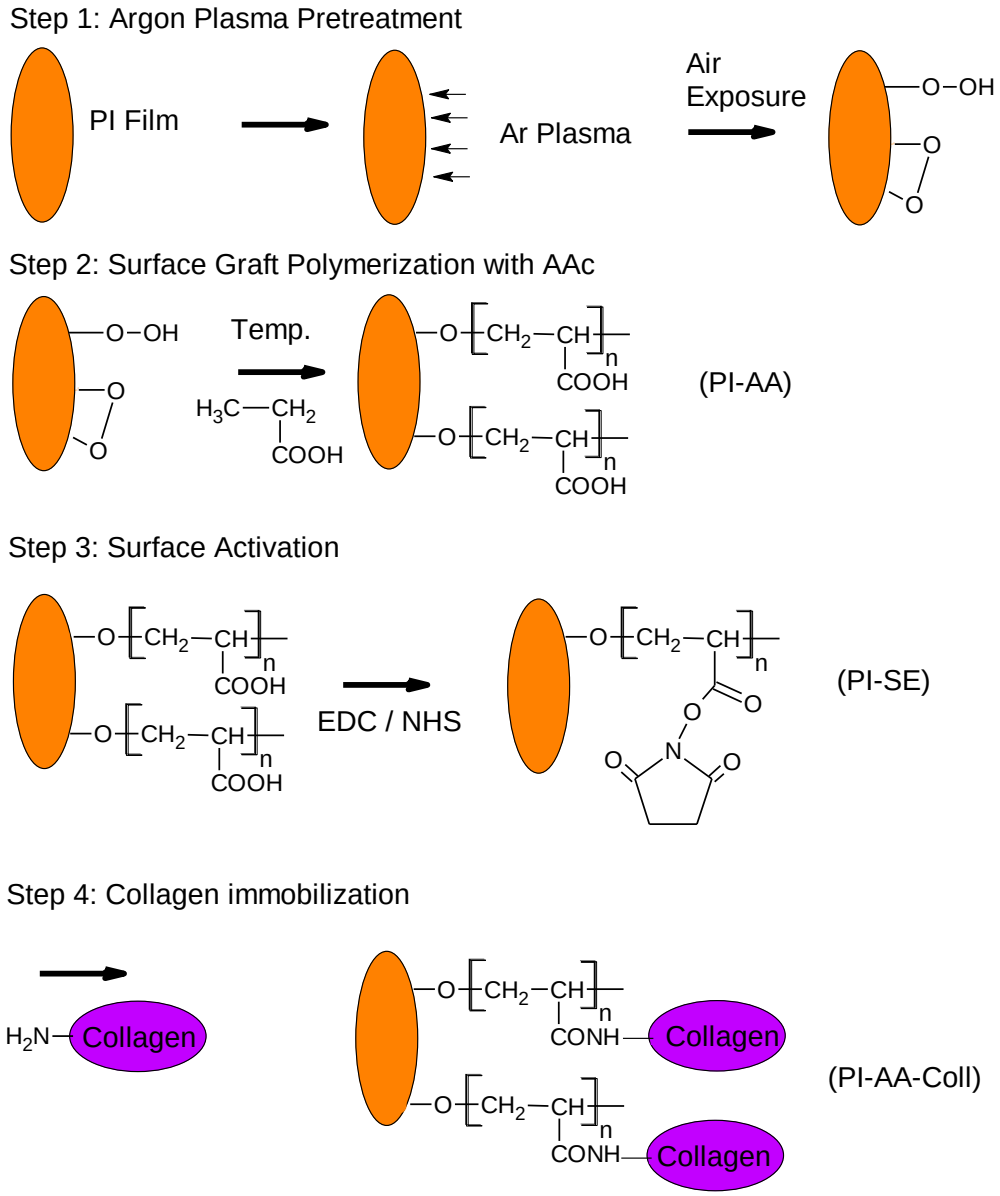

Figure 4.2. *Schematic representation of the processes of thermal-induced AAc grafting and collagen immobilization.*

4.2.1. Argon plasma pretreatment

PI membranes were pretreated with Ar plasma (Vision 320 MK II RIE, Advance Vacuum, Sweden) before the thermal-induced graft polymerization of AAc. In order to remove any impurity from the chamber, the chamber was first cleaned by oxygen (O_2) plasma treatment for 2 min at O_2 pressure of 30 mTorr, with flow rate of 30 sccm and plasma power of 30 W (recipe GC version 1.00).

For Ar plasma treatment, the membranes were fixed in CellCrown^{TM} 12 inserts (Scaffdex, Finland) and then placed inside the chamber for 60 s at an Ar pressure of 250 mTorr and flow rate of 100 sccm. The plasma power was kept at 60 W at a radio frequency of 13.6 kHz. After plasma treatment, the membranes were taken out from the reactor into the air and preserved in a desiccator containing dry air at atmospheric pressure and RT for 20 min. The whole process facilitates the formation of surface peroxides and hydroperoxides, which were used for subsequent AAc grafting. Parameters used in plasma treatment are based on the existing literature. [17-21]

4.2.2. Acrylic acid graft polymerization

Acrylic acid graft polymerization was immediately performed after peroxide formation onto the surface. Ar plasma treated PI membranes were placed in the bottom of 12-well plate. The membranes were still fixed in the CellCrowns^{TM} to keep the AAc solution on the shining side of the membrane inside the CellCrown^{TM}, and to prevent the spreading of AAc solution between the well and the lower surface of the membrane. The CellCrowns^{TM} were sterilized by immersion once in 70 % and 90 % ethanol (5 min each) for cell culture studies.

Graft polymerization of AAc onto the plasma treated PI membranes was carried out under nitrogen (N_2) atmosphere inside the chamber modified of the pressure cooker (Figure 4.3). The head of pressure cooker is connected by a tube to the N_2 tank. When the ball valve is open, the N_2 spreads into the chamber with 362 Torr pressure and fills the space. Then, the pressure inside the chamber increases and the pressure regulator allows the excess pressure to be released out. The N_2 insertion is repeated several times for an appropriate time depending on the amount of solution added on the membrane. As a result, the O_2 molecules inside the solution diffuse out to the chamber cavity and the air inside the chamber is replaced by N_2.

Figure 4.3. *The chamber modified of the pressure cooker used in this study to remove the O_2 molecules from solutions.*

For AAc graft polymerization, the membrane was covered by 1 ml of AAc solution of predetermined concentrations (25 % and 35 %) inside the CellCrown^{TM}. N_2 was inserted into the pressure cooker for 30 min to remove oxygen from the solution and the whole system. The pressure cooker was subsequently placed in an incubator (Termaks INCU 4) maintained at 60 °C for 6 h. After one hour, the amount of solution on the films was checked and then the N_2 was inserted to the pressure cooker for 2 min. After the second hour, again the amount of solution was checked and 500 µl of AAc solution was added to each sample and N_2 was inserted for 15 min. On the fourth hour, the sample was checked again, the amount of solution on the membrane was enough, the N_2 was inserted for 2 min and the process stopped after 6 h. In general, adding 1.5 ml of AAc solution on the membrane inside the CellCrown^{TM} and 1 ml of AAc solution outside the CellCrown^{TM} would be enough to have solution on the membrane for the mentioned period of AAc graft polymerization at 60 °C. The added solution outside the CellCrown^{TM} prevents the flow of solution from inside the CellCrown^{TM} to outside. Parameters used in AAc graft polymerization are based on the existing literature. [2, 15, 16] For cell culture studies, AAc solution was added to the samples through a 0.2 µm filter (Whatman$^{®}$, Germany).

After graft copolymerization, the AA-grafted PI, termed as PI-AA (25 %) or PI-AA (35 %) (depending on the monomer concentration used for grafting) was removed from the reaction mixture and washed with copious amounts of deionized water for 24 h to remove the residual homopolymer adsorbed on the surface. The films were dried in desiccator containing dry air for later surface characterization and/or collagen immobilization.

4.2.3. Dulbecco's phosphate buffered saline

Dulbecco's Phosphate Buffered Saline (DPBS) was used in this study. It was prepared at RT according to the formula presented in Table 4.1. The solution was stirred overnight and the pH was adjusted to 7.3-7.7 at RT by Na_2HPO_4. Then, the DPBS was stored in refrigerator (+ 2 °C) for maximum 1 month. [115] The DPBS was sterilized by autoclave (cycle ca. 20 min, 121 °C, and steam program) prior to use in cell culture studies.

Table 4.1. *Required materials for preparation of 1 liter of DPBS. [115]*

Material	**Abb.**	**Weight (g)**
Potassium chloride	KCl	0.2
Potassium dihydrogen phosphate	KH_2PO_4	0.2
Sodium chloride	NaCl	8
Sodium hydrogen phosphate anhydrous	Na_2HPO_4	1.15

4.2.4. Stock solution of collagen IV

A stock solution of collagen IV was prepared in sterile 0.5 M acetic acid into concentration of 1 mg/ml. The stock solution was occasionally swirled for 4 h at 2 °C in refrigerator. Then, it was divided into 45 sterile containers and they were stored at - 20 °C before using. The mixing and division processes were done under laminar hood. Also, deionized water and all the dishes were autoclaved before use.

4.2.5. Collagen immobilization

2.9.2.1. Surface activation

10 mM EDC/NHS solution was prepared in DPBS. 1.5 ml of solution was added on PI-AA (25 %) membrane fixed in CellCrown^{TM} and 1 ml outside the CellCrown^{TM}. For cell culture studies, the solution was added to the samples through a 0.2 µm filter. The solution was deoxygenated for 15 min. The membranes were soaked in solution at RT with occasionally shaking manually for 1 h, leading to succinimidyl esterification of the carboxyl groups on PI-AA (25 %). Then, the membranes were rinsed with DPBS for two times and went to next step for collagen immobilization. Also, number of the membranes were dried under the stream of N_2 and stored in the refrigerator for surface char-

acterization. The resulting films are designated as PI-SE. The parameters are based on the relevant articles. [3, 10-14]

2.9.2.2. Collagen immobilization

The amount of stock solution per one insert (V_s) was calculated considering the exposed surface area of the CellCrown^{TM} (1.54 cm^2), the concentration of collagen in stock solution (C_s), and the desired amount of collagen on the surface (C_d, 5 µg/cm^2).

$$V_s = (C_d / C_s) * \text{Surface area} \quad (1)$$

According to the equation 1, the amount of stock solution per insert is 7.7 µl. Therefore, 8 µl of collagen IV stock solution was diluted in 492 µl of DPBS and mixed well by vortex and pipetting up and down for several times. Then, it was added on the PI-SE membrane fixed with the CellCrown^{TM} inside the well plate. The linking reaction was performed at + 2 °C for 24 h. After incubation, the films were washed twice with DPBS to remove any remaining of the acetic acid. The resulting films, called PI-AA-Coll, were stored in a refrigerator before characterization.

4.3. Preparation of reference samples

The reference samples were prepared by traditional dipping method. This method is commonly used when culturing cells on the substrates [60, 72]. The PI membranes were fixed in CellCrown^{TM} 12 inserts. According to the surface area of the CellCrown^{TM}, 8 µl of collagen IV stock solution was mixed well with 492 µl of PBS solution. Then the dilution was applied on a PI membrane placed on the bottom of each well plate. The plate was carefully swirled so that the coating dilution is distributed evenly and the membranes were incubated at 4 °C for 24 h [105]. After incubation, the membranes were washed twice with PBS (5 min) to remove any remaining of the acetic acid. The resulting films, designated as PI-Coll, were stored in a refrigerator before surface characterization.

4.4. Surface characterization

4.4.1. Surface density of carboxyl groups

The number of carboxyl groups on PI-AA membranes introduced on PI membrane in AA graft polymerization step was determined by a colourimetric method using Toluidine Blue O (TBO). TBO can combine with a carboxyl group in alkaline solution to form a stable electrostatic complex which can be detached from the surface in acetic acid or other organic solvents, as shown in Figure 4.4.

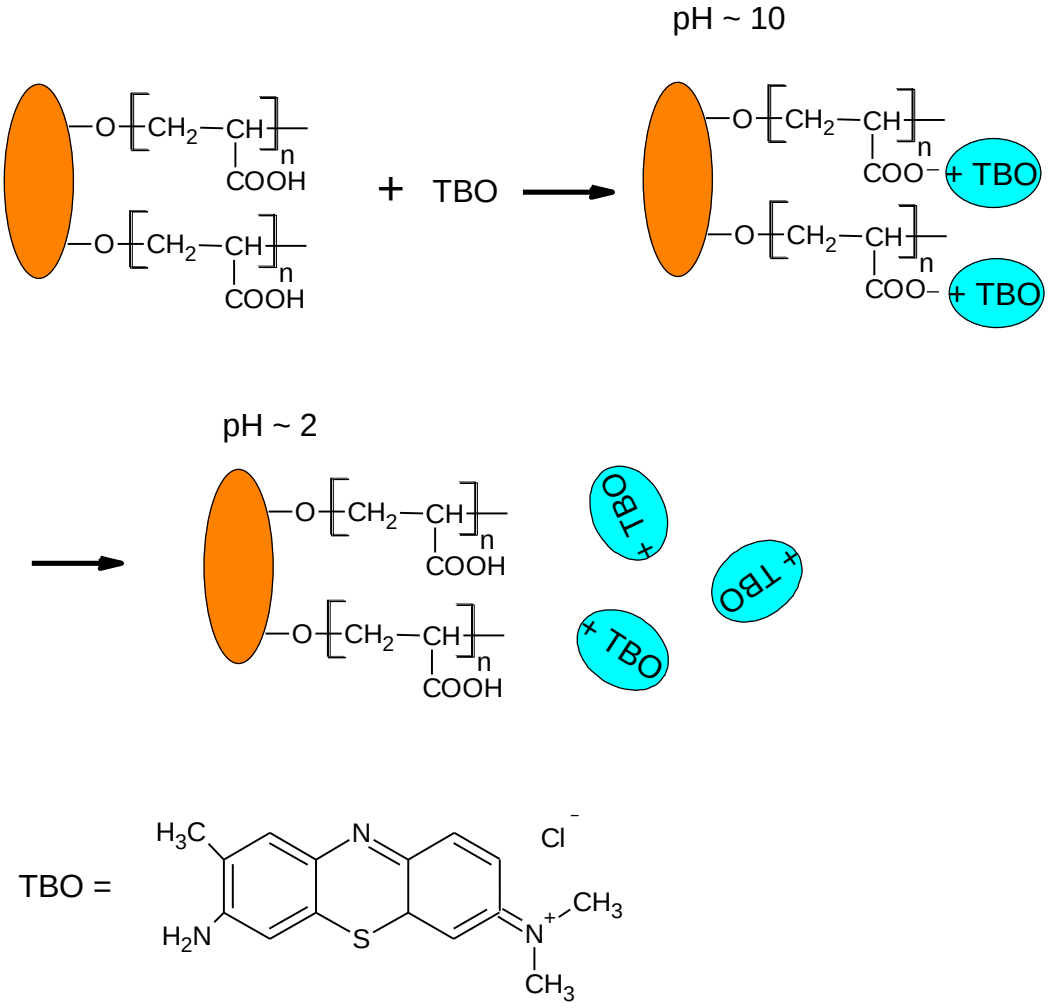

Figure 4.4. *Quantitative analysis of COOH-groups on PI surface. In basic solution (pH ~ 10), a complex is formed between positively charged TBO and –COO⁻, while in acidic solution (pH < 2), the TBO molecules are released from the surface. Drawn according to [101].*

One sample from each membrane (unmodified PI, PI-AA (25 %), PI-AA (35 %)) was used in the analysis of carboxyl surface functionality. The membrane was cut into one-quarter pieces and the test was repeated for two pieces in each case. The 0.5 mM TBO solution was prepared with 0.1 mM NaOH solution (pH 10). Then, 3 ml of solution was added to each PI-AA membrane. The formation of ionic complexes between the COOH-groups of the grafted pAAc chains and the cationic dye was allowed to proceed for 6 h under constant agitation at 37 °C in a shaker. The membrane was subsequently removed and thoroughly rinsed with an excess amount of fresh NaOH solution (pH~9) to wash away the unbound dye molecules.

After thorough rinse, the reacted surface was placed in 3 ml of 50 % acetic acid solution for 30 min at 37 °C while stirring. During this step, the TBO molecules bound to

the acidic groups of PI-AA film were eluted from the analyzed surface and diffused into solution, coloring it blue. The light absorbance of the solution was measured at 634 nm wavelength on a Unicam UV 540 UV/VIS Spectrophotometer (Thermo Spectronic, Cambridge, England).

The number of reactive carboxyl groups on the membrane was calculated from a calibration curve (concentration versus absorbance) of TBO, with the assumption that 1 mol of TBO combine with 1 mol of the carboxyl groups of the AAc-grafted polymer. Therefore, the surface concentration calculations were performed by using the formula (2):

$$\rho_A\ (\mu g/cm^2) = C_{TBO}\ (mmol/l) \times V_d\ (ml) \times M_{w\ (TBO)} / A_d\ (cm^2) \qquad (2)$$

where

ρ_A = surface density of carboxyl groups
C_{TBO} = concentration of TBO
V_d = desorbing volume (3.0 ml)
A_d = desorbing area of PI membrane (0.385 cm^2)
$M_{w\ (TBO)}$ = molecular weight of TBO (305.83 g/mol)

The test was repeated one more time where in second test, another one-quarter of same membranes were tested to check the accuracy of the assay. The absorbance of unmodified PI film was measured as background control once. Parameters used in TBO test are based on the existing literature. [2, 15, 16, 101, 116]

To construct the carboxyl quantification calibration curve, TBO solutions of 0.0025, 0.005, 0.0075, 0.01, 0.0125, 0.015, 0.0175, 0.02, 0.0225, 0.025 mM concentrations were prepared by dissolving the dry TBO powder in 50 % acetic acid at pH 1.36. Then, the optical density of TBO solutions was measured at 634 nm by UV/VIS Spectrophotometer.

Carboxyl quantification calibration curve

Figure 4.5 shows the light absorbance of solutions containing a known amount of TBO at a 634 nm wavelength and a path length of 1 cm. The experimental data were best fitted to a linear plot (3):

$$y = a \times x + b \qquad (3)$$

where y is the absorbance, a and b are constants, and x is the concentration of TBO in the solution. The values of a and b are equal to 76.817 and 0.0004, respectively. Therefore, the equation of calibration curve is as follow:

$$y = 76.817\ x - 0.0004 \qquad (4)$$

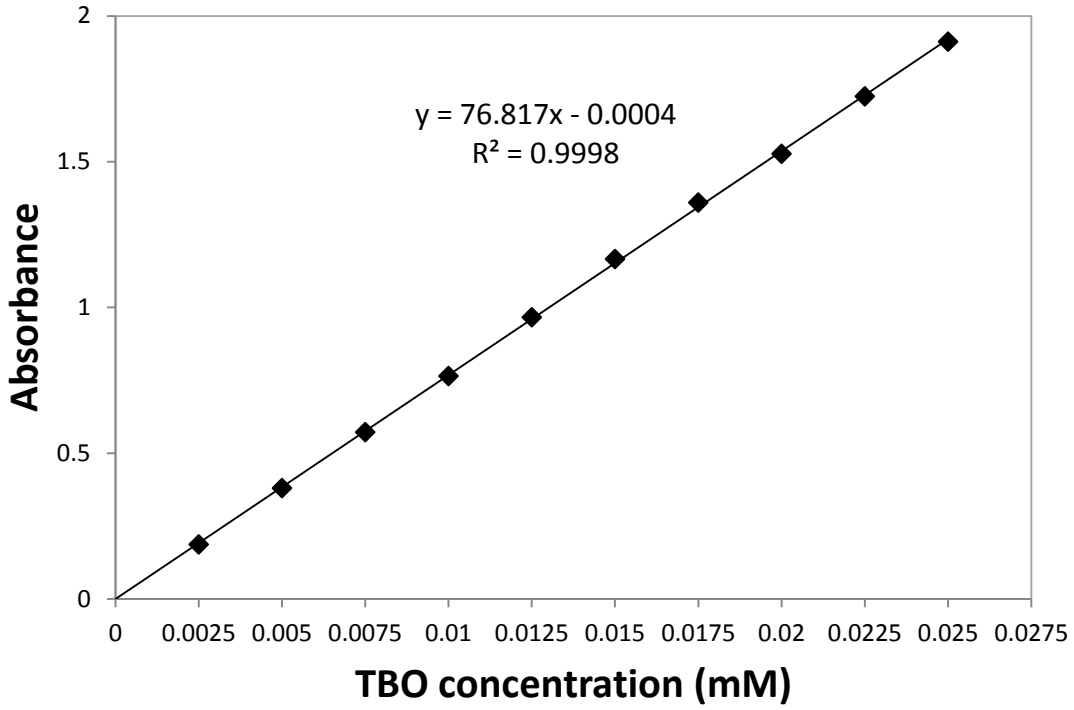

Figure 4.5. *Calibration curve for the concentration of TBO dye using optical density at 630 nm wavelength and 1 cm path length. Linear fit is shown for the experimental data.*

4.4.2. Contact angle measurements

The surface wettability of plasma treated PI, PI-AA, PI-SE, PI-AA-Coll and PI-Coll membranes was measured at RT using a theta optical tensiometer (Biolin Scientific). A water droplet was placed on the dry membrane surface, photographed exactly at the time of water contact with surface and digitized. However, the membranes have pores on the surface so that after dropping the water on the surface the water penetrates the membrane just in few seconds. Therefore, the water contact angle were measured on non-porous PI membranes at the time that water droplet stabilizes on the surface. To measure the contact angle, a tangent was applied at the spot where the drop met the surface of the substrate. The resulting angle indicates the degree of hydrophobicity of the substratum where an angle below 90° signifies hydrophilicity and obtuse angle signifies hydrophobicity [117].

The measurements on the membranes were carried out 5 days after collagen immobilization for two times. For each membrane reported, the measurements are made at one part of the membrane (6 mm diameter) with deionised water.

4.4.3. Atomic force microscopy

The surface morphologies of unmodified PI and PI-AA membranes were characterized using atomic force microscope (XE-100, Park Systems Corp, USA). In each case, an area of 1 μm^2 was scanned in non-contact mode, under air, and at RT. The probe was supported on an APPNANO^{TM} AFM cantilever (Type: ACTA, L: 125 µm, tip-radius: < 10 nm, f = 200-400 kHz, spring constant: 25-75 Nm^{-1}; coating aluminium). The scan rate was 1 Hz. The surface roughness average (R_a) was calculated from the roughness profile determined by AFM with XEI image processing software (Park Systems).

4.4.4. Attenuated total reflectance-Fourier transform infrared (ATR-FTIR) spectroscopy (measurements)

ATR-FTIR measurements of unmodified PI, PI-AA, PI-SE, PI-AA-Coll were carried out using a FT-IR Spectrometer (Perkin Elmer Instruments, Spectrum One, USA). The samples were analyzed in the reflectance mode in the range of 650-4000 cm^{-1}. For each spectrum obtained, a total of 8 scans were accumulated at a resolution of 4.00 cm^{-1}.

4.4.5. Immunostaining and fluorescence microscopy

After collagen immobilization, the PI-AA-Coll and PI-Coll membranes were cut into disks (6 mm diameters) with punch, placed in 96-well plate and washed 2 times with DPBS (5 min) at room temperature. Samples were blocked with 10 % normal donkey serum (NDS, Merck Millipore) and 1 % albumin from bovine serum (BSA, lyophilized powder, ≥ 96 %, Sigma Aldrich) in DPBS for 45 min at RT to minimize background signal. The membranes were rinsed once with DPBS containing 1 % (m/v) NDS and 1 % (m/v) BSA. Collagen IV Ab-3 (Clone PHM-12+CIV 22) mouse monoclonal antibody (Thermo scientific) was diluted (1:100) in DPBS containing 1 % (m/v) NDS and 1 % (m/v) BSA. Then, each sample was incubated in 100 µl of primary antibody dilution for 1 hour at room temperature. The membranes were washed three times (5 min) with DPBS containing 1 % (m/v) BSA. Then, 100 µl of Alexa Fluor® 568 goat anti-mouse IgG (H+L) (Invitrogen/Life technologies) diluted in 1 % BSA/ DPBS (1:800) was added to each membrane at room temperature for 1 hour in dark. Membranes were washed for three times (each time 5 min) with DPBS and dried at room temperature for five minutes. 10 µl of VECTASHIELD® Mounting Medium with DAPI (Vector Laboratories Inc., Burlingame, CA) was applied on the collagen coated side of the membrane and the membrane was put between the coverslips, and the edges were sealed with superglue. The fluorescently labeled samples were kept in the dark at 4 °C until use. The PI membrane was also used as control sample and the whole process was applied for it. Images were acquired by Nikon Eclipse TS100-F with Manta GigE camera (ALLIED Vision Technologies). The surface density of collagen on the membrane was calculated from the images by the ImageJ-program. This protocol was repeated for two times, once with one sample in each group and the other one with 3 samples in each group.

4.4.6. Stability of immobilized collagen

The stability of covalent immobilization of collagen on PI was compared with collagen coated onto PI by traditional dipping method (termed PI-Coll). The PI-AA membranes with a diameter of 6 mm inside the 96-well plate were surface activated and coated covalently with collagen. PI-Coll membranes were also prepared inside the 96-well plates. One mini tablet of Complete Protease Inhibitor Cocktail (Roche, Switzerland) was dissolved in 10 ml of DPBS (pH 7.4), and stored at -20 °C. The membranes were immersed in 250 µl of DPBS or 250 µl DPBS containing Complete Protease Inhibitor Cocktail (DPBS+cocktail) at 37 °C for 14 days. The Inhibitor Cocktail was used with a parallel set of samples to prevent the activity of proteinases in solution and subsequently prevent the degradation of collagen. PI membrane was also used as the control and was immersed only in DPBS. There were 3 parallel samples in each group and the solutions were replaced every 7 days. At time points of 0, 7 and 14 days, the samples were immunostained and observed by fluorescence microscope to compare the density of collagen on them.

4.5. Cell culturing

4.5.1. Continuous cell culturing

The media from the cultured cells in a cell culture flask was removed and the cells were washed with Ca^{2+} and Mg^{2+} - free PBS (2.5 ml) two times; PBS was gently inserted to the bottom of bottles to prevent shear stresses on the cells. This washing process is required since trypsin does not function properly in the presence of serum. Then after removing the PBS, 1.5 ml of 1x trypsin was added to the bottom of flask and after 1 min most of the trypsin was aspirated (leaving just 1 drop of it to prevent cells from drying). In order to enhance the action of trypsin the cell flask was then transferred to the incubator for 3 min at 37 °C. Next, the effect of trypsin was checked under the microscope if cells had changed from spindle to the spherical shape cells (meaning that they have detached from growth substrata). The final detachment of cells was done by shaking the flasks planarly on the table. Then, trypsinization was halted by transferring 4 ml of medium to the flask. The cells were then plated to new culture flasks in 1:4 dilution. The main flask of cell suspension was checked under microscope to be empty of cells and same for new flasks to be full of cells. The cells were incubated at 37 °C and the medium was changed with fresh one every second day.

4.5.2. Cell plating for experiment

The same protocol for PBS washing and trypsinization were used for plating cells needed for experiments. Then 1 ml of medium was used per each flask and the cells were triturated with medium from up to down of the flask. Finally, cell suspension was collected in a container tube and the cells were counted.

To count the cells, 40 µl of cell suspension without using trypan blue was inserted to a haemocytometer (Depth 0.1 mm, Bürker, Germany) by gently resting the end of the tip at the edge of the chambers. It was considered not to overfill the chamber and the fluid runs to the edges of the grooves only. The full grid on a hemacytometer contains nine squares, each of which is 1 mm square (Figure 4.6). The central counting area of the hemacytometer contains 25 large squares and each large square has 16 smaller squares. [118] The cell concentration was estimated by counting 3 squares in the 25 large middle squares in both chambers and the average value was calculated. The raised edges of the hemocytometer hold the coverslip 0.1 mm off the chamber, giving 10 nl volume of cell suspension to 1 mm^2 square [119]. Therefore, the average value was multiplied by 10,000 to obtain the number of cells in ml of medium. Then the amount of required cell suspension was obtained considering the desired cell density on the samples. Cells were seeded at a density of 80000 cells/cm^2 onto the PI, PI-Coll, and PI-AA-Coll membranes. To prevent the flow of fluid outside of the CellCrown™, first 1 ml of medium was added to the outside of the CellCrown™ and then 500 µl cell suspension and medium was added to the inside of the CellCrown™. Experiments were performed at 3 days of culture. Medium was replenished on every second day.

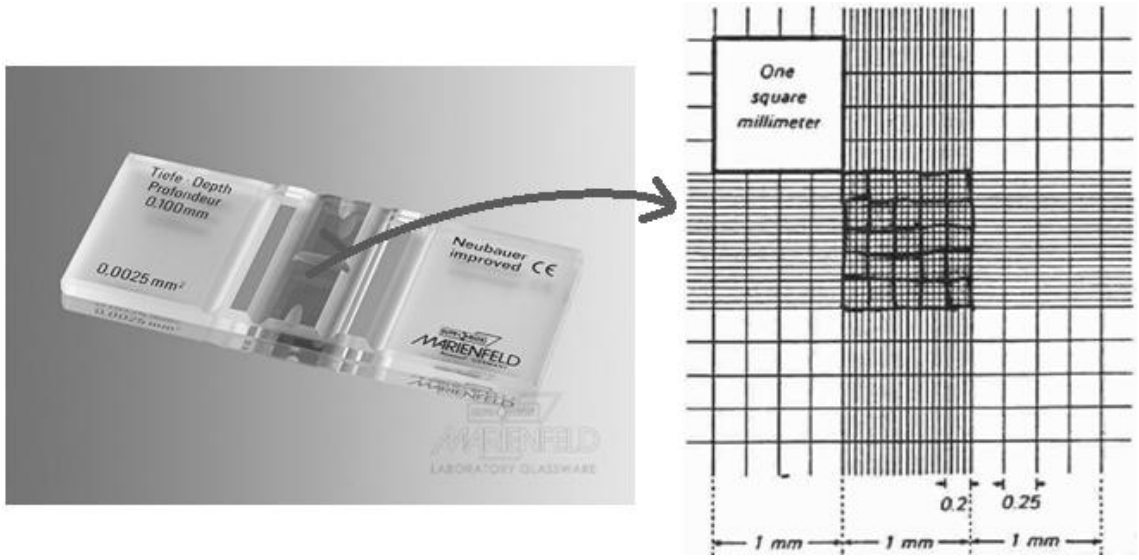

Figure 4.6. *The hemacytometer with two full grids that contain nine squares each. [118, 120]*

4.5.3. Immunocytochemistry

After 3 days of culture, the cell culture wells were drained empty of medium and washed once with Ca^{2+} and Mg^{2+} - free PBS solution. The ARPE-19 cells grown on the membranes were fixed with 4 % paraformaldehyde (PFA, pH 7.4; Sigma-Aldrich) for 10 min at RT. The PFA was then drained and wells were washed by PBS for 3 times.

The process was followed by permeabilization with detergent, 0.1 % Triton X-100/PBS (Sigma-Aldrich), for 10 min. The samples were washed for 3 times with PBS for 5 min. Then, nonspecific binding sites were blocked with 3 % bovine serum albumin in PBS for 1 h at RT. The processes until this step were done under hood. Then PBS was added to samples and the samples were cut into four pieces suitable for 96-well plate. Adding PBS was not included in the main immunostaining protocol and it was done only for 3 days samples in the first round. Primary antibody incubations were done in 0.5 % BSA-PBS for 1 h at RT. Tight junction formation was visualized with mouse anti-Zonula occludens-1 (ZO-1, Invitrogen, USA, 1:250), and RPE cell specific proteins with rabbit anti-Bestrophin (BEST, Abcam, Cambridge, UK, 1:200), and mouse anti-cellular retinaldehyde-binding protein (CRALBP, Abcam, 1:500). The incubation with primary antibodies was followed by three times washing with PBS for 5 min. The secondary antibody incubations were done in 0.5 % BSA-PBS with donkey anti-rabbit IgG (H+L), and donkey anti-mouse IgG (H+L) (both Alexa Fluor® 488, Invitrogen, Molecular Probes, USA) in a 1:800 for 1 h. Amanita toxin, Phalloidin conjugated with Tetramethylrhodamine B (Sigma Aldrich, 1:300) was also used to visualize filamentous actin. Aliquot of Neurotoxic phalloidin + methanol was first dried under laminar flow hood and 0.5 % BSA in PBS and secondary antibody (anti-mouse) were added to it. The wells were washed three times with PBS for 5 min. Lastly, the membranes were placed on a coverslip and two drops of anti-fade reagent VECTASHIELD® with DAPI was applied on the membrane with a cover slip on top. The nuclei were counterstained with 4´, 6´ diamidino-2-phenylidole (DAPI) included in the mounting medium. After staining, the samples were stored at - 20 °C before imaging.

The immunostaining results were visualized using fluorescence microscope (Olympus IX51, Olympus Corporation, Tokyo, Japan) and images were captured and combined with DP Manager and DP Controller software (Olympus Corporation, Tokyo, Japan). Six images were captured from each membrane. Confocal images were obtained with an LSM 700 confocal microscope (Carl Zeiss, Jena, Germany) using 63x oil immersion (Immersol™, Germany) objective. Overlays and image processing of confocal images were done in ZEN-software (Carl Zeiss).

5. RESULTS

The previous chapters showed the need for surface modification of polymers to improve the final biocompatibility or the cell-interactive character of implants. Also, the importance of PI membranes as implants for ocular diseases, including AMD, and the need for modification of this biopolymer for better RPE cell attachment were mentioned. Therefore, in this study, the PI surface is modified by covalent coupling of adhesive molecule collagen IV, a major constituent of the RPE basal lamina.

The collagen type IV immobilization onto the PI membrane surface was achieved by four steps: First, the PI film was pretreated by Ar plasma and exposed to air. This created peroxides on the surface which are thermally labile in nature. Second, graft polymerization of AAc was carried out under the effect of polymerization initiator (peroxides) and thermal energy. Third, the EDC/NHS reactivated the carboxyl groups by formation of amine-reactive NHS-esters. Lastly, a peptide bond was produced between collagen and AAc as the NHS was replaced by the collagen. In all steps, the membranes were fixed in CellCrowns^{TM} to modify one side of the membrane surface. The CellCrown^{TM} prevented the membrane from floating in solution and kept it immersed in solution.

5.1. AFM measurements

The surface morphology of unmodified PI, PI-AA, and collagen coated membranes were observed by atomic force microscopy (AFM). Figure 5.1 shows the surface morphology of (a) unmodified PI, (b) PI-AA (25 %), and (c) PI-AA-Coll as a result of the AAc graft polymerization and collagen immobilization. The R_as of the all membranes are also presented in Figure 5.2. The untreated PI membrane showed a smooth surface with a R_a of 0.75 nm. After AAc grafting with 25 % monomer concentration, the surface roughness slightly decreased to a R_a of 0.71 nm, while after collagen immobilization, R_a increased to 1.15 nm.

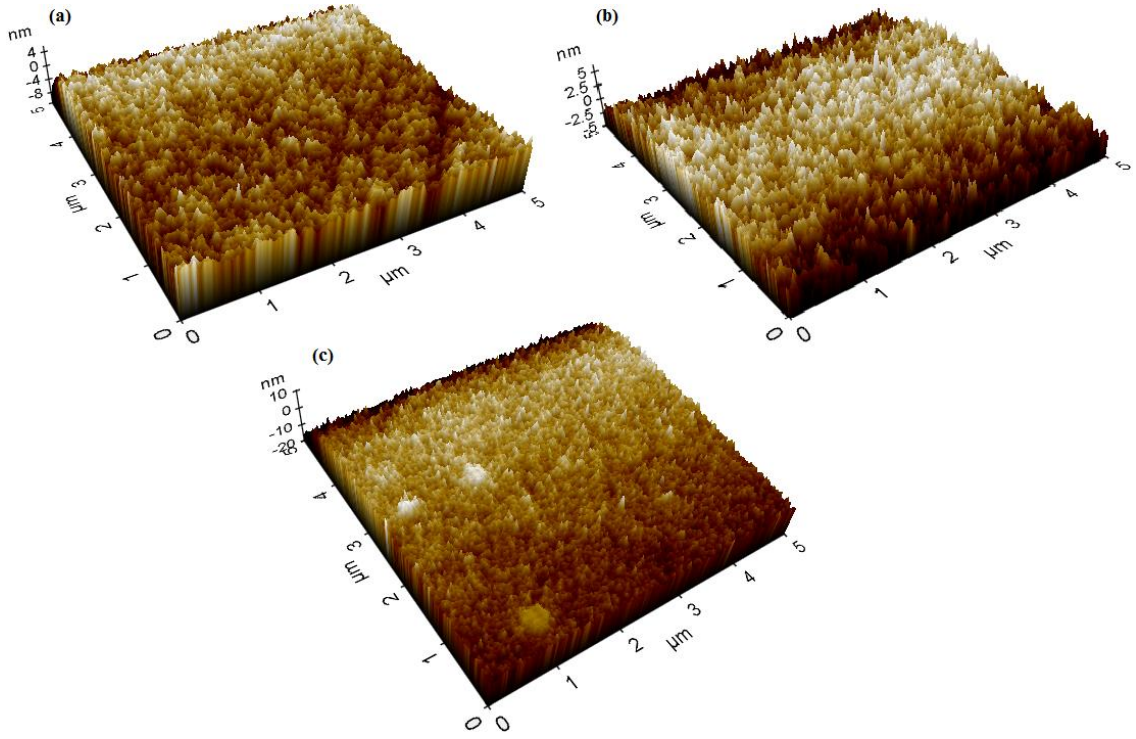

Figure 5.1. *AFM images of (a) unmodified PI, (b) PI-AA (25 %), and (c) PI-AA-Coll.*

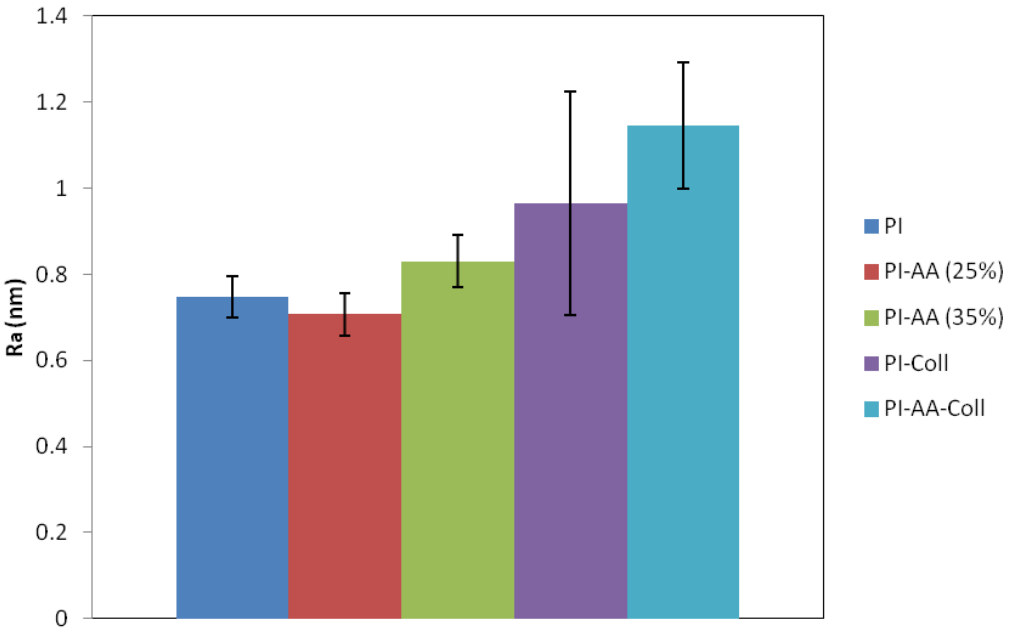

Figure 5.2. *Average R_as and their deviations for PI membranes. The data are averaged values from totally 9 areas of 1 µm^2 in 3 parallel scans for each membrane.*

5.2. Surface density of carboxyl groups

The amount of carboxyl groups on AAc-grafted membranes were determined by quantifying the amount of bound TBO molecules. After immersing the membranes in TBO solution and washing them with NaOH solution, the membranes got different colour due to the reaction with TBO, and the PI-AA (25 %) membrane was darker compare to PI-AA (35 %) (Figure 5.3).

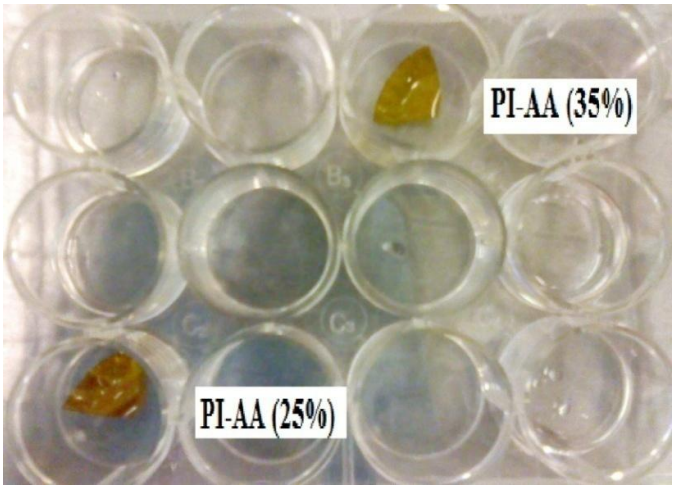

Figure 5.3. *The changes in colour of AAc grafted membranes after reaction with TBO.*

The absorbances of solutions observed by UV/VIS Spectrophotometer are presented in Table 5.1.

Table 5.1. *The absorbance values of TBO solutions after reaction with PI-AA membranes (n=1).*

Absorbance	**PI-AA (25 %)**	**PI-AA (35 %)**	**Unmodified PI**
First test	0.399	0.2665	0.1947
Second test	0.3857	0.2382	

The concentration of TBO in solutions was calculated using the data in Table 5.1 and the equation (4). The results are shown in Table 5.2.

Table 5.2. *The concentration of TBO in acetic acid 50 % solution measured by absorbance values and equation 4.*

Concentration (µM)	PI-AA (25 %)	PI-AA (35 %)	Unmodified PI
First test	5.20	3.47	2.54
Second test	5.02	3.10	

The surface concentration calculations were performed by using the formula (2) and the results are shown in Table 5.3. The surface density of carboxyl group of PI-AA (25 %) membrane was calculated to be 12.17 µg/cm^2, and was obviously higher than that of PI-AA (35 %) (7.83 µg/cm^2). The concentration of carboxyl groups on unmodified membrane was 6.04 µg/cm^2. Therefore, after step II of AAc graft polymerization, the surface density of carboxyl groups on PI-AA (25 %) increased by 6.13 µg/cm^2.

Table 5.3. *The surface density of carboxyl group on unmodified and modified PI membranes.*

Surface density (µg/cm^2)	PI-AA (25 %)	PI-AA (35 %)	Unmodified PI
First test	12.38	8.27	6.04
Second test	11.97	7.39	
Average value of first and second tests	12.17	7.83	

5.3. Water contact angle of the modified surface

To compare the hydrophilicity of the modified and unmodified membrane surfaces, water contact angles were measured.

Figure 5.4 shows the photo images of water drops on the surface of (a) control PI, (b) plasma treated PI, (c) PI-AA (25 %), (d) PI-AA (35 %), (e) PI-SE, (f) PI-AA-Coll, and (g) PI-Coll, respectively. The results of contact angle measurements are presented in Table 5.4. The water contact angle decreased as the polyacrylic acid chains were grafted on the surface. Also, after surface activation and collagen immobilization on PI-AA (25 %) membrane, the water contact angle of the membranes were lower than that of the control sample, while the hydrophilicity of PI-Coll was near to the control sample.

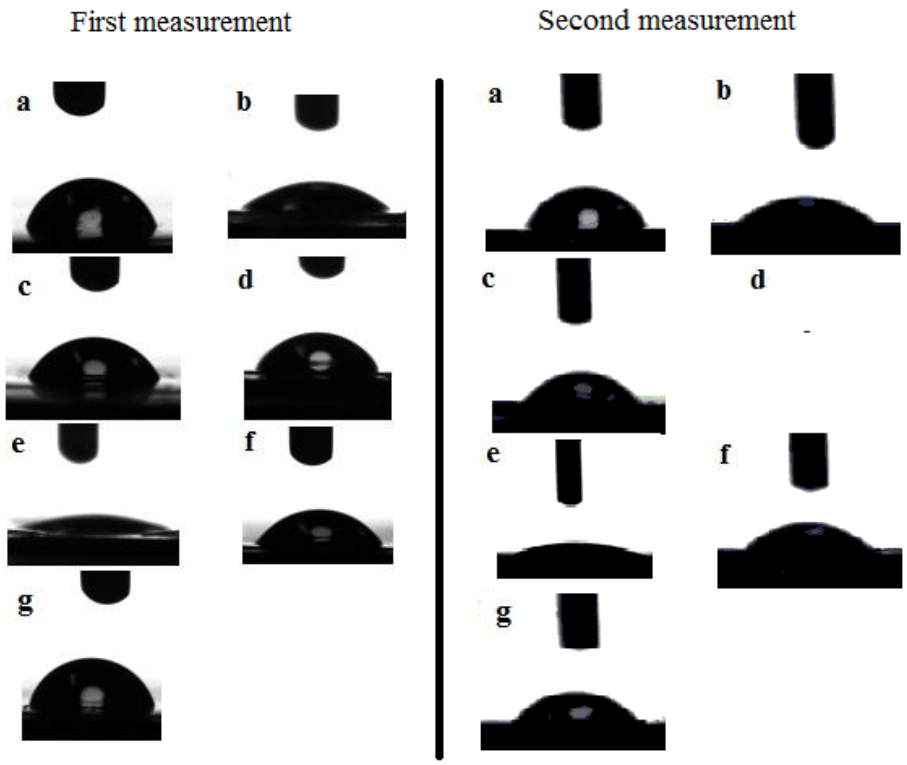

Figure 5.4. *Photo images of water drops on the (a) control PI, (b) plasma treated PI, (c) PI-AA (25 %), (d), PI-AA (35 %), (e) PI-SE, (f) PI-AA-Coll, and (g) PI-Coll for first and second measurements.*

Table 5.4. *The water contact angle measurements (n=1).*

Membrane	PI (control)	Plasma treated	PI-AA (25 %)	PI-AA (35 %)	PI-SE	PI-AA-Coll	PI-Coll
Contact angle, 1st test	75	40	61	56	17	59	78
Contact angle, 2nd test	71	37	49	-	19	37	57

5.4. Attenuated total reflectance-Fourier transform infrared (ATR-FTIR) measurements

The chemical structure of the modified membrane surface was studied by ATR-FTIR. Figure 5.5 shows the respective ATR-FTIR spectra of the unmodified PI (a), PI-AA (25 %) (b), PI-AA (35 %) (c), PI-SE (d) and PI-AA-Coll membrane (e). The spectra for grafted PI membranes were found to be close to the unmodified PI membrane. The

major absorption bands and their characteristic bonds in unmodified PI membrane spectrum are listed in Table 5.5. [121]

Table 5.5. *The ATR-FTIR absorption bands of unmodified PI membrane. [121]*

Absorption bands (cm^{-1})	**Bond**
722	C=O bending
1090	C-O-C bond
1166	C-C bending
1240 1374	C-N stretching
1498 1599	aromatic C=C ring stretch
1714	C=O symmetrical stretching
1776	C=O asymmetrical stretching

The same peaks were also found in the spectrum of PI-AA (25 %), PI-AA (35 %), PI-SE, and PI-AA-Coll membranes. However, in b and c, the broader peaks in the region 3000-2800 cm^{-1} may indicate the presence of more H-bonding of carboxylic acid groups in PI-AA (25 % and 35 %) membranes (also see Figure 6.1).

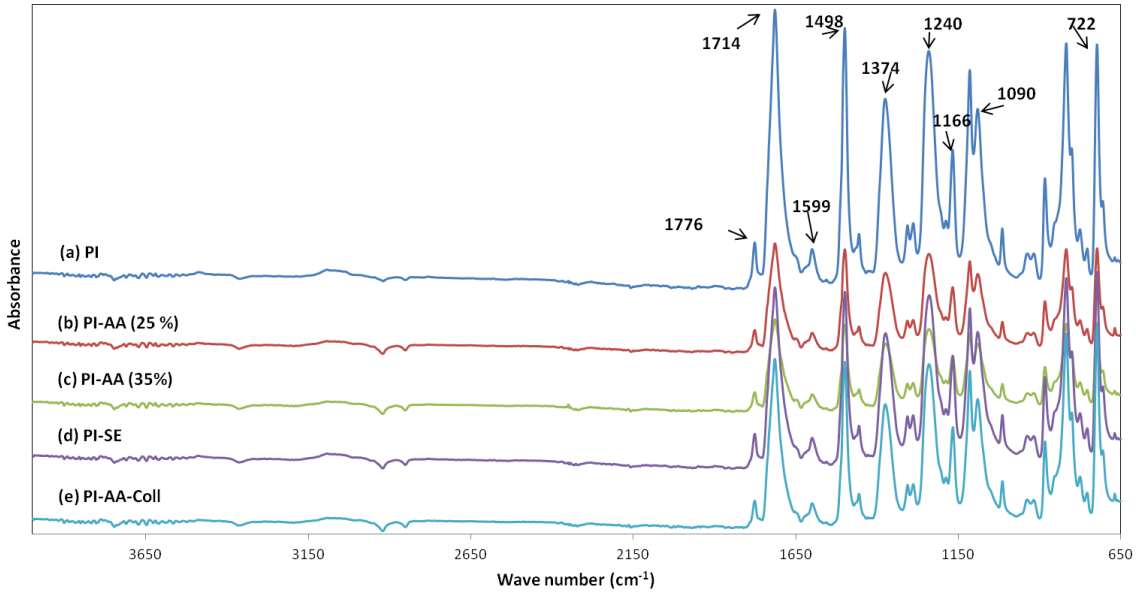

Figure 5.5. *ATR-FTIR of PI membranes (a) unmodified, (b) PI-AA (25%), (c) PI-AA (35%), (d) PI-SE, and (e) PI-AA-Coll.*

5.5. Fluorescence microscopy and image analysis

In order to compare the surface density of collagen on PI-AA-Coll and PI-Coll membranes, the fluorescence microscopy imaging was applied.

In the first test, the increase in intensity (per percent) of light as a result of dipping and covalent surface modification, compared to the uncoated control were 19 % and 32 %, respectively (Table 5.6). Then the contrast and the brightness of the images were modified in the paint.net program. As can be seen in Figure 5.6, the control PI had background fluorescence. However, the intensity of light in PI-AA-Coll is significantly higher than that in PI-Coll and PI samples.

Table 5.6. *The mean intensities of membranes (First test, n=1).*

Membrane	PI	PI-Coll	PI-AA-Coll
Mean intensity	20.20	24.40	26.87

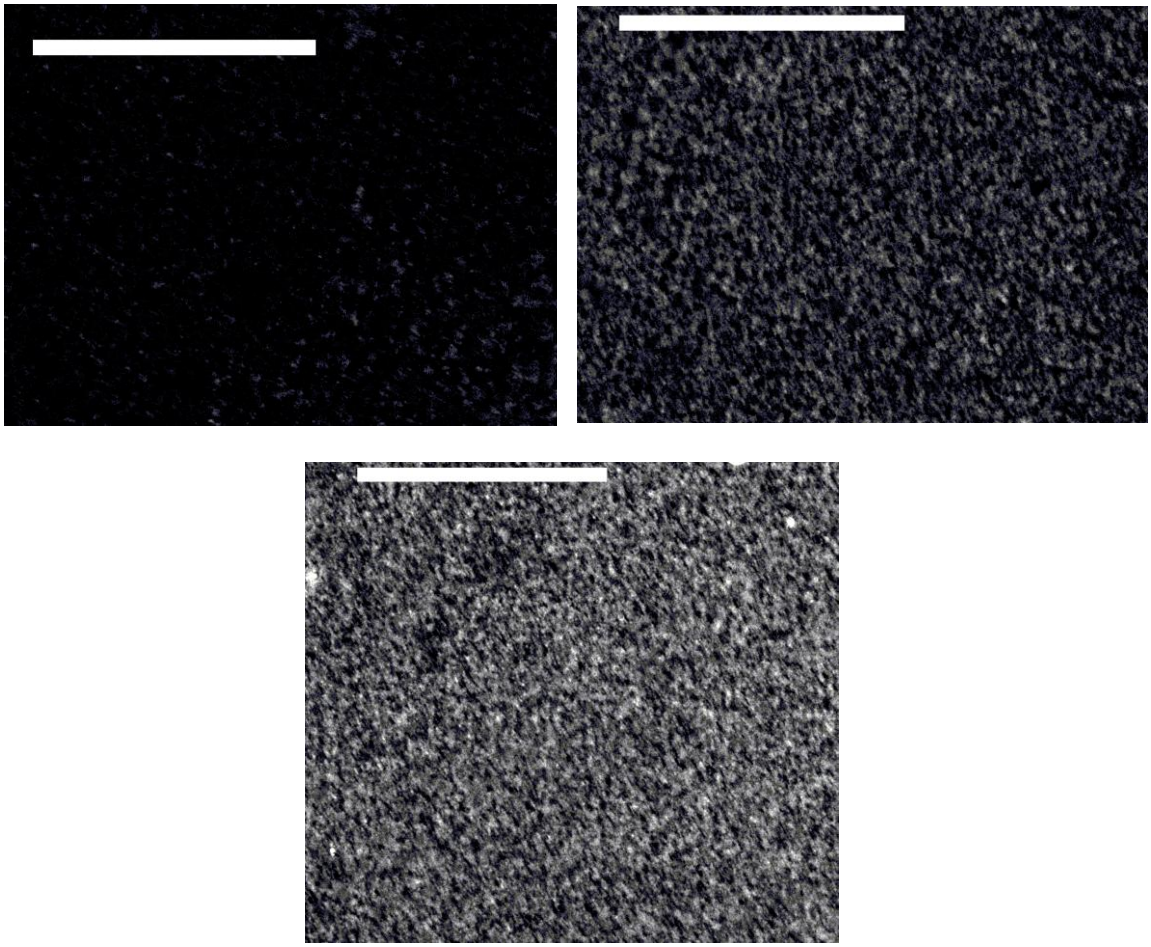

Figure 5.6. *Fluorescent microscopy images of (a) control PI, (b) PI-Coll, and (c) PI-AA-Coll membranes taken with a 4X microscope objective after 1s exposure. The white block represents 500 µm.*

In the second test, the results show higher amount of intensity for the PI and PI-Coll membranes. It is noticeable that the standard deviation is significantly high for PI and PI-AA-Coll membranes. (Figure 5.7)

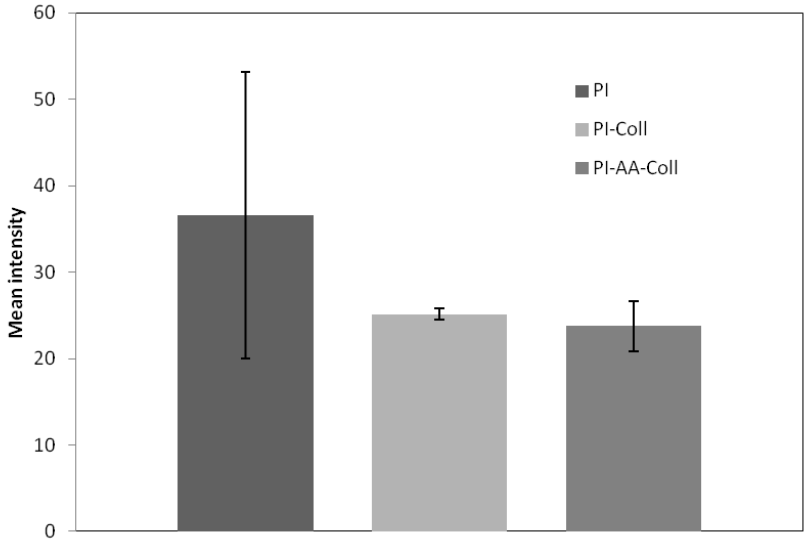

Figure 5.7. *The mean intensities of membranes (Second test, n=3).*

5.6. Stability of immobilized collagen

The stability of immobilized collagen was investigated by immersing PI, PI-Coll and PI-AA-Coll membranes in DPBS and DPBS+cocktail over 14 days. The surface density of collagen on samples was compared by the intensity of light in fluorescence images before and after immersion.

Indicated in Figure 5.8, for PI membrane, the intensity is not constant during 14 days and on the first week in DPBS solution, the highest intensity value of 24.12 (± 0.80) for PI can be observed. PI-Coll membrane in DPBS has an intensity of 17.23 (± 1.48) for 0 week which unexpectedly increases to intensity of 39.72 (± 19.77) on 1st week. This value decreases to 17.28 (± 0.57) on 2nd week quite near its value for 0 week. For PI-AA-Coll, the intensity slightly decreases during 14 days; however, it must be considered the high standard deviation on 0 week.

To compare the effect of solution on mean intensity, the difference between the intensities of PI-AA-Coll membranes in DPBS and DPBS+cocktail after 1 and 2 weeks are 0.46 and 0.72, respectively. Also, the difference between the intensities of PI-Coll membranes in DPBS and DPBS+cocktail on 2nd week is 0.75.

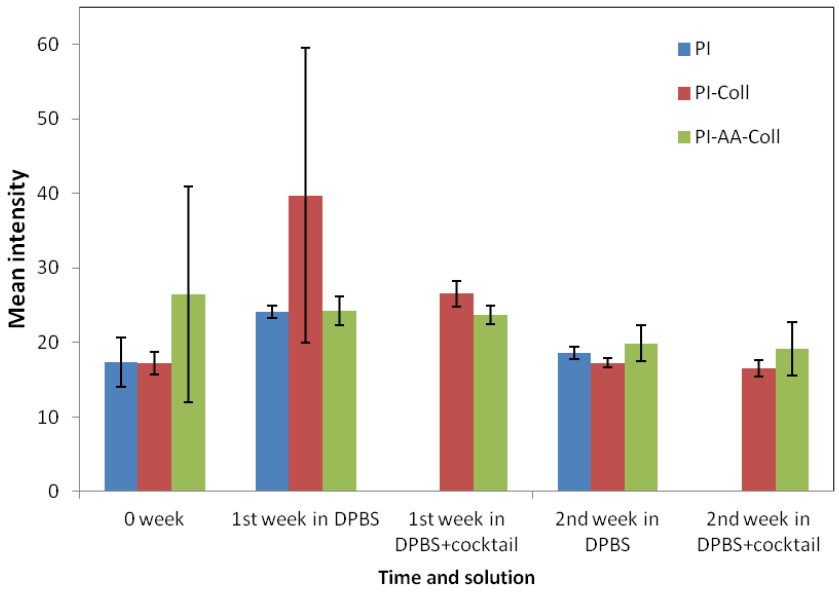

Figure 5.8. *The mean intensities of membranes after 14 days immersion in DPBS and/or DPBS+cocktail solutions (n=3).*

5.7. Cell culture and immunocytochemistry

ARPE-19 cells were grown on modified PI membranes (PI-AA-Coll) for 3 days. Unmodified PI and PI-Coll membranes were used as controls. The attachment and proliferation of ARPE-19 cells on investigated membranes were analyzed with immunocytochemistry.

On covalently modified membranes, ARPE-19 cells displayed a more hexagonal cell morphology whereas on PI-Coll and PI membranes the cell morphology was fibroblast-like (Figure 5.9). The protein ZO-1 was observed more on PI-AA-Coll membranes compared to PI and PI-Coll membranes, however, cells had divided in aberrant way on PI-AA-Coll membranes (Figures 5.9 and 5.10).

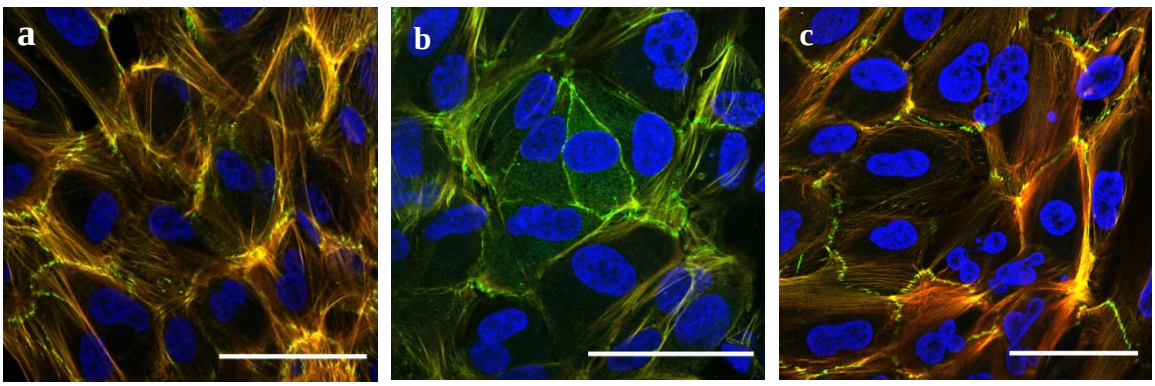

Figure 5.9. *Immunocytochemistry of ARPE-19 cultured on PI membranes for 3 days, (a) control PI, (b) PI-Coll, and (c) PI-AA-Coll. The protein ZO-1(in green) was localized at the tight junctions on the cell membranes. The filamentous actin (F-actin) (seen in red) is either on the stress fibers or on the cellular junctions. The nuclei were counterstained with DAPI (blue). Z-position from the surface 6 µm. Scale bars 50 µm.*

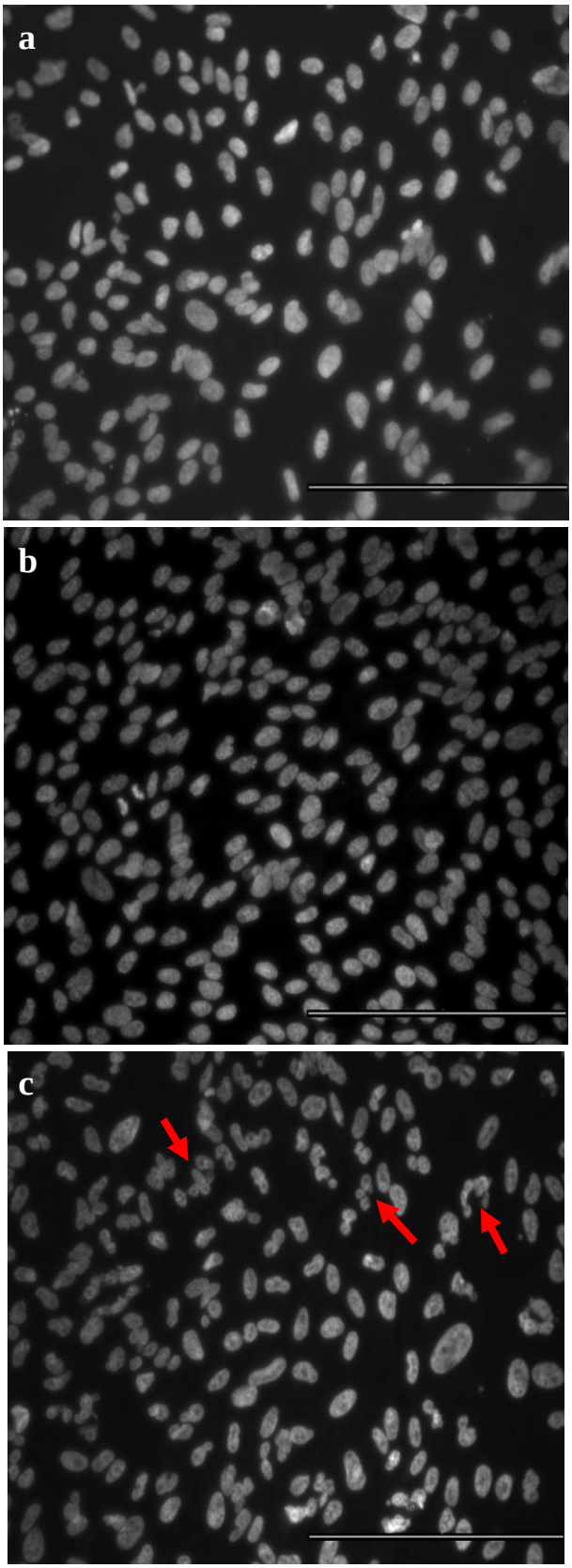

Figure 5.10. *Fluorescence images of ARPE-19 cells cultured for 3 days on (a) control PI, (b) PI-Coll, and (c) PI-AA-Coll membranes. Examples of aberrant ARPE-19 cell division on PI-AA-Coll membranes are shown by red arrows in (c). The nuclei were counterstained with DAPI (shown in white for better contrast). Taken by 20X microscope objective. Scale bars 200 µm.*

In addition, phalloidin staining showed filamentous actin (F-actin) distribution in stress fibers on all investigated samples. However, the amount of detected stress fibers was higher in control PI compared to the PI-Coll and PI-AA-Coll samples (Figure 5.11). In figures 5.9 and 5.11, a and c are from different sz section of Z-stack images where the actin fibers are seen better in Figure 5.11.

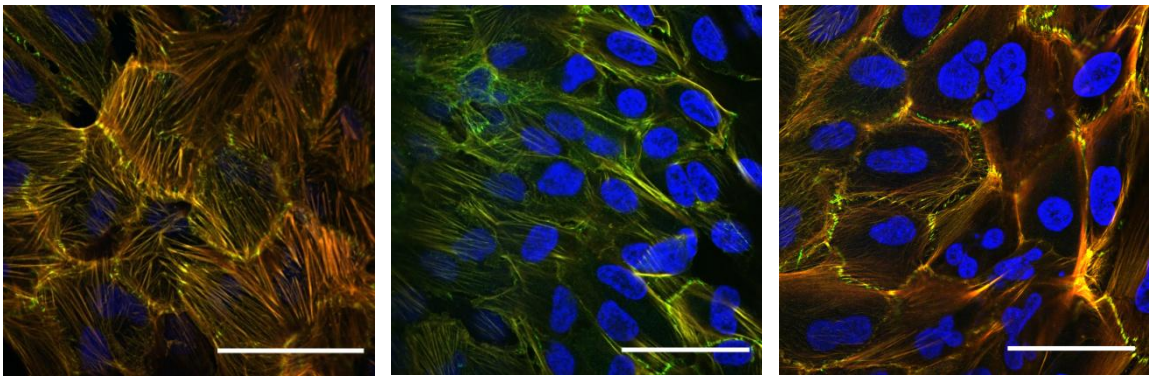

Figure 5.11. *Immunocytochemistry of ARPE-19 cultured on PI membranes for 3 days, (a) control PI, (b) PI-Coll, and (c) PI-AA-Coll. F-actin was visualized with phalloidin (red) that represents the presence of stress fibers. The protein ZO-1(in green) was localized at the tight junctions on the cell membranes. Z-position from the surface 7 µm. Scale bars 50 µm.*

6. DISCUSSION

The surface chemistry and topology of biomaterials have both an important role in biological response to biomaterials and the final biocompatibility of implant. Hence, the principle of surface modification of biomaterials is to keep the main physical properties of biomaterials while modifying the surface to influence the bio-interactions. [104] In order to improve the retinal cell-interaction with PI substrates, a four-step surface modification was developed and evaluated in this study. Collagen IV was selected to modify the PI surface in this study because of acceptable differentiation and maturation of hESC toward RPE phenotype in presence of collagen IV. The effect of surface modification protocol on the degree of grafted carboxyl groups, surface roughness, hydrophilicity of membranes, and surface density of immobilized collagen were studied. At the end, some probable methods to improve the behavior of ARPE-19 cells with modified PI membranes were suggested.

6.1. Surface density of carboxyl groups

Thermal-induced acrylic acid grafting on plasma-pretreated PI membrane was carried out with two monomer concentrations of 25 % and 35 %. The incorporation of carboxyl groups was quantified by TBO interaction method. The results show that the 25 % AAc monomer concentration provides more carboxyl groups on the membrane surface compared to 35 % AAc monomer concentration. Previous studies reported that by the increase in AAc monomer concentration used for graft copolymerization, the concentration of the surface-grafted carboxyl groups increases [2, 16]. Also, it has been observed that there is a maximum peak in surface concentration of carboxyl groups by the increase in the AAc monomer concentration, and the subsequent sharp decrease attributed to extensive homopolymerization in the system (Figure 3.6) [15, 16]. In our study, more AAc monomer concentrations are needed to test in order to find the optimum monomer concentration to achieve the maximum carboxyl density on the surface. However, it is supposed that 25 % AAc monomer concentration is located in the rising region of the curve and 35 % AAc monomer concentration is located in the decrease part of the curve where the carboxyl concentration on the surface tends to decrease by increase in monomer concentration.

It was reported that the concentration of immobilized collagen on the surface increases as the surface density of carboxyl groups increases since the COOH-group acts as a spacer to bond with collagen [3, 107]. Therefore, in this study, the PI-AA (25 %)

membrane was selected for further surface activation and collagen immobilization processes.

The AAc monomer concentration used for graft polymerization has an effect on the surface composition, in particular, the concentration of the COOH-groups from the grafted AAc polymer on the modified PI surface. The surface density of carboxyl group of PI-AA (25 %) membrane was calculated to be 12.17 μg/cm^2, which was comparable with published results. Gupta et al. reported that their surface density of carboxyl groups on the AAc-grafted PET monofilament (AAc grafted at 50 °C for the reaction time of 4 h) was 0.5–10.80 μg/cm^2, depending on the AAc monomer concentration from 20 to 80 %. [16]

6.2. Atomic force microscopy

The surface topography of membranes do not undergo significant changes as a result of the AAc grafting process and collagen immobilization and the membranes did not get damaged. The AFM imaging from PI samples was not successful which might be due to the electrical properties of surface or the size of cantilever tip. However, it is expected that the surface roughness of the PI membranes increases after Ar plasma treatment due to the etching effect of plasma treatment [2, 19, 107]. It was observed that after graft polymerization with AAc, the surface roughness was about 0.83 nm for the PI-AA (35%) which was quite near to the surface roughness of unmodified membrane. The phenomenon indicates that the graft poly(acrylic acid) chains form their own domains and exist as an overlayer on the PI membrane so that decrease the roughness of surface after plasma treatment [2, 107]. As the grafting increases, the domain size of graft chains increases, thus the nearby domains agglomerate to a larger one, and leads to flattening of the surface. Therefore, the surface roughness of PI-AA (25 %) was lower than that of PI-AA (35 %). Moreover, the covalently attached collagen to polyacrylic acid chains, broadened the polyacrylic acid domains on the membrane surface, which led to increase of the surface roughness [3].

6.3. Water contact angle of the modified surface

The effect of surface modification on hydrophilicity of PI membrane is also studied. The results of contact angle measurements in Table 5.4 indicated that AAc graft copolymerization increased the wettability of PI membrane due to the presence of -OH and -C=O [16], and the AAc grafted membranes are more hydrophilic compared to control sample.

Furthermore, after collagen immobilization of PI-AA (25 %) membrane, a part of carboxyl functional groups are blocked with collagen. Therefore, it is expected that the membrane surface becomes less hydrophilic compared to PI-AA (25 %) membrane, while in the first test the water contact of PI-AA (25 %) and PI-AA-Coll are close to each other, and in the second test PI-AA-Coll membrane is more hydrophilic compared

to PI-AA (25 %). This might be due to the presence of residual hydrophilic NHS-esters on the surface of PI-AA-Coll. However, the contact angle of collagen immobilized membrane is lower than that of unmodified membrane, and shows improvement in hydrophilicity of the membrane. However, the water contact angle measurements can be repeated for at least two more set of samples to know the exact effect of each step on hydrophilicity of the surface.

6.4. ATR-FTIR studies

The adsorption peak at 1730 cm^{-1} corresponds to the COO of a carboxyl group. [3, 107] But the adsorption peak overlapped with the adsorption peak of C=O stretching group at 1714 cm^{-1}, which is the backbone chain in PI membrane. Only small differences were observed between the spectra of untreated and treated samples. This may be due to the fact that the penetration depth of ATR-FTIR is around 1 to 10 microns [122]. When the thickness of the "surface treatment layer" prepared in this work is assumed to be in nanometer scale, it can be hypothesized that information is mostly gained from the bulk PI membrane.

The only additional feature in AAc grafted membranes is the broader peaks in the region 3000-2800 cm^{-1} (see Figure 6.1). This may be due to the higher extent of H-bonding of carboxylic acid groups in AAc grafted membranes. Since, the carboxylic acid O-H stretch appears as a very broad band in the region 3300-2500 cm^{-1}, centered at about 3000 cm^{-1} [123]. Also, it can be seen in Figure 6.2, there are new peaks formed in the region of 1440-1400 cm^{-1} which are related to the presence of O-H bend in carboxyl group [124, 125]. In general, it is difficult to determine the presence of grafted poly(acrylic acid) chains at the membrane surface from the results.

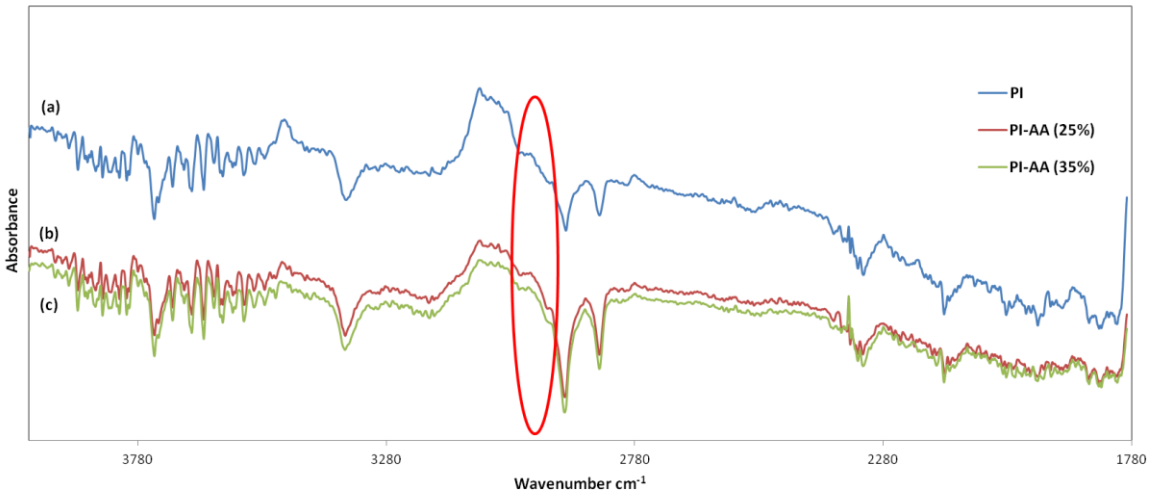

Figure 6.1. *ATR-FTIR of PI membranes (a) unmodified, (b) PI-AA (25 %), (c) PI-AA (35 %); the broader peaks in the region 3000-2800 cm^{-1} are marked with the red circle.*

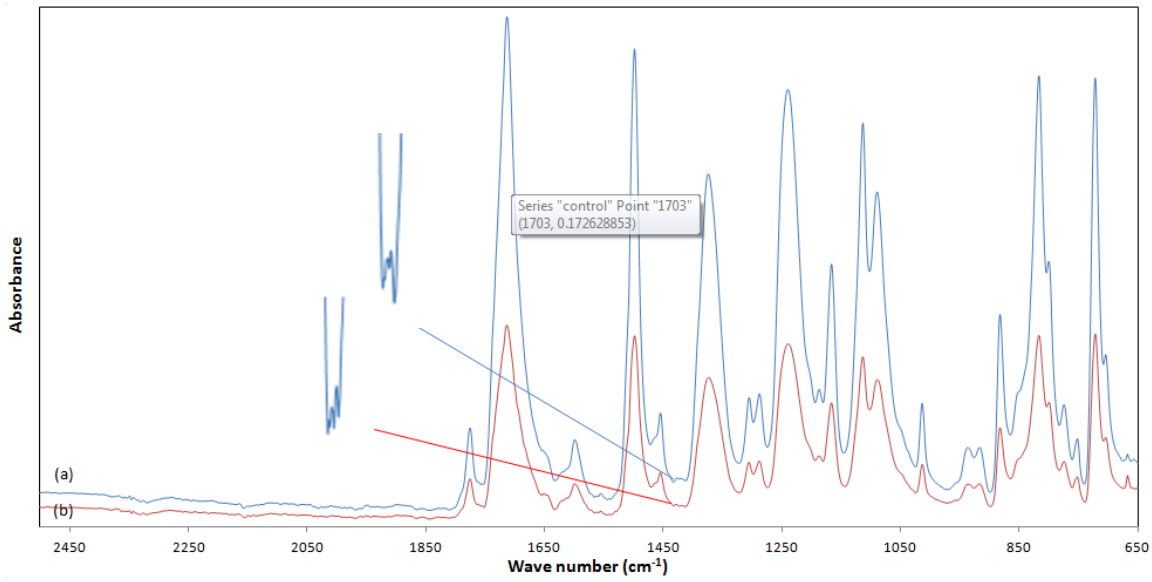

Figure 6.2. *ATR-FTIR of PI membranes (a) unmodified, (b) PI-AA (25 %), the peaks in the region of 1440-1400 cm^{-1} are magnified.*

Collagen type IV shows characteristic peaks at 1454, 1403, 1340, 1282, 1240, 1205, 1659 and 1555 cm^{-1} representing respectively CH_2 bend, CH_3 bend, C-N stretch, N-H stretch, amid I, and amid II. [58] However, in ATR-FTIR spectrum of PI-AA-Coll in Figure 5.5, all these peaks are also hidden by the peaks from the bulk of the PI membrane.

6.5. Collagen density and stability test

The collagen density and its stability on the surface of PI-AA-Coll membranes were investigated. The PI and PI-Coll samples were used as control. The results showed high range of variation in the intensities between the parallel samples that made the analysis difficult. The inhibitor cocktail was added to inhibit the activity of possible proteinases in the solution to show the "real effects" of incubation to the coatings. However, the observed intensities of membranes incubated in DPBS and DPBS+cocktail were not significantly different.

One of the reasons for high standard deviation may be the lack of enough amount of VECTASHIELD® Mounting Medium with DAPI on the membranes. The places with less amount of VECTASHIELD® have shown photobleaching properties with higher intensity of light. To improve the result of this experiment, enough amount of VECTASHIELD® must be used per each sample to cover the whole surface of membrane and remove all the air between the membrane and the coverslip. Also, the membranes can be cut with surgical knife instead of punch as it prevents the probable contact of membrane surface with the punch wall. Moreover, the light membranes in the 96-well plate might rotate by adding solution when the air bubbles stay below them. In or-

der to decrease the risk of rotation, the membranes can be cut to small pieces later, one step before primary antibody addition.

6.6. Cell culture

One of the identifier of RPE maturation is expression of adhesion proteins like tight junction (TJ) protein ZO-1 [126]. In the results, the protein ZO-1 was observed more on PI-AA-Coll membranes compared to PI and PI-Coll membranes. ZO-1 localized at the tight junctions on the cell membrane, suggesting that cells were more mature on covalently modified membranes. The maturation of RPE cells is also accessed by their morphology starting from fusiform, followed by rounding to more epithelioid cells, and finally to cobblestone morphology [127, 128]. The hexagonal cell morphology of ARPE-19 cells on PI-AA-Coll membranes which can be due to the covalent crosslink between the collagen and the membrane, however the cells were dividing in aberrant way.

In a study done by Kearns et al., ARPE-19 cells showed successful attachment on acrylic acid plasma treated culture plates at 1 day, with cell proliferation over the ten-day period in culture. After 7 to 10 days, cells formed a confluent monolayer, with the rate of increase in cell number similar to that on the tissue culture plate surface. [129] In another study, it was also demonstrated that different carboxylic acid concentrations influenced the degree of human keratinocyte attachment to the surface [130, 131]. Thus, acrylic acid grafted surfaces have the potential to provide appropriate substrate for the growth of RPE once the growth conditions are optimized. In accordance with these findings, our study indicated that the probable presence of acrylic acid on polyimide membranes might not have adverse effect on ARPE-19 cells to have proliferation in aberrant way. However, it would be informative to check the behavior of ARPE-19 cells on PI-AA membranes with different carboxylic acid concentrations.

Jui-Yang Lai investigated that ARPE-19 cells are able to maintain typical epithelial-like morphology and relatively high viability after a 3-day exposure to EDC cross-linked HA hydrogel membranes. Only a few red-stained nuclei were noted in Live/Dead assay, indicating negligible cytotoxicity. To prevent the deactivation of water-soluble carbodiimide, the crosslinking reaction was allowed to proceed in acetone/water mixtures, followed by washing and then drying for 24 h. [132] In another study done by the same author, corneal stromal cells exhibited different cell adhesion and proliferation activity on gelatin/chondroitin sulfate (CS) scaffolds modified at different NHS/EDC molar ratios. In the molar ratio range of NHS to EDC from 0 to 0.5 (at a constant EDC concentration of 10 mM), the cell number on the scaffold represents an upward trend after 5 days in culture, with subsequent decrease for molar ratio of 1. The author correlates this behavior to changes in CS content of the scaffold. As the CS content increased with increase in the NHS/EDC molar ratio range from 0 to 0.5 and then decreased by increasing the EDC/NHS molar ratio to 1. However, the cells did not show toxicity in contact with the scaffolds. [133]

Regarding the coated protein, type IV collagen from human placenta was selected as being the natural constituent of RPE basal lamina. In a study done by Subrizi et al., the hESC-RPE cells acquired RPE monolayer morphology and pigmentation on PI membranes physically coated with collagen IV. While the uncoated PI membrane, or coated PI membranes with synthetic laminin peptides, HS and HA did not support hESC-RPE cell attachment and growth. [9] Therefore, it is also expected that collagen IV does not have adverse effect on ARPE-19 cell proliferation on PI membranes.

One of the probable reasons for proliferation of ARPE-19 in aberrant way might be the presence of residual NHS-esters on the PI-AA-Coll samples. The hydrolysis rate of NHS-esters by water is fast and no more surface deactivation steps are needed. The deactivation of residual NHS-esters proceeds along with the protein immobilization after 21 min of surface treatment with buffers of pH 8–9 at 25 °C. [134] In our study, the collagen immobilization reaction occurred in pH of 7.3 for 24 h at 4 °C which might first bring the idea that the excess NHS-esters will be hydrolyzed back to carboxylate anions in these conditions and the surface is completely deactivated. However, the water contact angle results for PI-AA-Coll, represents the presence of residual NHS-esters on the surface. It is supposed to observe higher water contact angle for PI-AA-Coll compared to PI-AA (25 %) due to the carboxyl groups blocking effect by collagen.

One of the methods to deactivate residual NHS-esters is to quench the PI-AA-Coll samples with ethanolamine solution to block non-specific reactions of the un-reacted carboxylic groups with the ARPE-19. [111, 135] Also, the washing process after collagen immobilization can be performed for a longer time with subsequent 24 h drying step. [132, 136] The other solution could be to change the NHS/EDC molar ratio to find an appropriate ratio for collagen immobilization and optimized conditions for normal ARPE-19 cell growth.

7. CONCLUSIONS

The aim of this study was to chemically modify the PI membrane using a controlled surface modification method, involving argon-plasma treatment, acrylic acid graft polymerization, surface activation, and covalent immobilization of collagen IV. In collagen immobilization, a peptide bond was produced between collagen and grafted carboxyl groups on the membrane by means of carbodiimides and N-hydroxysuccinimide crosslinkers. One of the future goals that this study is leading is to find ways to improve the attachment and maturation of hESC-RPE cells and immortalized cell lines (such as ARPE-19).

As a conclusion, the concentration of AAc grafted on the membrane surface was strongly dependent on the concentration of AAc monomer solution used for grafting. Thereafter, the membrane with higher amount of carboxyl groups was chosen for surface activation and collagen immobilization. The TBO test was quite a useful and easy method that allows a quantitative estimate of the total number of carboxyl groups on the membrane. The use and detection of the cationic TBO required basic instrumentation.

AFM images were also successful on non-porous membranes but on porous membranes, cantilevers with lower tip-radius may be required. Despite the etching effect of plasma treatment on the membranes, the surface modification protocol did not significantly affect the final surface roughness of membranes.

The water contact angle measurement method for the track etched PI membrane was challenging as the membranes had pores on the surface and water did not stabilize on the surface for enough time. However, the measurements on non-porous PI membranes represent the effect of each step on hydrophilicity of the membranes. After surface activation, the water contact angle significantly decreased representing the presence of NHS-ester groups on the surface. Collagen-modified PI membrane was found to be more hydrophilic in comparison with PI and PI-Coll. The other challenge with this method was that mostly between the membranes and the carbon tape on the sample holder, small air bubbles were entrapped so that prevent a flat surface for water contact angle measurements.

Furthermore, the ATR-FTIR spectroscopy was not a suitable method to detect the NHS-esters and collagen on the membrane surface. However, the presence of grafted poly(acrylic acid) chains at the acrylic acid grafted membrane surface was determined in spectra. The information from ATR-FTIR data were almost from the bulk of sample due to the fact that ATR-FTIR is not a surface sensitive technique and its penetration depth is at the level of micron. Thus a more surface sensitive method like XPS is suggested to detect the presence of different coatings on the membrane surface.

Throughout the experiments, the autofluorescence property of the membranes was the main issue in determination of collagen surface density. However, the risk of high range of variation in the intensities between the parallel samples could be decreased by applying more amount of VECTASHIELD® Mounting Medium with DAPI on the membranes and changing some practical methods mentioned in discussion part.

In addition, under light and fluorescence microscopes, it was impossible to observe ARPE-19 cells on the yellowish and autofluorescent membranes. However, the confocal microscope compensated the absence of clear ZO-1 and phalloidin in fluorescence images. Results from in vitro study using ARPE-19 cells have shown more mature cells on the covalently modified membranes compared to control samples. However, the cells were dividing in aberrant way. One of the probable reasons for proliferation of ARPE-19 in aberrant way might be the presence of residual NHS-esters on the PI-AA-Coll samples. Some of the methods to deactivate residual NHS-esters are to quench the PI-AA-Coll samples with ethanolamine solution, longer washing process after collagen immobilization, and changes in the NHS/EDC molar ratio.

REFERENCES

[1] Fully Implantable Retinal Prosthesis Chip with Photodetector and Stimulus Current Generator. Electron Devices Meeting, IEEE International; 2007.

[2] Ying L, Yin C, Zhuo RX, Leong KW, Mao HQ, Kang ET, et al. Immobilization of galactose ligands on acrylic acid graft-copolymerized poly(ethylene terephthalate) film and its application to hepatocyte culture. Biomacromolecules 2003;4(1):157-165.

[3] Cheng Z, Teoh S. Surface modification of ultra thin poly (ε-caprolactone) films using acrylic acid and collagen. Biomaterials 2004;25(11):1991-2001.

[4] Kang ET, Neoh KG, Huang SW, Lim SL, Tan KL. Surface-Functionalized Polyaniline Films. J Phys Chem B 1997;101(50):10744-10750.

[5] Van Vlierberghe S, Sirova M, Rossmann P, Thielecke H, Boterberg V, Rihova B, et al. Surface modification of polyimide sheets for regenerative medicine applications. Biomacromolecules 2010;11(10):2731-2739.

[6] Zrenner E, Bartz-Schmidt KU, Benav H, Besch D, Bruckmann A, Gabel VP, et al. Subretinal electronic chips allow blind patients to read letters and combine them to words. Proc Biol Sci 2011;278(1711):1489-1497.

[7] Sachs HG, Schanze T, Wilms M, Rentzos A, Brunner U, Gekeler F, et al. Subretinal implantation and testing of polyimide film electrodes in cats. Graefe's Archive for Clinical and Experimental Ophthalmology 2005;243(5):464-468.

[8] A retinal implant technology based on flexible polymer electrode and optical/electrical stimulation. Biomedical Circuits and Systems, IEEE International; 2004.

[9] Subrizi A, Hiidenmaa H, Ilmarinen T, Nymark S, Dubruel P, Uusitalo H, et al. Generation of hESC-derived retinal pigment epithelium on biopolymer coated polyimide membranes. Biomaterials 2012;33(32):8047-8054.

[10] Zhang C, Thompson ME, Markland FS, Swenson S. Chemical surface modification of parylene C for enhanced protein immobilization and cell proliferation. Acta Biomater 2011;7(10):3746-3756.

[11] Sam S, Touahir L, Salvador Andresa J, Allongue P, Chazalviel JN, Gouget-Laemmel AC, et al. Semiquantitative study of the EDC/NHS activation of acid terminal groups at modified porous silicon surfaces. Langmuir 2010;26(2):809-814.

[12] Jonkheijm P, Weinrich D, Schroder H, Niemeyer CM, Waldmann H. Chemical strategies for generating protein biochips. Angew Chem Int Ed Engl 2008;47(50):9618-9647.

[13] Zhang F, Shi ZL, Chua PH, Kang ET, Neoh KG. Functionalization of Titanium Surfaces via Controlled Living Radical Polymerization: From Antibacterial Surface to Surface for Osteoblast Adhesion. Ind Eng Chem Res 2007;46(26):9077-9086.

[14] Wong DM, Jameson SS. General Approaches for Chemical Cross-Linking. Chemistry of Protein and Nucleic Acid Cross-Linking and Conjugation. Second ed.: CRC Press; 2011. p. 297-320.

[15] Gupta B, Hilborn JG, Bisson I, Frey P. Plasma-induced graft polymerization of acrylic acid onto poly(ethylene terephthalate) films. J Appl Polym Sci 2001;81(12):2993-3001.

[16] Gupta B, Srivastava A, Grover N, Saxena S. Plasma induced graft polymerization of acrylic acid onto poly(ethylene terephthalate) monofilament. IJFTR 2010;35(1):9-14.

[17] Yang GH, Kang ET, Neoh KG, Zhang Y, Tan KL. Electroless deposition of copper on polyimide films modified by surface graft copolymerization with nitrogen-containing vinyl monomers. Colloid & Polymer Science 2001;279(8):745-753.

[18] Yu ZJ, Kang ET, Neoh KG. Electroless plating of copper on polyimide films modified by surface grafting of tertiary and quaternary amines polymers. Polymer 2002;43(15):4137-4146.

[19] Bhusari D, Hayden H, Tanikella R, Allen SAB, Kohl PA. Plasma Treatment and Surface Analysis of Polyimide Films for Electroless Copper Buildup Process. Journal of The Electrochemical Society 2005;152(10):F162-F170.

[20] Suzuki M, Kishida A, Iwata H, Ikada Y. Graft copolymerization of acrylamide onto a polyethylene surface pretreated with glow discharge. Macromolecules 1981;19(7):1804-1808.

[21] Pauleau Y editor. Materials Surface Processing by Directed Energy Techniques. 1st Edition ed.: European materials research society; 2006.

[22] Meyer J. Retina implant—a bioMEMS challenge. Sensors and Actuators A: Physical 2002;97–98(0):1-9.

[23] Eurell TE, Brown DR, Gerding PA, Hamor RE. Alginate as a new biomaterial for the growth of porcine retinal pigment epithelium. Vet Ophthalmol 2003;6(3):237-243.

[24] da Cruz L, Chen FK, Ahmado A, Greenwood J, Coffey P. RPE transplantation and its role in retinal disease. Prog Retin Eye Res 2007;26(6):598-635.

[25] Mazumder MA, Fitzpatrick SD, Muirhead B, Sheardown H. Cell-adhesive thermogelling PNIPAAm/hyaluronic acid cell delivery hydrogels for potential application

as minimally invasive retinal therapeutics. J Biomed Mater Res A 2012;100(7):1877-1887.

[26] Physiology of analyzers. 2013; Available at: http://intranet.tdmu.edu.ua/data/kafedra/internal/i_nurse/classes_stud/English/BSN-(4y)/1%20year/Fall%20semester/Physiology/PHYSIOLOGY%20OF%20ANALYZERS.htm.

[27] Curcio CA, Medeiros NE, Millican CL. Photoreceptor loss in age-related macular degeneration. Invest Ophthalmol Visual Sci 1996;37(7):1236-1249.

[28] Berson EL, Rosner B, Sandberg MA, Hayes KC, Nicholson BW, Weigel-DiFranco C, et al. A randomized trial of vitamin a and vitamin e supplementation for retinitis pigmentosa. Archives of Ophthalmology 1993;111(6):761-772.

[29] Santos A, Humayun MS, de Juan E,Jr, Greenburg RJ, Marsh MJ, Klock IB, et al. Preservation of the inner retina in retinitis pigmentosa. A morphometric analysis. Arch Ophthalmol 1997;115(4):511-515.

[30] Hynes SR, Lavik EB. A tissue-engineered approach towards retinal repair: scaffolds for cell transplantation to the subretinal space. Graefes Arch Clin Exp Ophthalmol 2010;248(6):763-778.

[31] Chow AY, Bittner AK, Pardue MT. The artificial silicon retina in retinitis pigmentosa patients (an American Ophthalmological Association thesis). Trans Am Ophthalmol Soc 2010;108:120-154.

[32] Humayun MS. Intraocular retinal prosthesis. Trans Am Ophthalmol Soc 2001;99:271-300.

[33] Portable Biomimetic Retina for Learning, Perception-based Image Acquisition. Neural Networks, International Joint Conference; 2007.

[34] Klauke S, Goertz M, Rein S, Hoehl D, Thomas U, Eckhorn R, et al. Stimulation with a Wireless Intraocular Epiretinal Implant Elicits Visual Percepts in Blind Humans. Investigative Ophthalmology & Visual Science 2011;52(1):449-455.

[35] Fernandes RA, Diniz B, Ribeiro R, Humayun M. Artificial vision through neuronal stimulation. Neurosci Lett 2012;519(2):122-128.

[36] Rizzo III JF, Shire DB, Kelly SK, Troyk P, Gingerich M, McKee B, et al. Development of the boston retinal prosthesis. Conf Proc IEEE Eng Med Biol Soc 2011:3135-3138.

[37] Chow AY, Chow VY, inventors. IMI INTELLIGENT MEDICAL IMPLANTS AG, assignee. Artificial retina device with stimulating and ground return electrodes disposed on opposite sides of the neuroretina and method of attachment. United States patent US 2011/0238134 A1. 2011 .

[38] Weiland JD, Cho AK, Humayun MS. Retinal prostheses: current clinical results and future needs. Ophthalmology 2011;118(11):2227-2237.

[39] Novel Retinal Prosthesis System with Three Dimensionally Stacked LSI Chip. Solid-State Device Research Conference, Proceeding of the 36th European; 2006.

[40] Zrenner E. Will retinal implants restore vision? Science 2002;295(5557):1022-1025.

[41] Maynard EM. Visual prostheses. Annu Rev Biomed Eng 2001;3:145-168.

[42] Lee SW, Seo JM, Ha S, Kim ET, Chung H, Kim SJ. Development of microelectrode arrays for artificial retinal implants using liquid crystal polymers. Invest Ophthalmol Vis Sci 2009;50(12):5859-5866.

[43] Schanze T, Hesse L, Lau C, Greve N, Haberer W, Kammer S, et al. An optically powered single-channel stimulation implant as test system for chronic biocompatibility and biostability of miniaturized retinal vision prostheses. IEEE Trans Biomed Eng 2007;54(6 Pt 1):983-992.

[44] Margalit E, Maia M, Weiland JD, Greenberg RJ, Fujii GY, Torres G, et al. Retinal Prosthesis for the Blind. Surv Ophthalmol 2002;47(4):335-356.

[45] Scholz C. Perspectives on: Materials Aspects for Retinal Prostheses. Journal of Bioactive and Compatible Polymers 2007;22(5):539-568.

[46] Güven D, Weiland JD, Maghribi M, Davidson JC, Mahadevappa M, Roizenblatt R, et al. Implantation of an inactive epiretinal poly(dimethyl siloxane) electrode array in dogs. Exp Eye Res 2006;82(1):81-90.

[47] Walter P, Kisvarday ZF, Gortz M, Alteheld N, Rossler G, Stieglitz T, et al. Cortical activation via an implanted wireless retinal prosthesis. Invest Ophthalmol Vis Sci 2005;46(5):1780-1785.

[48] Majji AB, Humayun MS, Weiland JD, Suzuki S, D'Anna SA, de Juan E,Jr. Long-term histological and electrophysiological results of an inactive epiretinal electrode array implantation in dogs. Invest Ophthalmol Vis Sci 1999;40(9):2073-2081.

[49] Kim ET, Kim C, Lee SW, Seo JM, Chung H, Kim SJ. Feasibility of microelectrode array (MEA) based on silicone-polyimide hybrid for retina prosthesis. Invest Ophthalmol Vis Sci 2009;50(9):4337-4341.

[50] Seo J, Kim SJ, Chung H, Kim ET, Yu HG, Yu YS. Biocompatibility of polyimide microelectrode array for retinal stimulation. Materials Science and Engineering: C 2004;24(1–2):185-189.

[51] Seo J, Paik SJ, Kim ET, Byun SW, Lee AR, Cho D, et al. Silicon retinal tack for the epiretinal fixation of the polyimide electrode array. Current Applied Physics 2006;6(4):649-653.

[52] Margalit E, Fujii GY, Lai JC, Gupta P, Chen SJ, Shyu JS, et al. Bioadhesives for intraocular use. Retina 2000;20(5):469-477.

[53] Tunc M, Cheng X, Ratner BD, Meng E, Humayun M. Reversible thermosensitive glue for retinal implants. Retina 2007;27(7):938-942.

[54] Tunc M, Humayun M, Cheng X, Ratner BD. A reversible thermosensitive adhesive for retinal implants: in vivo experience with plasma-deposited poly(N-isopropyl acrylamide). Retina 2008;28(9):1338-1343.

[55] Lu L, Yaszemski MJ, Mikos AG. Retinal pigment epithelium engineering using synthetic biodegradable polymers. Biomaterials 2001;22(24):3345-3355.

[56] Lu JT, Lee CJ, Bent SF, Fishman HA, Sabelman EE. Thin collagen film scaffolds for retinal epithelial cell culture. Biomaterials 2007;28(8):1486-1494.

[57] Gomes M, Azevedo H, Malafaya P, Silva S, Oliveira J, Silva G, et al. Chapter 6 - Natural Polymers in tissue engineering applications. In: Clemens van Blitterswijk, Peter Thomsen, Anders Lindahl, et al., editors. Tissue Engineering Burlington: Academic Press; 2008. p. 145-192.

[58] Belbachir K, Noreen R, Gouspillou G, Petibois C. Collagen types analysis and differentiation by FTIR spectroscopy. Anal Bioanal Chem 2009;395(3):829-837.

[59] Nair LS, Laurencin CT. Biodegradable polymers as biomaterials. Progress in Polymer Science 2007;32(8–9):762-798.

[60] Shadforth AM, George KA, Kwan AS, Chirila TV, Harkin DG. The cultivation of human retinal pigment epithelial cells on Bombyx mori silk fibroin. Biomaterials 2012;33(16):4110-4117.

[61] Fitzpatrick SD, Jafar Mazumder MA, Lasowski F, Fitzpatrick LE, Sheardown H. PNIPAAm-grafted-collagen as an injectable, in situ gelling, bioactive cell delivery scaffold. Biomacromolecules 2010;11(9):2261-2267.

[62] Vaajasaari H, Ilmarinen T, Juuti-Uusitalo K, Rajala K, Onnela N, Narkilahti S, et al. Toward the defined and xeno-free differentiation of functional human pluripotent stem cell-derived retinal pigment epithelial cells. Mol Vis 2011;17:558-575.

[63] Wikstrom J, Elomaa M, Syvajarvi H, Kuokkanen J, Yliperttula M, Honkakoski P, et al. Alginate-based microencapsulation of retinal pigment epithelial cell line for cell therapy. Biomaterials 2008;29(7):869-876.

[64] Jani D, Salamone CJ, inventors. AnonymousAlginate viscoelastic composition, method of use and package. EP1720518 B1. 2009 .

[65] Wikstrom J, Elomaa M, Nevala L, Raikkonen J, Heljo P, Urtti A, et al. Viability of freeze dried microencapsulated human retinal pigment epithelial cells. Eur J Pharm Sci 2012;47(2):520-526.

[66] Prestwich GD. Hyaluronic acid-based clinical biomaterials derived for cell and molecule delivery in regenerative medicine. J Control Release 2011;155(2):193-199.

[67] Gross-Jendroska M, Lui GM, Song MK, Stern R. Retinal pigment epithelium-stromal interactions modulate hyaluronic acid deposition. Invest Ophthalmol Vis Sci 1992;33(12):3394-3399.

[68] D. Y. W. Intra-articular hyaluronic acid injections for knee osteoarthritis. Am Fam Physician 2000;62(3):565-570.

[69] Liu Y, Wang R, Zarembinski TI, Doty N, Jiang C, Regatieri C, et al. The application of hyaluronic acid hydrogels to retinal progenitor cell transplantation. Tissue Eng Part A 2013;19(1-2):135-142.

[70] Aumailley M, Bruckner-Tuderman L, Carter WG, Deutzmann R, Edgar D, Ekblom P, et al. A simplified laminin nomenclature. Matrix Biology 2005;24(5):326-332.

[71] Timpl R, Rohde H, Robey PG, Rennard SI, Foidart JM, Martin GR. Laminin--a glycoprotein from basement membranes. Journal of Biological Chemistry 1979;254(19):9933-9937.

[72] Redenti S, Neeley WL, Rompani S, Saigal S, Yang J, Klassen H, et al. Engineering retinal progenitor cell and scrollable poly(glycerol-sebacate) composites for expansion and subretinal transplantation. Biomaterials 2009;30(20):3405-3414.

[73] Pritchard CD, Arner KM, Neal RA, Neeley WL, Bojo P, Bachelder E, et al. The use of surface modified poly(glycerol-co-sebacic acid) in retinal transplantation. Biomaterials 2010;31(8):2153-2162.

[74] Yurchenco PD, Patton BL. Developmental and pathogenic mechanisms of basement membrane assembly. Curr Pharm Des 2009;15(12):1277-1294.

[75] Laminin. 2013; Available at: http://www.sigmaaldrich.com/life-science/metabolomics/enzyme-explorer/learning-center/structural-proteins/laminin.html.

[76] Yao J, Tao SL, Young MJ. Synthetic Polymer Scaffolds for Stem Cell Transplantation in Retinal Tissue Engineering . Polymers 2011;3(2):899-914.

[77] Baldwin SP, Mark Saltzman W. Materials for protein delivery in tissue engineering. Adv Drug Deliv Rev 1998;33(1–2):71-86.

[78] Lavik EB, Klassen H, Warfvinge K, Langer R, Young MJ. Fabrication of degradable polymer scaffolds to direct the integration and differentiation of retinal progenitors. Biomaterials 2005;26(16):3187-3196.

[79] Rai R, Tallawi M, Grigore A, Boccaccini AR. Synthesis, properties and biomedical applications of poly(glycerol sebacate) (PGS): A review. Progress in Polymer Science 2012;37(8):1051-1078.

[80] Redenti S, Tao S, Yang J, Gu P, Klassen H, Saigal S, et al. Retinal tissue engineering using mouse retinal progenitor cells and a novel biodegradable, thin-film poly(e-caprolactone) nanowire scaffold. J Ocul Biol Dis Infor 2008;1(1):19-29.

[81] Bordes C, Fréville V, Ruffin E, Marote P, Gauvrit JY, Briançon S, et al. Determination of poly(ε-caprolactone) solubility parameters: Application to solvent substitution in a microencapsulation process. Int J Pharm 2010;383(1–2):236-243.

[82] Poly(methyl methacrylate) . 2013; Available at: http://chemsrv1.uwsp.edu/macrogcss/pmma.html.

[83] Tao S, Young C, Redenti S, Zhang Y, Klassen H, Desai T, et al. Survival, migration and differentiation of retinal progenitor cells transplanted on micro-machined poly(methyl methacrylate) scaffolds to the subretinal space. Lab Chip 2007;7(6):695-701.

[84] Julien S, Peters T, Ziemssen F, Arango-Gonzalez B, Beck S, Thielecke H, et al. Implantation of ultrathin, biofunctionalized polyimide membranes into the subretinal space of rats. Biomaterials 2011;32(16):3890-3898.

[85] Guenther E, Troger B, Schlosshauer B, Zrenner E. Long-term survival of retinal cell cultures on retinal implant materials. Vision Res 1999;39(24):3988-3994.

[86] Blawas AS, Reichert WM. Protein patterning. Biomaterials 1998;19(7–9):595-609.

[87] Neves-Petersen MT, Snabe T, Klitgaard S, Duroux M, Petersen SB. Photonic activation of disulfide bridges achieves oriented protein immobilization on biosensor surfaces. Protein Science 2006;15(2):343-351.

[88] Chang TY, Yadav VG, De Leo S, Mohedas A, Rajalingam B, Chen C, et al. Cell and Protein Compatibility of Parylene-C Surfaces. Langmuir 2007;23(23):11718-11725.

[89] Sinz A. Chemical cross-linking and mass spectrometry for mapping three-dimensional structures of proteins and protein complexes. Journal of Mass Spectrometry 2003;38(12):1225-1237.

[90] Baslé E, Joubert N, Pucheault M. Protein Chemical Modification on Endogenous Amino Acids. Chem Biol 2010;17(3):213-227.

[91] Kannoujia DK, Kumar S, Nahar P. Covalent immobilization of ascorbate oxidase onto polycarbonate strip for l-ascorbic acid detection. Journal of Bioscience and Bioengineering 2012;114(4):402-404.

[92] Pei Z, Yu H, Theurer M, Waldén A, Nilsson P, Yan M, et al. Photogenerated Carbohydrate Microarrays. ChemBioChem 2007;8(2):166-168.

[93] Cheng N, Cao X. Photosensitive chitosan to control cell attachment. J Colloid Interface Sci 2011;361(1):71-78.

[94] Amine-reactive crosslinker chemistry. 2012; Available at: http://www.piercenet.com/browse.cfm?fldID=F330F14F-EBCC-97DB-7F6E-9664D3ACE886.

[95] Goddard JM, Hotchkiss JH. Polymer surface modification for the attachment of bioactive compounds. Progress in Polymer Science 2007;32(7):698-725.

[96] Rusmini F, Zhong Z, Feijen J. Protein Immobilization Strategies for Protein Biochips. Biomacromolecules 2007;8(6):1775-1789.

[97] Puleo DA, Nanci A. Understanding and controlling the bone–implant interface. Biomaterials 1999;20(23–24):2311-2321.

[98] Jose B, Antoci Jr. V, Zeiger AR, Wickstrom E, Hickok NJ. Vancomycin Covalently Bonded to Titanium Beads Kills Staphylococcus aureus. Chem Biol 2005;12(9):1041-1048.

[99] Wissink MJB, Beernink R, Pieper JS, Poot AA, Engbers GHM, Beugeling T, et al. Immobilization of heparin to EDC/NHS-crosslinked collagen. Characterization and in vitro evaluation. Biomaterials 2001;22(2):151-163.

[100] Ma Z, Gao C, Ji J, Shen J. Protein immobilization on the surface of poly-L-lactic acid films for improvement of cellular interactions. European Polymer Journal 2002;38(11):2279-2284.

[101] Ma Z, Mao Z, Gao C. Surface modification and property analysis of biomedical polymers used for tissue engineering. Colloids and Surfaces B: Biointerfaces 2007;60(2):137-157.

[102] Siow KS, Britcher L, Kumar S, Griesser HJ. Plasma Methods for the Generation of Chemically Reactive Surfaces for Biomolecule Immobilization and Cell Colonization - A Review. Plasma Processes and Polymers 2006;3(6-7):392-418.

[103] Inagaki N, Tasaka S, Hibi K. Surface modification of Kapton film by plasma treatments. Journal of Polymer Science Part A: Polymer Chemistry 1992;30(7):1425-1431.

[104] Xia Y, Boey F, Venkatraman S. Surface modification of poly(L-lactic acid) with biomolecules to promote endothelialization. Biointerphases 2010;5(3):FA32-FA40.

[105] Lee S, Hsiue G, Chang PC, Kao C. Plasma-induced grafted polymerization of acrylic acid and subsequent grafting of collagen onto polymer film as biomaterials. Biomaterials 1996;17(16):1599-1608.

[106] Bisson I, Kosinski M, Ruault S, Gupta B, Hilborn J, Wurm F, et al. Acrylic acid grafting and collagen immobilization on poly(ethylene terephthalate) surfaces for adherence and growth of human bladder smooth muscle cells. Biomaterials 2002;23(15):3149-3158.

[107] Gupta B, Plummer C, Bisson I, Frey P, Hilborn J. Plasma-induced graft polymerization of acrylic acid onto poly(ethylene terephthalate) films: characterization and human smooth muscle cell growth on grafted films. Biomaterials 2002;23(3):863-871.

[108] Protein cross-linkers handbook & selection guide. 2011; Available at: http://www.gbiosciences.com/default.aspx.

[109] Drumheller P, Hubbell J. Surface Immobilization of Adhesion Ligands for Investigations of Cell-Substrate Interactions. In: Palsson B, Hubbell J, Plonsey R, Bronzino JD, editors. Tissue Engineering: CRC Press; 2003.

[110] Briand E, Salmain M, Compère C, Pradier C. Immobilization of Protein A on SAMs for the elaboration of immunosensors. Colloids and Surfaces B: Biointerfaces 2006;53(2):215-224.

[111] Wei F, Sun B, Guo Y, Zhao XS. Monitoring DNA hybridization on alkyl modified silicon surface through capacitance measurement. Biosens Bioelectron 2003;18(9):1157-1163.

[112] Slocik JM, Beckel ER, Jiang H, Enlow JO, Zabinski JS, Bunning TJ, et al. Site-Specific Patterning of Biomolecules and Quantum Dots on Functionalized Surfaces Generated by Plasma-Enhanced Chemical Vapor Deposition. Adv Mater 2006;18(16):2095-2100.

[113] van Wachem PB, Plantinga JA, Wissink MJB, Beernink R, Poot AA, Engbers GHM, et al. In vivo biocompatibility of carbodiimide-crosslinked collagen matrices: Effects of crosslink density, heparin immobilization, and bFGF loading. J Biomed Mater Res 2001;55(3):368-378.

[114] Kudo H, Sudo S, Oka T, Hama Y, Oshima A, Washio M, et al. Ion-beam irradiation effects on polyimide-UV-vis and infrared spectroscopic study. Radiat Phys Chem 2009;78(12):1067-1070.

[115] Dulbecco's Phosphate Buffered Saline. 2013; Available at: http://www.sigmaaldrich.com/catalog/product/sigma/d5652?lang=en&region=CA.

[116] Tiraferri A, Elimelech M. Direct quantification of negatively charged functional groups on membrane surfaces. J Membr Sci 2012;389(0):499-508.

[117] Thumann G, Viethen A, Gaebler A, Walter P, Kaempf S, Johnen S, et al. The in vitro and in vivo behaviour of retinal pigment epithelial cells cultured on ultrathin collagen membranes. Biomaterials 2009;30(3):287-294.

[118] Use of a Hemacytometer. Available at: http://www.animal.ufl.edu/hansen/protocols/hemacytometer.htm.

[119] Hemocytometer square size. Available at: http://hemocytometer.wordpress.com/2013/04/11/hemocytometer-square-size/.

[120] Neubauer Sperm counting chamber and coverslips. Available at: http://www.tekevent.com/counting-chambers/neubauer-sperm-counting-chamber/index.shtml.

[121] Garg M, Quamara J. FTIR analysis of high energy heavy ion irradiated kapton-H polyimide. Indian Journal of Pure & Applied Physics 2007;45:563-568.

[122] Kallioinen M, Nyström M. Membrane Surface Characterization. Advanced Membrane Technology and Applications: John Wiley & Sons, Inc.; 2008. p. 841-877.

[123] IR Spectroscopy Tutorial: Carboxylic Acids. Available at: http://orgchem.colorado.edu/Spectroscopy/irtutor/carbacidsir.html.

[124] Infrared Spectroscopy IR Absorptions for Representative Functional Groups. 2007; Available at: http://www.chemistry.ccsu.edu/glagovich/teaching/316/ir/table.html.

[125] Infrared Spectroscopy. 2013; Available at: http://www2.chemistry.msu.edu/faculty/reusch/virttxtjml/spectrpy/infrared/infrared.htm

[126] Burke JM. Epithelial phenotype and the RPE: is the answer blowing in the Wnt? Prog Retin Eye Res 2008;27(6):579-595.

[127] Burke JM, Skumatz CM, Irving PE, McKay BS. Phenotypic heterogeneity of retinal pigment epithelial cells in vitro and in situ. Exp Eye Res 1996;62(1):63-73.

[128] McKay BS, Burke JM. Separation of phenotypically distinct subpopulations of cultured human retinal pigment epithelial cells. Exp Cell Res 1994;213(1):85-92.

[129] Kearns V, Mistry A, Mason S, Krishna Y, Sheridan C, Short R, et al. Plasma polymer coatings to aid retinal pigment epithelial growth for transplantation in the treatment of age related macular degeneration. J Mater Sci Mater Med 2012;23(8):2013-2021.

[130] M. France R, D. Short R, A. Dawson R, Macneil S. Attachment of human keratinocytes to plasma co-polymers of acrylic acid/octa-1,7-diene and allyl amine/octa-1,7-diene. Journal of Materials Chemistry 1998;8(1):37-42.

[131] Haddow DB, France RM, Short RD, MacNeil S, Dawson RA, Leggett GJ, et al. Comparison of proliferation and growth of human keratinocytes on plasma copolymers of acrylic acid/1,7-octadiene and self-assembled monolayers. J Biomed Mater Res 1999;47(3):379-387.

[132] Lai J. Solvent Composition is Critical for Carbodiimide Cross-Linking of Hyaluronic Acid as an Ophthalmic Biomaterial. Materials 2012;5(10):1986-2002.

[133] Lai J. Corneal Stromal Cell Growth on Gelatin/Chondroitin Sulfate Scaffolds Modified at Different NHS/EDC Molar Ratios. International Journal of Molecular Sciences 2013;14(1):2036-2055.

[134] Vaisocherova H, Yang W, Zhang Z, Cao Z, Cheng G, Piliarik M, et al. Ultralow fouling and functionalizable surface chemistry based on a zwitterionic polymer enabling sensitive and specific protein detection in undiluted blood plasma. Anal Chem 2008;80(20):7894-7901.

[135] Du Y, Chia S, Han R, Chang S, Tang H, Yu H. 3D hepatocyte monolayer on hybrid RGD/galactose substratum. Biomaterials 2006;27(33):5669-5680.

[136] Park BW, Yang HS, Baek SH, Park K, Han DK, Lee TS. The efficacy of acrylic acid grafting and arginine-glycine-aspartic acid peptide immobilization on fibrovascular ingrowth into porous polyethylene implants in rabbits. Graefes Arch Clin Exp Ophthalmol 2007;245(6):855-862.

[137] Doraiswamy A, Jin C, Narayan RJ, Mageswaran P, Mente P, Modi R, et al. Two photon induced polymerization of organic-inorganic hybrid biomaterials for microstructured medical devices. Acta Biomater 2006;2(3):267-275.

[138] Szmigiel D, Domanski K, Grabiec P. Polysiloxane Coatings on Biomedical Micro Devices: Plasma Etching and Properties of Protection Layer. Advances in Science and Technology 2008;57:220-225.

[139] Hao X, Jeffery JL, Le TPT, McFarland G, Johnson G, Mulder RJ, et al. High refractive index polysiloxane as Injectable, in situ curable accommodating intraocular lens. Biomaterials 2012;33(23):5659-5671.

[140] Norton JN, Kohnen T, Hackett RB, Patel A, Koch DD. Ocular biocompatibility testing of intraocular lenses: a 1 year study in pseudophakic rabbit eyes. Journal of Cataract & Refractive Surgery 1999;25(11):1467-1479.

[141] MacCarthy N, Wood T, Ameri H, O'Connell D, Alderman J. A laser release method for producing prototype flexible retinal implant devices. Sensors and Actuators A: Physical 2006;132(1):296-301.

[142] Sonn M, Feist WM. A prototype flexible microelectrode array for implant-prosthesis applications. Med Biol Eng 1974;12(6):778-791.

[143] Metallo C, White RD, Trimmer BA. Flexible parylene-based microelectrode arrays for high resolution EMG recordings in freely moving small animals. J Neurosci Methods 2011;195(2):176-184.

[144] Haas K-, Amberg-Schwab S, Rose K, Schottner G. Functionalized coatings based on inorganic–organic polymers (ORMOCER®s) and their combination with vapor deposited inorganic thin films. Surface and Coatings Technology 1999;111(1):72-79.

[145] Fujii T, Yokoi T, Hiramatsu M, Nawata M, Hori M, Goto T, et al. Low dielectric constant film formation by oxygen-radical polymerization of laser-evaporated siloxane. Journal of Vacuum Science & Technology B: Microelectronics and Nanometer Structures 1997;15(3):746-749.

[146] Characterization of Polymethyl Methacrylate (PMMA) Layers for OTFTs Gate Dielectric. Devices, Circuits and Systems, Proceedings of the 6th International Caribbean Conference on; 2006.

[147] Treichel H, Withers B, Ruhl G, Ansmann P, Würl R, Müller C, et al. Chapter 1 - Low Dielectric Constant Materials for Interlayer Dielectrics. Handbook of Low and High Dielectric Constant Materials and Their Applications Burlington: Academic Press; 1999. p. 1-71.

[148] Popall M, Kappel J, Pilz M, Schulz J, Feyder G. A new inorganic-organic polymer for the passivation of thin film capacitors. Journal of Sol-Gel Science and Technology 1994;2:157-160.

[149] Polysiloxanes. 2004; Available at: http://www.eng.buffalo.edu/Courses/ce435/Polysiloxanes/.

[150] Lloyd AW, Faragher RGA, Denyer SP. Ocular biomaterials and implants. Biomaterials 2001;22(8):769-785.

[151] Sapsford KE, Ligler FS. Real-time analysis of protein adsorption to a variety of thin films. Biosensors and Bioelectronics 2004;19(9):1045-1055.

[152] Kron J, Amberg-schwab S, Schottner GS. Functional coatings on glass using ORMOCER®-systems. Journal of Sol-Gel Science and Technology 1994;2(1):189-192.

[153] Pielichowski K, Njuguna J. Inorganic polymers. Thermal degradation of polymeric materials: Rapra technology; 2005. p. 173-188.

[154] Klinge PM, Vafa MA, Brinker T, Brandis A, Walter GF, Stieglitz T, et al. Immunohistochemical characterization of axonal sprouting and reactive tissue changes after long-term implantation of a polyimide sieve electrode to the transected adult rat sciatic nerve. Biomaterials 2001;22(17):2333-2343.

[155] Bodas DS, Gangal SA. Structural characterization of sputtered PMMA in argon plasma. Mater Lett 2005;59(23):2903-2907.

[156] Licari JJ. 2 - Chemistry and Properties of Polymer Coatings. Coating Materials for Electronic Applications Norwich, NY: William Andrew Publishing; 2003. p. 65-200.

[157] Houbertz R, Domann G, Cronauer C, Schmitt A, Martin H, Park J-, et al. Inorganic–organic hybrid materials for application in optical devices. Thin Solid Films 2003;442(1–2):194-200.

[158] Seo J, Zhou J, Kim E, Koo K, Ye J, Kim S, et al. A Retinal Implant System Based on Flexible Polymer Microelectrode Array for Electrical Stimulation. In: Tombran-Tink J, Barnstable C, Rizzo J, editors. Visual Prosthesis and Ophthalmic Devices: Humana Press; 2007. p. 107-119.

[159] Loeb GE, Bak MJ, Salcman M, Schmidt EM. Parylene as a chronically stable, reproducible microelectrode insulator. IEEE Trans Biomed Eng 1977;24(2):121-128.

[160] Flueckiger J, Bazargan V, Stoeber B, Cheung KC. Characterization of postfabricated parylene C coatings inside PDMS microdevices. Sensors Actuators B: Chem 2011;160(1):864-874.

[161] Schizas C, Karalekas D. Mechanical characteristics of an Ormocomp® biocompatible hybrid photopolymer. Journal of the Mechanical Behavior of Biomedical Materials 2011;4(1):99-106.

[162] ORMOCER® (hollow) fibers and nanoporous SiO_2 hollow fibers. 2013; Available at: http://www.ormocer.de/ORMOCER-R-hollow-fibers-and.816.0.html?&L=1.

[163] Jiao L, Fan B, Xian X, Wu Z, Zhang J, Liu Z. Creation of nanostructures with poly(methyl methacrylate)-mediated nanotransfer printing. J Am Chem Soc 2008;130(38):12612-12613.

[164] Chen Y, Lai H, Lin S, Cho C, Chao W, Liao C, et al. Design and fabrication of a polyimide-based microelectrode array: Application in neural recording and repeatable electrolytic lesion in rat brain. J Neurosci Methods 2009;182(1):6-16.

[165] Chen P, Chen M, Sun J, Chen M, Tsai C, Lin F. Biocompatibility of NGF-grafted GTG membranes for peripheral nerve repair using cultured Schwann cells. Biomaterials 2004;25(25):5667-5673.

[166] Yang W, Yang C, Huang C, Chen K, Lin S. Bostrycin, a novel coupling agent for protein immobilization and prevention of biomaterial-centered infection produced by Nigrospora sp. No. 407. Enzyme Microb Technol 2012;50(6–7):287-292.

[167] Choi HJ, Kim NH, Chung BH, Seong GH. Micropatterning of biomolecules on glass surfaces modified with various functional groups using photoactivatable biotin. Anal Biochem 2005;347(1):60-66.

[168] Ko H, Lee E, Lee G, Kim J, Jeon B, Kim M, et al. One step immobilization of peptides and proteins by using modified parylene with formyl groups. Biosensors and Bioelectronics 2011;30(1):56-60.

[169] Jeon B, Kim M, Pyun J. Application of a functionalized parylene film as a linker layer of SPR biosensor. Sensors Actuators B: Chem 2011;154(2):89-95.

[170] Yu G, Ji J, Zhu H, Shen J. Poly(D,L-lactic acid)-block-(ligand-tethered poly(ethylene glycol)) copolymers as surface additives for promoting chondrocyte attachment and growth. Journal of Biomedical Materials Research Part B: Applied Biomaterials 2006;76B(1):64-75.

[171] Shukla SP, Devi S. Immobilization of pepsin on an acrylamide/2-hydroxyethyl methacrylate copolymer and its use in casein hydrolysis. J Appl Polym Sci 2005;96(5):1544-1549.

[172] Nilsson K, Mosbach K. Immobilization of ligands with organic sulfonyl chlorides. Methods in Enzymology: Academic Press. p. 56-69.

[173] Horlacher T, Seeberger PH. Carbohydrate arrays as tools for research and diagnostics. Chem Soc Rev 2008;37(7):1414-1422.

[174] Vegas AJ, Fuller JH, Koehler AN. Small-molecule microarrays as tools in ligand discovery. Chem Soc Rev 2008;37(7):1385-1394.

[175] Sharkawi T, Darcos V, Vert M. Poly(DL-lactic acid) film surface modification with heparin for improving hemocompatibility of blood-contacting bioresorbable devices. Journal of Biomedical Materials Research Part A 2011;98A(1):80-87.

[176] Ferrero VEV, Andolfi L, Di Nardo G, Sadeghi SJ, Fantuzzi A, Cannistraro S, et al. Protein and Electrode Engineering for the Covalent Immobilization of P450 BMP on Gold. Anal Chem 2008;80(22):8438-8446.

[177] Ichihara T, Akada JK, Kamei S, Ohshiro S, Sato D, Fujimoto M, et al. A Novel Approach of Protein Immobilization for Protein Chips Using an Oligo-Cysteine Tag. Journal of Proteome Research 2006;5(9):2144-2151.

[178] Kunath K, Merdan T, Hegener O, Häberlein H, Kissel T. Integrin targeting using RGD-PEI conjugates for in vitro gene transfer. J Gene Med 2003;5(7):588-599.

[179] Delaittre G, Greiner AM, Pauloehrl T, Bastmeyer M, Barner-Kowollik C. Chemical approaches to synthetic polymer surface biofunctionalization for targeted cell adhesion using small binding motifs. Soft Matter 2012;8(28):7323-7347.

[180] Rizzi SC, Hubbell JA. Recombinant protein-co-PEG networks as cell-adhesive and proteolytically degradable hydrogel matrixes. Part I: Development and physicochemical characteristics. Biomacromolecules 2005;6(3):1226-1238.

[181] Mateo C, Torres R, Fernandez-Lorente G, Ortiz C, Fuentes M, Hidalgo A, et al. Epoxy-amino groups: a new tool for improved immobilization of proteins by the epoxy method. Biomacromolecules 2003;4(3):772-777.

[182] Gauvreau V, Chevallier P, Vallières K, Petitclerc É, Gaudreault RC, Laroche G. Engineering Surfaces for Bioconjugation: Developing Strategies and Quantifying the Extent of the Reactions. Bioconjugate Chem 2004;15(5):1146-1156.

APPENDIX 1. SOME CANDIDATE POLYMERS FOR RETINAL PROSTHESIS AND THEIR PROPERTIES

Properties	ORMOCER (ORMOCOMP)	Polysiloxane	PMMA	Polyimide	Parylene C Poly(2-chlor-para-xylylene)
Biocompatible	–Non-toxic and biologically inert –Acceptable cell viability and cell growth profiles against neuroblast and epithelial cells [137]	–Biocompatible [138] –Noncytotoxic and ocular biocompatibility [139]	Ocular biocompatibility [140]	–Biostable and non-toxic [141] –Ocular biocompatibility [50]	–blood compatibility [142] / biocompatible [143] –Tight retinal cellular adhesion for 4 weeks [51] – Low fibroblasts attachment on PC [10]
Electrical property	Control the electrical surface conductivity in order to produce antistatic coatings [144]	Low dielectric constant [145]	High electrical resistivity [146]	low dielectric constant e with respect to processing [147]	High dielectric strength and electrical insulation resistance [10, 143]
Corrosion	–Corrosion resistant layer [144] –Reduction of water permeation [144, 148]	–High chemical resistance [138] –High gas permeability [149]	–Acceptable surface wettability –Low oxygen permeability [150]	Chemically inert, water and ion impermeable [151]	Moisture/chemical barrier properties [142, 143]
Durability	Stability against weathering and resistance towards corrosive delamination [152]	–Thermally stable to 300 °C [153] –Too hydrophobic [149]	Exceptional durability [150]	Biostable for at least 11 months [154]	Biostable for many years once implanted [10]
Adhesion	Good adhesion to a variety of substrates [137, 144, 148, 152]	Good adhesion to the substrate [138]	Good adhesion when it is coated with DC sputtering [155]	Good adhesion to electrode [8]	Excellent adhesion to most surfaces [156]

APPENDIX 1. SOME CANDIDATE POLYMERS FOR RETINAL PROSTHESIS AND THEIR PROPERTIES

Properties	ORMOCER (ORMO-COMP)	Polysiloxane	PMMA	Polyimide	Parylene C Poly(2-chlor-para-xylylene)
Coating method	– All conventional coating techniques (dipping, spraying, spin on, blade, curtain, etc.) [144, 157] – Two photon induced polymerization [137]	Plasma etching [138]	plasma polymerization, thermal deposition, RF sputtering, DC sputtering [155]	Spin coating [154, 158]	Chemical vapour deposition (CVD) process [10, 142, 143, 159, 160]
Application	Electronics, micromechanical systems, corrosion coatings, and medical technology [152, 161]	Protection layer on cochlear implant, intraocular lens, electrical insulator [138, 139, 153]	– Ocular devices/contact lenses [150] – Coatings, adhesives, sensors, biomaterials [155] – Electronic photoresists [146]	Biosensor encapsulation, retinal tissue prosthesis [5-7]	Insulator for biomedical probes, retinal tissue prosthesis [10, 143]
Flexibility	Flexible hollow fibers [162]	High flexibility [138]	Flexible [163]	180° bends with no cracks [151]	Flexible [143, 164]

APPENDIX 2. INTERACTION BETWEEN FUNCTIONAL GROUPS ON THE SURFACE, CROSSLINKER, AND PROTEIN

Surface	Crosslinker	Crosslinker-Surface	Final product References
Protein functional group: 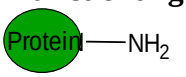			
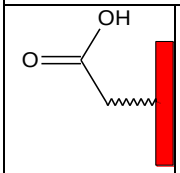	Carbodiimides (EDC or EDAC) 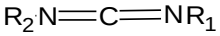	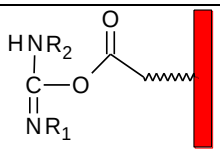	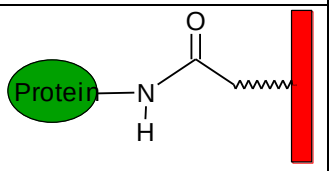 Amide [3, 89, 100, 136, 165]
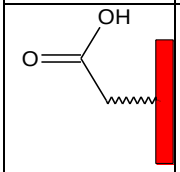	N-hydroxysuccinimide (NHS), Carbodiimides 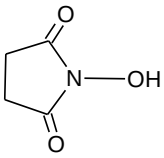	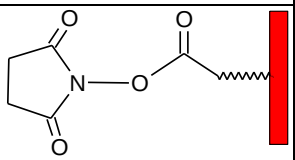	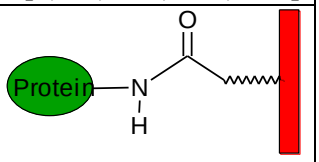 Amide [2, 10, 12, 13, 61, 89, 96, 99, 104, 111, 135]
	Aldehydes 	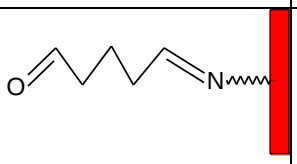	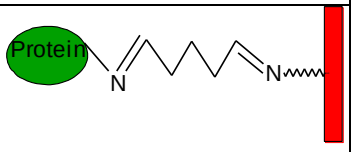 [12, 96, 166-169]
	Sulfonyl Chlorides 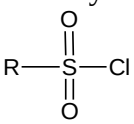	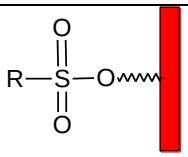	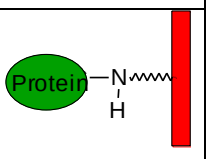 [100, 170-172]
	Epoxides 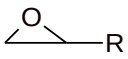	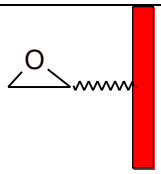	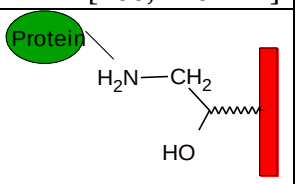 [96, 173, 174]

APPENDIX 2. INTERACTION BETWEEN FUNCTIONAL GROUPS ON THE SURFACE, CROSSLINKER, AND PROTEIN

Surface	Crosslinker	Crosslinker-Surface	Final product References
Protein functional group: 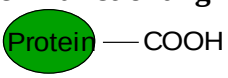			
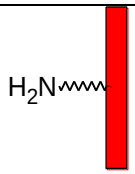	Carbodiimides 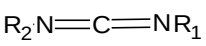	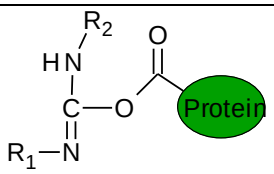	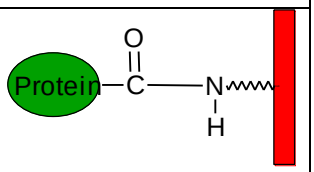 [12, 90, 108]
	N-hydroxysuccinimide (NHS), Carbodiimides 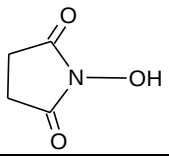	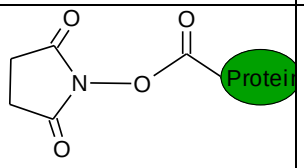	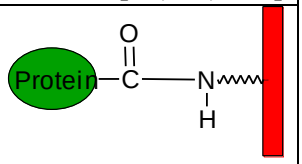 [61, 93, 175]
Protein functional group: 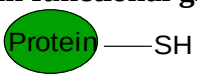			
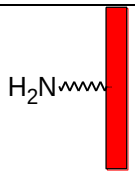	Maleimides 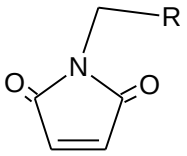	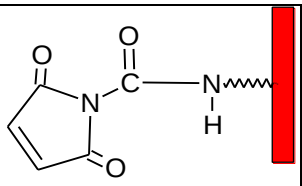	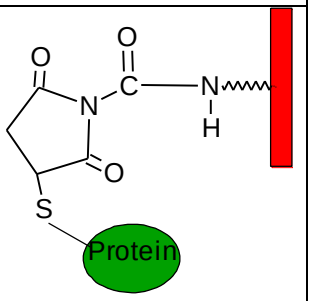 [89, 96, 176, 177]
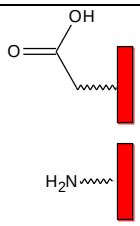	Disulfide reagents 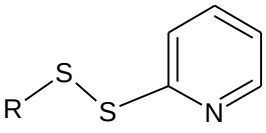	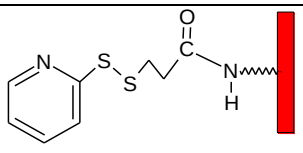	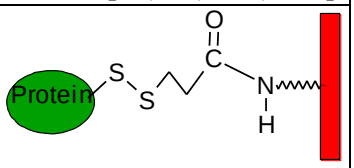 [96, 178, 179]
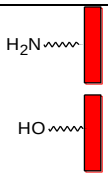	Vinyl sulfone 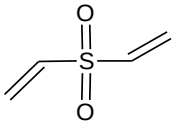	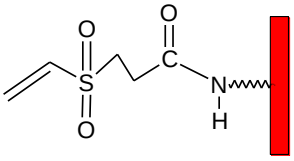	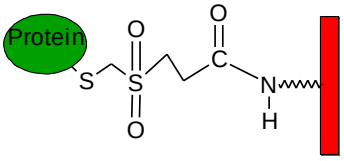 [12, 96, 178, 180]

APPENDIX 3. GRAFTING METHODS OF FUNCTIONAL GROUPS ONTO THE SUBSTRATE

Functional Groups	Methods of Grafting
Hydroxyl (-OH)	• Photooxidization and subsequent UV-induced polymerization (using PHEMA) [100] • Oxygen plasma treatment , or Ar plasma treatment followed by exposure to atmospheric oxygen [102]
Amino ($-NH_2$)	• Using compounds such as 1,6-hexanediamine [175], Ethylenediamine [181], polyethyleneimine [166], and 3-aminopropyltriethoxysilane (APTES) [167] • Ammonia plasma treatement [101, 182]
Carboxyl (-COOH)	• Plasma treatment with CO_2 , CO, or monomers like acrylic acid [102, 103, 136] • Photooxidization and subsequent UV-induced polymerization [100, 101] • Gas plasma pretreatment and subsequent graft polymerization with COOH- terminated compounds [2, 3, 16, 105-107, 135]